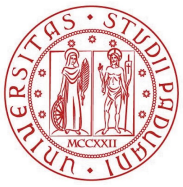

UNIVERSITÀ
DEGLI STUDI
DI PADOVA

UNIVERSITÀ DEGLI STUDI DI PADOVA
DIPARTIMENTO DI FISICA E ASTRONOMIA
SCUOLA DI DOTTORATO DI RICERCA IN ASTRONOMIA
CICLO XXIV

Stellar models with rotation in intermediate mass regime

Direttore della Scuola di Dottorato:
Ch.mo Prof. GIAMPAOLO PIOTTO
Supervisore: Dr.ssa ANTONELLA VALLENARI
Co-Supervisore: Dr. FREDERIC THEVENIN

Dottoranda: **LUCA SANTORO**
Matricola: 966277-DR

ANNO ACCADEMICO 2012

Contents

List of Figures

List of Tables

x

Riassunto

Malgrado i progressi dell'evoluzione stellare nel recente passato, rimangono molti problemi aperti. Ci sono molti effetti che influenzano sensibilmente le magnitudini stellari, il tempo di vita, la durata della fase di bruciamento a necessitano di essere calibrate per paragonare modelli e osservazioni. Le osservazioni che forniscono i dati di input per questo tipo di analisi richiedono comunque buoni dati fotometrici e spettroscopici cos come la determinazione di appartenenza. La missione ESA Gaia fornirá parallassi, moti propri, velocit radiali, magnitudini e colori per tutti i tipi di stelle di tutte le popolazioni stellari (fino a G=20) nella nostra galassia. I dati astrometrici di Gaia forniranno grandi campioni di membri di ammasso con probabilit molto alta per diverse decine di cluster vicini, coprendo un'ampia gamma di tipi spettrali. Questi dati potranno essere paragonati con le isocrone teoriche preparata per composizione chimica simile ed etá e le differenze tra le isocrone osservate e teoriche potranno essere esplorate per raffinamenti dei modelli che sono alla base delle isocrone teoriche. Questo potrebbe portare a un sensibile miglioramento nell'attendibilit di questi modelli e la loro applicazione in differenti campi, come il fornire stima di et per le stelle di campo. La determinazione dell'etá e della massa delle stelle di Gaia (FLAMES) ha un'importanza fondamentale per studiare la formazione e l'evoluzione di varie popolazioni galattiche. Le osservazioni campioneranno le popolazioni di cluster per una grande gamma di ammassi aperti in etá e composizione chimica. Il diagramma HR sar calibrato includendo tutte le fasi di evoluzione stellare, dalle stelle di pre-sequenza principale fino alle nane bianche e le fasi transienti e tutte le possibili masse dalle nane brune fino alle pi massicce stelle O. Grazie alla grande accuratezza dei dati di Gaia, per interpretarli é necessario avere modelli stellari di accuratezza paragonabile. In piú questo tipo di informazione é molto importante per comprendere l'evoluzione stellare. Ci sono un numero di incertezze associate ai modelli stellari, come il mixing, la diffusione, rate nucleare, la convezione, il campo magnetico. In particolare é cruciale prendere in considerazione la rotazione delle stelle per studiare il diagramma HR delle popolazioni stellari come quelle degli ammassi aperti. In questa tesi noi ci focalizzeremo sullo studio della rotazione nel regime di masse basso-intermedio. L'effetto della rotazione sul mixing e sulla luminositá delle stelle significativo per stelle di bassa massa, influenzando la determinazione di etá e di masse dal diagramma HR. In questa tesi di dottorato noi affrontiamo lo studio della rotazione la sua influenza nell'interpretazione delle caratteristiche degli ammassi aperti, in particolare per 5 ammassi: Iadi, Praesepe, Pleadi, Blanco 1 e Alpha Persei. In praticolare noi testeremo l'implementazione della velocitá di rotazione nel codice di evoluzione stellare Cesam2k, calibrando i coefficienti di diffusione; calcoleremo insiemi adeguati di modelli stellari con una velocitá di rotazione ad-hoc per riprodurre i dati degli ammassi aperti selezionati. Infine applichiamo questi modelli alla determinazione di etá di questi ammassi. Nel capitolo 1 descriviamo il disegno generale della missione Gaia, com' é organizzata e che tipo di problemi scientifici affronta: lo studio della formazione e

dell'evoluzione della Via Lattea, ci concentriamo sull'importanza dell'accuratezza dei modelli stellari per la missione. Nel capitolo 2 discutiamo la rotazione nelle stelle: lo status della ricerca in questo campo e in particolare perch la rotazione importante nello studio di stelle giovani di bassa massa. Presentiamo l'effetto della rotazione sul diagramma HR e sulle abbondanze chimiche superficiali. infine discutiamo l'effetto von Zeipel. Nel capitolo 3 presentiamo il quadro osservazionale presentando il metodo di misura della velocitá di rotazione. Nello stesso capitolo discutiamo il metodo di Chandrasekhar-Munch per invertire statisticamente la distribuzione delle velocitá di rotazione proiettate. Nel capitolo 4 selezioniamo dai cataloghi esistenti dati adeguati per 5 ammassi aperti aventi membership, magnitudini, colori, distanze e velocitá di rotazione proiettate accurate. Ci focalizziamo sulle Iadi, Praesepe, Blanco 1, Pleadi, Alpha Persei. Nel capitolo 5 presentiamo il codice di evoluzione stellare Cesam2k in cui la rotazione é stata implementata e testata. Nel capitolo 6 presentiamo le griglie di modelli stellari al cambiare della velocit di rotazione per essere paragonate con le osservazioni del nostro campione di ammassi aperti. Questi modelli saranno paragonati con griglie di modelli con rotazione esistenti. Nel capitolo 7 discutiamo come otteniamo la vera velocit di rotazione da quella proiettata, l'inversione statistica, il suo test con i sistemi binari nell'ammasso delle Iadi e anche usando le stelle aventi misure di $Vsini$ e periodi di rotazione. Nel capitolo 8 facciamo uso dei modelli ottenuti con Cesam2k per derivare l'etá degli ammassi aperti. Infine verificheremo se la relazione usuale etá-velocitá (legge di Skumanich) verificata.

Abstract

In spite of the progresses of the stellar evolution in the recent past, still several open problems remain. All those effects significantly influence the stellar magnitudes, lifetimes, burning phase duration and need to be calibrated comparing models with observations. The observational input data for such exercise will, however, require good photometric and spectroscopic data, as well as very reliable cluster-membership determinations. Gaia Mission is an ESA Cornerstone which will provide parallaxes, proper motions, radial velocities, magnitudes and colors for all type of stars of all stellar populations (down to G= 20) in the Galaxy. The Gaia astrometric data will provide large samples of very high probability cluster members for several tens of nearby clusters, covering wide ranges of spectral types. These data should then be compared with theoretical isochrones prepared for similar chemical compositions and ages, and differences between the theoretical and observed isochrones can then be explored further for refinements of the models underlying the theoretical isochrones. This should ultimately lead to a significant improvement in the reliability of those models and their application in various fields, such as providing age estimates for field stars. The age and mass determination of the Gaia stars (FLAMES) has a fundamental importance in order to study the formation and evolution of the various Galactic populations. The observations will sample the cluster population, for a wide range of OCs in age and chemical composition. The H-R diagram will be calibrated, including all phases of stellar evolution, from pre-main sequence stars to white dwarfs and the existing transient phases and all possible masses from brown dwarfs to the most massive O stars. . Due to the high accuracy of Gaia data, to interpret them it is necessary to have stellar models of comparable accuracy. In addition, this kind of information is very important to understand the stellar evolution. There are a number of uncertainties associated with stellar evolution models, like mixing, diffusion, nuclear rate, convection, magnetic field. In particular, it is crucial to take into account the rotation of the stars to study the HR diagram of a population like those of open clusters. In this Thesis, we will focus on the study of the rotation in the low-intermediate mass regime. The effect of the rotation on the mixing and the luminosity of stars is significant for low mass stars masses influencing the determination of ages and masses from the HR diagram.

In this PhD thesis we the study of rotation and it's influence on the interpretation of the characteristic of the open clusters, in particular for 5 clusters: Hyades, Praesepe, Pleiades, Blanco 1 and Alpha Persei. In particular, we will test the implementation of the rotational velocity in the stellar evolutionary code Cesam2K, calibrating the diffusion coefficients; we will calculate suitable sets of stellar models with ad-hoc rotational velocity to reproduce the data of the selected open clusters. Finally we will apply these models to the determination of the age of these clusters. In Chapter 1 we describe the general design of the Gaia mission, how it is organized and what kind of scientific problems it handles: the study of the Milky Way formation and evolution. We focus on the importance of the

accurate stellar models for the mission. In Chapter 2 we discuss the rotation in stars: the status of the research in this field and in particular why the rotation is important in the study of relatively young low mass stars. We present the effect of rotation on the HR diagram, on the surface chemical abundances. Finally we discuss the von Zeipel effect. In Chapter 3 we present the observational framework, presenting the methods to measure the stellar rotation velocity. In the same chapter we discuss the Chandrasekhar-Munch method to statistically invert the projected rotational velocity distribution. In Chapter 4 we select from existing Catalogs, suitable data for 5 open clusters, having accurate memberships, magnitudes, colours, distances, and projected rotational velocities. We focus on Hyades, Praesepe, Pleiades, Blanco 1, Alpha Persei. In Chapter 5 we present the evolutionary code Cesam2k where the rotation was implemented and tested. In Chapter 6 we present the grids of stellar models at changing rotational velocities to be compared with the observations of our sample of open clusters. These models will be compared with existing grids of stellar models with rotation. In Chapter 7 we discuss how we obtain the true rotational velocity from the projected rotational velocity, the statistical inversion, its test with wide binary systems in Hyades cluster and using low mass stars having both $Vsini$ determinations and rotational periods. In Chapter 8 we make use of the Cesa2k stellar models to derive the age of the open clusters. Finally we will verify whether the usual age-velocity relation (the Skumanich law) is verified.

Chapter 1

Gaia and the Galaxy

1.1 Introduction

The formation and evolution of galaxies is one of the most studied problems in Astrophysics and detailed studies on our Galaxy are the fist step to understand these complex processes. The distributions in space, the kinematics and the chemical abudances of all of Galaxy components such as stars, planets, dark matter, radiation, dust, interstellar gas give information on the history of the formation. This knowledge has importance for the study of the high-redshift universe. To this aim, three type of observations are necessary: a census of large part of the Galaxy components, the knowledge of the component distances and the measure of the motions in three dimensions. In this way we can have a significant statistical descriptions of present spatial structure of Galaxy. This in turn can provide information about the gravitational field and the stellar orbits. The astrometric measurements provide model-indipendent distances and transverse kinematics. The photometric measurements are necessary to complete astrophysical information of individual objects. The Gaia mission is the cornerstone ESA mission that will provide all this information. In the following we will describe the main principles of the Gaia mission and the expected scientific outcome.

1.2 General design

In this Section we discuss the performance of the Gaia mission. The Gaia design has arisen from the requirements on astrometric precision and completeneness, the provision of accurate spectrophotometry for astrophysical diagnostics, the acquisition of radial velocities and the need for on-board object detection (Perryman et al., 2001). The main goal of the Gaia mission is to perform global (wide field) astrometry as opposed to local (narrow field) astrometry. In local astrometry, the star positions are measured with respect to a neighbouring star in the same field. Even with an accurate instrument, the propagation of errors is prohibitive when making a sky survey. The principle of global astrometry is to link stars with large angular distances in a network where each star is connected to a large number of other stars in every direction. Global astrometry requires the simultaneous observation of two fields of view in which the star positions are measured and compared.

It will make use of a continuous scanning motion ensuring that every object is observed in at least six distinct epochs per year in patterns that are geometrically favorable for the determination of the astrometric parameters. The angle between the Sun and spin axis is 45°, the spin period is 6 hours and the basic angle is 106.5°, as illustrate in the figure (1.1).

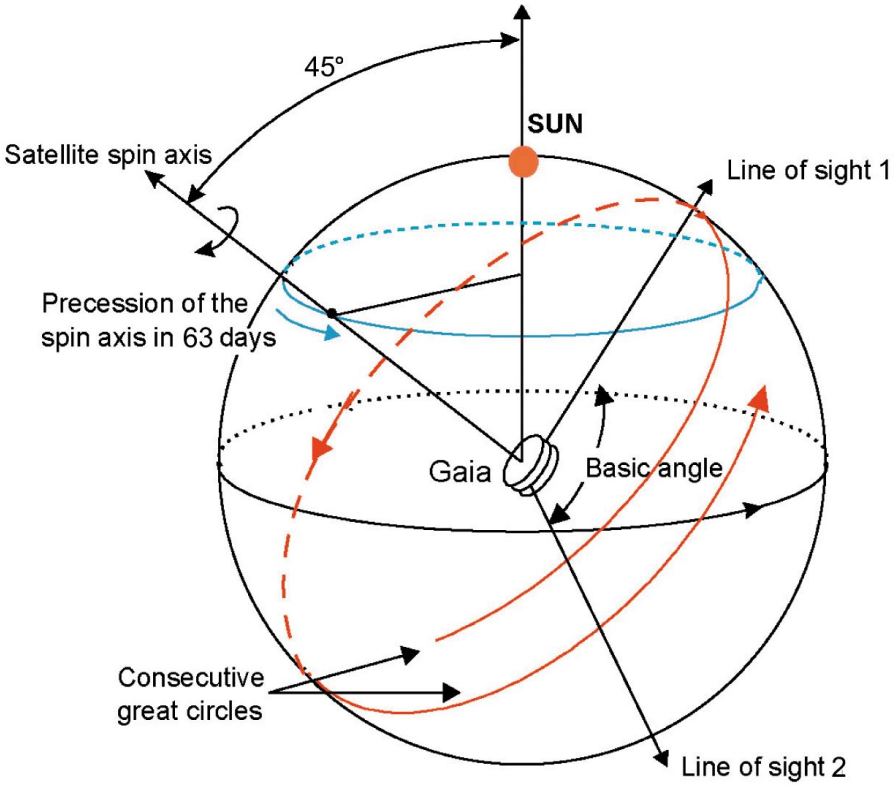

Figure 1.1: Scheme of the instrument movements. The line of sight 1 and 2 are the 2 directions of the observation for the 2 mirrors on board, they are separeted by the basic angle of 106.5°. The direction of the spin axis and of the precession motion are shown.

Gaia optical configuration is based on two telescopes looking at two different fields of view mapped on the same focal plane. Each of the two fields of view has an entrance pupil of $1.45 \times 0.5m^2$. The CCDs have a pixel size of $10 \times 30\mu m^2$, matched to the optical resolution of the instrument and the effective focal length of 35 m. In the figure (1.3) there is a scheme of the Gaia focal plane and how the focal plane is organized.

The on-board processing system detects any object brighter than 20 mag as it enters the focal plane, then tracks the object across a sequence of CCDs dedicated to the astrometric, photometric and radial-velocity measurements. The photometric and radial-velocity measurements share the same telescope and focal plane as the astrometry. For the photometry there are thus two rows of CCDs, referred to as the blue and red photometers (BP and RP). Each of them is prism spectrophotometer, sampling the dispersed image covering the spectral interval 330-680 nm (BP) and 640-1050 nm (RP). Any object

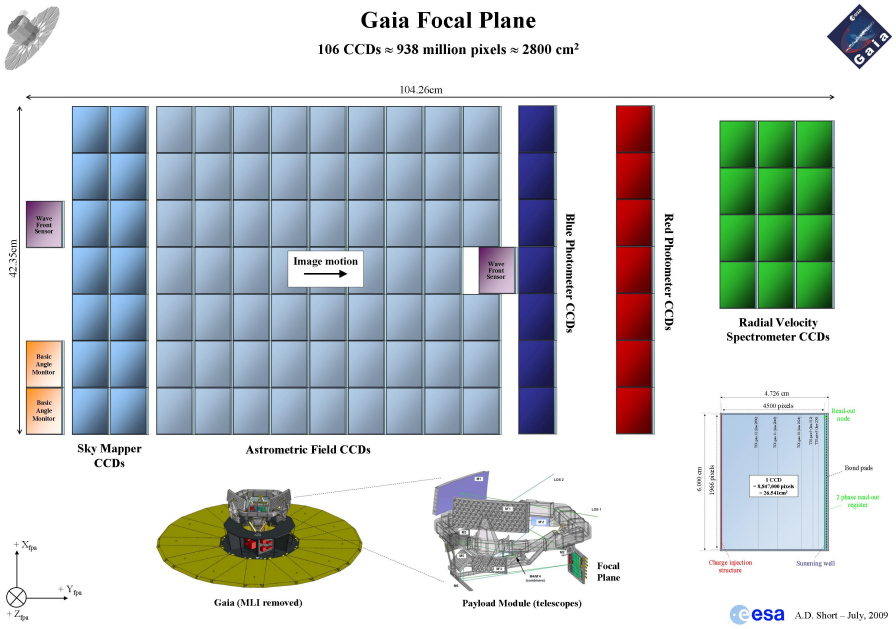

Figure 1.2: Gaia focal plane. In left bottom is illustrated where the focal plane is locate in the payload of the satellite where M1-M6 and M'1-M6 are the the 2 telescopes. In right bottom there are the dimensions of one CCD.

will be observed about 70 times by each photometer. Radial-velocity measurements will be made for stars brighter than 16 mag using the radial-velocity spectrometer (RVS). Its resolution (R 11, 500/7500) and wavelength range (847-874 nm) have been optimised to allow radial velocities to be measured, with a range of 1-10 km/s depending on spectral type and magnitude, for a wide range of spectral classes. It covers the Ca II triplet, which is strong for most intermediate to late type stars, as well as the hydrogen lines dominating the early type spectra, and many weaker lines of various species. For a given object there will be on average 40 transits across the three rows of CCDs used by the RVS.

1.2.1 Astrometry

Astrometry provides the only reliable way to measure distances in the local Universe. Gaia space astrometry mission is aimed to perfom global measurements. In this way the positions and change in positions are determined in a reference system defined over the whole sky. Hipparcos demonstrated that this can be achieved with mas accuracy with a continuously scanning observing two directions simultaneously. As described in the previous sections, this solution had been adopted for Gaia.

One challenging aspect of the Gaia mission is precisely how to build the catalogue of astrometric parameters from such elementary measurements. The image of each star will pass many times through the focal plane. In order to build the celestial map with the required accuracy (a few microarcsec, μas), it is necessary to recover the attitude of the spacecraft and calibrate the instruments to the same accuracy. The attitude is related

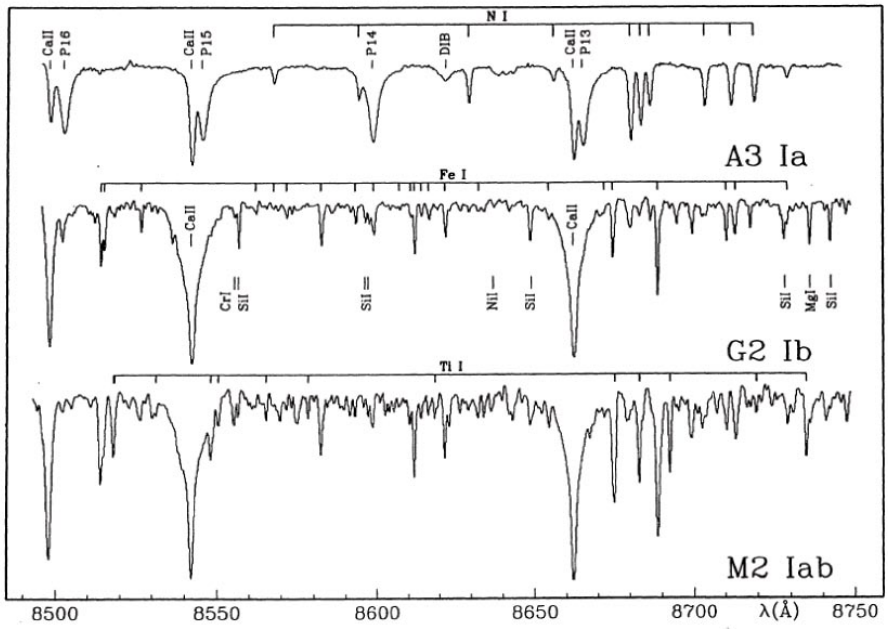

Figure 1.3: CaII triplet region for different spectral types (Munari, 1999)

	B1V	G2V	M6V
$V - I_c[mag]$	-0.22	0.75	3.85
Bright stars	5-14 μ as(6 mag<V<12 mag)	5-14 μ as (6 mag < V < 12 mag)	5-14 μ as (8 mag < V < 14 mag)
V = 15 mag	26 μ as	24 μ as	9 μas
V = 20 mag	330 μ as	290 μ as	100 μ as

Table 1.1: End of mission standard errors on the parallaxes averaged over the sky for an uniform distribution, for unreddened stars

to the orientation of the satellite and its rotation state. Currently the model implements the following effects: a copy of the on-board AOCS (Attitude and Orbit Control System) algorithms, thruster performance, torque due to the solar radiation pressure on the Deployable Solar Array, thermal infra-red emission from the surface of Gaia, impact of micro-meteoroids, clanks (discontinuities in the attitude). The global solution can only be achieved by considering the strong interconnection between all the unknowns throughout all the observations. Effectively it means that all the data must be treated together in a single solution, which makes this task computationally difficult. In the core astrometric solution all the calibration, attitude and primary source parameters must therefore be adjusted to fit all the measurements as best as possible. From a mathematical point of view the adjustment can be understood as a least squares problem. The astrometric solution links the astrometric parameters (the positions, parallaxes and proper motions) of the different sources by means of elementary measurements in the focal plane of Gaia.

These measurements, which thus form the main input to the astrometric solution, consist of the precisely estimated times when the centres of the star images cross over designated points on the CCDs. They are the product of a complex processing task, known as the initial data treatment. Table 1.1 gives the expected performances of Gaia on parallaxes at the end of mission, averaged over the sky, for unreddened stars as a function of magnitude and spectral type.

1.2.2 Photometry

The goal of the BP/RP photometric instrument is to measure the spectral energy distribution of all observed objects to allow on-ground corrections of image centroids measured in the main astrometric field for systematic chromatic shifts caused by aberrations. Besides the positional and kinematical information (position, parallax, proper motion, and radial velocity), Gaia will provide the spectral energy distribution of every object sampled by the dedicated spectrophotometric instrument that will provide low-resolution spectra in the blue and red. Gaia will yield G-magnitudes that will be monitored through the mission for variability. The integrated flux of the low-resolution BP (blue photometer) and RP (red photometer) spectra yield GBP and GRP-magnitudes as two broad passbands in the ranges 330680 nm and 640-1000 nm, respectively. As already discussed, the radial velocity instrument will disperse the light in the range 847874 nm (region of the CaII triplet) and the integrated flux of the resulting spectrum can be seen as measured with a photometric narrow band yielding GRVS magnitudes. In addition, these photometric observations will allow the classification of the sources by deriving the astrophysical parameters, such as effective temperature, gravity, and chemical composition for the all stars. The spectral resolution is a function of wavelength and varies in BP from 4 to 32 nm pixel-1 covering the wavelength range 330-680 nm. In RP, the wavelength range is 640-1000 nm with a resolution of 7 to 15 nm pixel-1.

1.2.3 Radial velocity

Gaia is essentially an astrometric mission. But this kind of measurements supply only two components of space motion of the target. The third component is the radial velocity. This type of information is important for kinematical and dynamical studies. Measurements of radial velocity is a powerful method to detect and characterize multiple system and it is important to give a 3D space motion for the observed targets observated. The accuracy depend strongly on the brightness of target. To maximize the radial velocity signal is used the region where is the Ca II triplet near 860 nm. The selected wavelength region is close to the peak of the energy distributions of the RVS' most numerous targets, G-K type stars. In addition, the extinction in the red domain is roughly a factor of two smaller than in the V band. This will allow the probing of the Galactic disk over greater distances than would be feasible at 5500 $\mathring{A}$. In Fig 1.3 we show the spectra of A, G, M supergiants with identification of some of the strongest lines. Sequences of NI, FeI and TiI absorption characterize the A, G, M spectra, respectively. CaII lines become visible at B8 and dominate throughout the M stars, while the Pashen lines disappear at $\sim$ F8. This allows the measurement of radial velocities even at very low signal-to-noise ratios

(i.e. $\sigma_{V_r} \sim 15$ kms^{-1} at S/N ~ 1 per pixel for a K1 V type star) as well as in very metal-poor stars. Although the strength of the triplet lines decrease with increasing gravity, it nevertheless remains very strong in dwarf stars: their equivalent widths are larger than 3 $\AA$ for stars of spectral type F8 V to M6 V. The triplet is non-resonant and therefore will not be affected by contributions from the interstellar medium (Munari 1999) In early type stars, this spectral region is dominated by lines of the Hydrogen Paschen series, whose equivalent widths are strongly anti-correlated with gravity. The Paschen lines are visible even in very rapidly rotating stars. The spectra of hot stars also exibit some other strong (e.g. Ca II, N I) and weak (e.g. He I, He II) lines.

1.3 Gaia Science goals

The first objective of Gaia mission is the study of the Galaxy. The mission will derive the astrophysical parameters, the kinematics and distribution of stars over a large fraction of its volume. These information will allow to reconstruct the evolutionary history of the Galaxy, but also to test the stellar evolutionary models. A summary of the Gaia science case can be found in ESA-SCI(2000)4 to whom we refer for more detail and references. Among the scientific Objectives of the Gaia mission, we would like to recall :

- **Galactic structure**

  The most credited scenario for the formation of the Milky Way stands on the initial collapse of Baryonic Matter into the potential well of Dark Matter (Eggen et al., 1962). The cosmological framework, the Λ cold dark matter (CDM) paradigm, broadly describes from first principles how structures in the Universe have evolved (Springel et al., 2006). In this model, galaxies form hierarchically, through the amalgamation of smaller proto-systems made of either stars or gas (Searle and Zinn, 1978). In this context, the Milky Way grew around a central body (most likely the Bulge) and accreting matter in later epochs formed the external Halo and the disc (Gilmore and Wyse, 2001). Despite the many successes of this theory, particularly on large scales, we do not yet understand in detail how galaxies form. Many of the shortcomings of this model have become evident through comparisons to the properties of our Galaxy and its nearest neighbors (the missing satellites problem,(Klypin et al., 1999), (Moore et al., 1999). Therefore, it becomes clear that studies of the Galaxy and its components are crucial for a proper and complete understanding of galaxy evolution in the Universe as (Eggen et al., 1962) nicely put it: '... a study of these subsystems allows us partially to reconstruct the Galactic past because the time required for stars in the Galactic system to exchange their energies and momenta is very long compared with the age of the Galaxy. Hence knowledge of the present energy and momenta of individual objects tells us something of the initial dynamic conditions under which they were formed'. The Milky Way is a spiral galaxy with three principle parts: the disk, the bulge and the halo (see Fig. 1.4).

- **The halo**

  The halo is a spherical region surrounding the entire galaxy. Kinematic analysis on Blue Horizontal-Branch (Xue et al., 2008) at 60 kpc from galactic centre provides

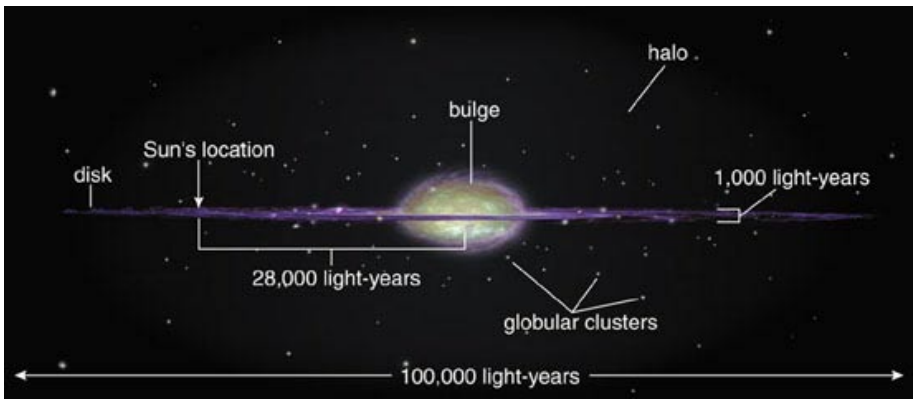

Figure 1.4: The MW components

a mass of $4.0 \pm 0.7 \times 10^{11}$ $M_{\odot}$. Recent studies (Carollo et al., 2007) suggest that the halo structure might be formed by two parts: stellar one and dark one. The stellar halo has a inner region, characterized by stars with metallicity [Fe/H]=-1.6, and an outer region with a metallicity [Fe/H]=-2.2. The most metal-poor stars in the Galaxy and possibly some of the oldest ones are found in the halo. It therefore provides us with a picture of the Milky Way in its early stages of evolution. Low-mass stars live for much longer than the present age of the Universe, and so retain in their atmospheres a record of the chemical elements of the environment in which they were born. The very metal-poor halo stars are thus fossils, whose chemical abundance and motions contain information of their sites of origin (Helmi, 2008). The structure of the stellar halo is intimately linked to how the Galaxy formed (Freeman and Bland-Hawthorn, 2002). Different scenarios predict different shapes and correlations with properties such as age, metallicity, etc. In the simplest case, the structure of the stellar halo could also give us insight into the structure of the dark matter halo. If a significant fraction of the dark matter had been baryonic (composed by MACHOs,(Paczynski, 1986)), then the stellar and dark halos would presumably be indistinguishable. However, this scenario appears unlikely, as the microlensing surveys are unable to assign more than 8% of the matter to compact dark objects (Tisserand et al., 2007).

- **The disks**

  The disks of spiral galaxies contain a substantial fraction of their baryonic matter and angular momentum. Much of the evolutionary activity in these galaxies, such as the formation of stars, takes place in the disks and these are the most prominent parts of late-type spiral galaxies. The disk of our own Milky Way Galaxy shows several arms with a spiral structure and its thickness is about 300 pc, its diameter is about 50 kpc and is formed by population I stars, open clusters and regions of star formation. The arms are the prominent part because there are the most luminous stars of entire galaxy itself. Quantitative surface photometry of disk Galaxy to study their structure and luminosity distributions shows the exponential nature of the radial surface brightness distributions of disk itself, that is observated also

in other spiral galaxy (van der Kruit and Freeman, 2011). Within the disk the star formation history was studied first in our Galaxy in the solar neighborhood. The stellar initial mass function IMF (the statistical distribution of stellar masses during star formation) was derived first by (Salpeter, 1959). Studies of the chemical evolution in the Galaxy identified the presence of a chemical radial gradient, very important for our understandings of formation and evolution scenario of Milky Way.

- **The bulge**

  The bulge is the spheroidal region at the centre of the Milky Way with a mass of 1.8×10^{10} $M_\odot$ (Sofue et al., 2009). There is a very hight density of population II stars and a black hole of about 2.6×10^6 $M_\odot$ (Melia and Falcke, 2001). The observations toward the bulge are limited by interstellar medium of the arms and they are possible only in particular regions. The nature of the bulge is matter of discussion, since it is unclear whether there is a classical bulge formed by collapse of the primordial matter, a pseudo-bulge/bar formed by secular evolution of the disk (see Zoccali et al 2010 for a review).

  How to probe and/or this model? If mergers/captures had such an important role, we must find the fossil relics of those events (such as age,metallicity, velocity differences and streaming motions) and determine the age at which they occurred. To this aim, the analysis of colour-magnitude diagrams, luminosity functions, chemical abundances for large samples of stars belonging to different Stellar Populations must be combined with that of kinematics and dynamics. It is worth recalling here that after GAIA (Perryman et al 1991), for a billion of stars brighter than V=20 the space velocity vectors, the distance, the temperature, gravity and metallicity will be known with high accuracy. Therefore, the direct determination of the 6D phase space distribution as well as of the chemical abundance of large and complete samples of objects will make it possible to interpret coherently the evolutionary scenarios of the whole Milky Way (Gilmore et al., 1989).

- **Stellar evolution: open clusters**

  Open clusters (OCs) are dynamically bound groups of stars that formed from the same giant molecular cloud, having a similar age and bulk chemical composition. The OC family includes loose SF regions with as few as 10 stars, up to super star clusters with $10^5 - 10^6$ members. OCs in the MW trace the young, intermediate-age, and old thin disc components; their ages cover the entire lifespan of the Galactic thin disc. The majority of the objects are younger than 1 Gyr, and only a few are as old as 8-10 Gyr. Although their metallicity is usually considered as solar, they span the range $-0.5 < [Fe/H] < +0.5$. OCs may be the dominant source of field stars. Gaia will make a complete census of OCs up to 5 kpc from the Sun, observing all known OCs and discovering a quantity of new ones. Distances and proper motions of individual stars will be derived with a precision of 1% for the OCs up to a distance of 1.5 kpc and of 10% for almost all known clusters, leading to an accurate and reliable definition of membership even for the most distant objects. OCs play a major role in studies of formation and evolution of stars and the Milky Way and the data on the OCs at

a wide range of Galactocentric radii (RGC), and with a large range of ages trace the formation process of the disk (Rosales-Ortega et al., 2010). The rates of OC loss of stars due to internal mechanisms or to interaction with the environment as a function of age can be used to trace the history of field star populations (de Grijs, 2010). OCs of different ages and RGC also reveal information on the abundance distribution in the thin disc, the radial gradient in particular, and on its evolution with time (Bragaglia and Tosi, 2006), (Molla et al., 1997), (Portinari and Chiosi, 1999), (Hou et al., 2000), (Chiappini et al., 1997),(Chiappini et al., 2001). Since the members are coeval, they have the same chemical composition as parental cloud, they share the same space motion to within the internal velocity dispersion of cluster and are distributed across the whole mass spectrum, depending on the cluster age. OCs are a perfect laboratory to study the stellar evolution. Using OCs, the H-R diagram will be calibrated, including all phases of stellar evolution, from pre-main sequence stars to white dwarfs and the existing transient phases and all possible masses from brown dwarfs to the most massive O stars. This kind of information is very important to understand the stellar evolution (Maeder and Meynet, 2000). The agreement between predicted and observed properties of stars remained qualitative due to the modest accuracy and relative scarcity of relevant observed quantities. The development of accurate astrometry with Hipparcos and high-resolution and high signal-to-noise ratio spectroscopy has allowed major progress in this area. The global stellar parameters used in the field of stellar structure and evolution will be obtained by Gaia. The stellar absolute luminosity is derived from parallax and apparent magnitude, corrected for extinction, which can be deduced from Gaia photometric and spectroscopic data. These also provide the effective temperature Teff, metallicity,the projected rotational velocity of stars $Vsini$ which can be directly compared with the predictions of the stellar models. Ages can be inferred from location of stars in the H-R diagram. These systems are important to understand the process of stellar formation.

- **Binary and multiple stars**

  The RVS will provide the radial velocities of about 100-150 million stars up to V=16 mag with a precision from 15 km/s at the faint end to 1 km/s (or better) at the bright end. The RVS will collect, on average, around 40 (transit) spectra per star over the 5 years of the mission. The associated multi-epoch radial velocity information will be ideally suited for identification and characterization of double and multiple systems for the brightest stars. In particular, Gaia will provide masses and radii accurate to a few per cent for thousands of eclipsing binaries. For those objects, the masses can be measured .The large number of this kind of systems, a few per cent for thousands of eclipsing binaries (Munari et al., 2004), for which mass will be measured by Gaia, will be used to validate stellar models, providing a better knowledge of the mass-luminosity relation

- **Extra-solar planets**

  Gaia will also make a systematic census of giant planets, providing insights into the frequency of giant planets as a function of the characteristics of their host stars and

their locations in the Galaxy. This will give unique information about the conditions favouring the formation of planets. Since the presence and location of one or several giant planets may severely affect the formation of smaller planets in a system, Gaia will provide important information on the likelihood of finding Earth-like planets orbiting their stars in the habitable zone (Rambaux et al., 2009).

- **Local group**

  Gaia will make a unique contributions to extragalactic astronomy, for example addressing the structure, dynamics and stellar populations in the Magellanic Clouds, M31 and M33. Even if a parallax accuracy better than 10 % cannot be derived for stars beyond 10 kpc, proper motions of individual giants and super giants in LMC and SMC will be accurate enough to allow to discriminate between the member and field stars and to derive the LMC and SMC space motions (Gilmore, 2002)(Kucinskas et al., 2005).

1.4 Gaia DPAC structure

The Gaia project is the result of a large and complex collaboration between many individuals, teams, and organizations. The consortium (DPAC) is divided into 9 units known as Coordination Units (CUs). These are the building blocks of DPAC, with each unit assigned a unique set of processing tasks. Scientists from ESA Member States in the Gaia Data Processing and Analysis Consortium will develop the procedures for the acquisition and analysis of data, and will produce the final catalogue. Gaia mission will yield an immense numbers of data for the observed objects, like positions and velocity. The role of the 9 CUs can be summarized as follows:

- CU1 System architecture: it takes the lead in helping the DPAC define the overall system processing philosophy, architecture and strategy.
- CU2 Data simulations: it has the responsibility to cover the simulation needs for the work of other CUs, ensuring that reliable data simulations are available for the various stages of the data processing development.
- CU3 Core processing: it covers the entire processing chain going from the raw telemetry to the astrometric core solution.
- CU4 Object processing: it will process all ill-behaved objects which pop up in CU3, CU5, or CU6 data reduction.
- CU5 Photometric processing: it provides the processed photometric data, as well as a number of related tasks, namely the PSF/LSF and CTI calibration for Astrometric Field/Sky Mapper and Blue Photometer/Red Photometer, the source environment analysis and photometric science alerts.
- CU6 Spectroscopic reduction: it will be in charge of the ground-based processing and analysis of the Gaia spectroscopic data, the data obtained with the Radial Velocity Spectrometer.

- CU7 Variability processing: it is in charge of detecting and studying the photometric and spectral variability.
- CU8 Astrophysical parameters: is responsible for "classification" tasks (see below).
- CU9 Catalogue: preparation of the final Gaia Catalog including all the objects, their astrometry, and APs and related errors.

1.5 CU8: Classification

As explained in the previous section, CU8 tasks concern the classification of Gaia objects. These tasks use fully calibrated photometry, spectroscopy and astrometry to classify objects and estimate their astrophysical parameters. As Gaia performs real time detection, the intrinsic properties of most of the objects that are entering in the Gaia's fields of view will not be known. Gaia will make use of the GSC2 as input Catalog, in the first passage, mainly to identify bright stars. The first part of the Gaia data processing requires classifying everything observed. If we consider the amount of data that Gaia will collect, we can conclude that the data processing clearly requires automated classification and parameterization methods for the detected sources.

In the Gaia project, the classification algorithms are base on both supervised and unsupervised methods (see (Smith et al., 2008)), first producing a discrete classification of the objects, i.e. dividing objects having higher probability of being stars, galaxies, and QSOs, then estimating the astrophysical parameters of all the stars and at some extent also of the galaxies, by comparison with a set of templates. Finally, the treatment of the outliers will rely on unsupervised methods.

The main objectives of the classification are:

• Discrete classification. Determination of whether an object is a star, galaxy, quasar or asteroid etc. The primary goal of Gaia classification is related to the QSO detection, which is fundamental to build the astrometric reference frame. Present QSOs catalogs are mainly based on radio positions. Their accuracy is not sufficient to calibrate Gaia astrometry. Instead, the large number of quasars observed by Gaia over the whole sky will define its own reference frame (Bailer-Jones et al., 2008). Thus, it is fundamental to identify a clean sample of Quasars. Gaia mission will allow a realization of the International Celestial Reference System (ICRS) based on optical detection and more accurate by two or three orders of magnitude than the present system.

• Estimation of Astrophysical Parameters(APs). For those objects identified as stars, it determines the intrinsic astrophysical properties. The relevant (and obtainable) ones are effective temperature, Teff, surface gravity, logg, metallicity, [Fe/H], and line-of-sight interstellar extinction, Av. Although this last one is of course not intrinsic to the star, we would ideally determine it on a star-by-star basis, so we can consider it as such. The summarized information of the astrophysical parameter precisions can be found in Tab. 1.2.

• Identification of unresolved binaries. Most stars are in multiple systems. Some of these can be recognized from the astrometry, and a few will be visual binaries, but most will go undetected in this way. Nonetheless, with favourable brightness ratios, a binary could be detected from the shape of its composite spectral energy distribution.

	Instrument	V[Mag]	Accuracy
Effective Temperature	BP/Rp	16	1% to 5%
Surface Gravity	BP/RP	16	0.1 to 0.4 dex
Metallicity	BP/RP	16	$\sim$ 0.2 dex
Extinction	RVS	Hot stars	0.05 to 0.1 mag

Table 1.2: Expected precision of astrophysical parameters

• Identification of new types of objects. As a major survey, Gaia must be open to the prospect of detecting new types of objects. This includes new types of variable stars, rare stars (e.g. brief phases of stellar evolution), abnormal abundance patterns or multiple systems.

Supervised classification methods will be used for all the object classes, but the last one. Supervised methods which are commonly used for determining stellar parameters from spectra, are generally forced to classify new types of objects into pre-existing classes. New objects would therefore go undetected (and samples of known types of objects would be contaminated). Thus special attention, including the use of unsupervised methods, is required to deal with this.

•. Determination of the mass and age of the single stars (FLAMES), using a comparison with a set of theoretical models.

1.6 The Importance of accurate stellar models for Gaia

The age and mass determination of the Gaia stars (FLAMES) has a fundamental importance in order to study the formation and evolution of the various Galactic populations. Due to the high accuracy of Gaia data, to interpret them it is necessary to have stellar models of comparable accuracy.

In spite of the progresses of the stellar evolution in the recent past, still several open problems remain. In particular we can mention the mixing in the stellar interiors (Charbonnel and Talon, 2008), (Gratton et al., 2000) (Smiljanic et al., 2009), the rotation, the magnetic fields. All those effects significantly influence the stellar magnitudes, lifetimes, burning phase duration and need to be calibrated comparing models with observations (Chiosi, 2009). The observational input data for such exercise will, however, require good photometric and spectroscopic data, as well as very reliable cluster-membership determinations. The Gaia astrometric data will provide large samples of very high probability cluster members for several tens of nearby clusters, covering wide ranges of spectral types. These data should then be compared with theoretical isochrones prepared for similar chemical compositions and ages, and differences between the theoretical and observed isochrones can then be explored further for refinements of the models underlying the theoretical isochrones. This should ultimately lead to a significant improvement in the reliability of those models and their application in various fields, such as providing age

estimates for field stars. The observations required will sample the cluster population, for a wide range of OCs in age and chemical composition.

There has been a great effort inside the Gaia community to provide new up-to date stellar models. A complete set of stellar models at changing He content, and chemical abundances was calculated by Padova Group (Bertelli et al., 2010)(Bertelli et al., 2009). However those models do not include stellar rotation, which can be critical to derive age and mass of the stars, even in the intermediate mass domain. Stellar models including rotation and their tests using open clusters, will be of great importance in view of the interpretation of Gaia data. This will be discussed in the next Chapter.

Chapter 2

Rotation in stars

In this Chapter we summarize the main effects of the rotation on low mass stars, during the pre-MS and MS phase. Finally we will discuss the rotationally induced mixing and the von Zeipel effect, due to the deviation from the spherical symmetry of the stellar surface.

2.1 Low mass stars PMS and MS evolution

Rotation is an important parameter for solar-like stars ($0.8 < M / M_{\odot} < 2.5$). Looking at the distribution of rotation periods and $Vsini$ distribution in clusters, some model-independent conclusions can be derived. The behavior of the stars on the Pre-main sequence (which is of the order of 30 Myr for a 1 $M_{\odot}$stars) and on the MS up to the age of the Hyades is strongly depending on the rotation rate. The slowest rotators in the ONC have a period of 10 days. If the angular momentum is conserved in the contraction of the star toward the MS, then the star should spin up. However, looking at the for these slowly-rotating stars, the period remains approximately constant until the age of NGC 2362 (5 Myr) is reached (Miller et al., 2008), and then going to the order of 8 days by the age of NGC 2547 ($\sim$ 40 Myr) (Irwin et al., 2008), when the contraction ceases . In the case of the fastest rotators , the period is going from 1 day at the age of the ONC, to 0.6 days at the age of NGC 2362 (5 Myr), and finally to 0.2 days for NGC 2547. It is clear that there is some mechanism removing the angular momentum only from the slow rotators for about 5-10 Myr (see (Irwin and Bouvier, 2009) for a review). This process result in a wide range of rotation rates in the early-MS clusters such as the Pleiades and M35. By the age of the Hyades only a single well defined sequence of rotation rate is present (Radick et al., 1987). This process is well underway by the age of M37 ($\sim$ 485 Myr). Clearly, another rotation-rate-dependent angular momentum loss mechanism is at work on the early-MS, such that more rapid rotators lose more angular momentum, to drive all the stars toward the same rotation rate between 100-600 My. The behavior of stars of masses below 0.8 $M_{\odot}$is completely different, but it will not be discussed here. Summarizing, two main mechanisms remove the angular momentum for stars of masses below 2-3 $M_{\odot}$: the first is operating for 5-10 Myr on the PMS, and the second one is at work on the main Sequence. Stars appear at the deuterium-burning birthline (Stahler, 1988) with a range of rotation rates, typically well below that expected

for accretion from a Keplerian disk. During the pre-main sequence phase, the interaction with a circumstellar disc drains angular momentum from the star, thus delaying its spin up for the duration of the disc lifetime. The process is not well understood yet (see,e.g., (Shu et al., 1994) (Matt et al., 2010), going from accretion-driven stellar wind (e.g. (Matt and Pudritz, 2005)), or disc locking (e.g. (Collier Cameron et al., 1995)). The disk lifetime is variable, and thus the stars will be released from this angular velocity regulation at a range of times, giving rise to a spread of rotation rates on the PMS and ZAMS. Moreover, examining early-PMS clusters show us a snapshot of this process in action. This result in a twofold distribution of the rotation periods of the stars in young OCs, being the fast rotators without disk or having recently dissipated disks. Observations of open clusters show that coeval stars of the same mass are born with a range of rotation rates (e.g. (Attridge and Herbst, 1992)). However, the majority of young stars arrive on the main sequence as slow rotators ((Stauffer et al., 1989) and (Hartman et al., 2010)). Much observational work has been invested in the study of star-disk coupling, with a diversity of results largely centered around the proper choice of disk proxies and disentangling evolutionary effects. Recently Spitzer studies (Rebull et al., 2006) have pointed in favour of a relationship between rotation and the presence of disks. This may reflect a coupling between the protostar and accretion disk .

Once on the main sequence, the rotational evolution is driven by the loss of angular momentum through a magnetised stellar wind (Weber and Davis, 1967), (Kawaler, 1988),(Chaboyer et al., 1995). Finally, a nearly solid-body rotation is established at the age of the Sun (Thompson et al., 2003). This mechanism is however not completely understood. The time dependence of rotation rates in this age range has been established observationally for solar type stars from the age of the Hyades to the Sun, and for the majority of the stars from the ages of the Pleiades to the age of the Hyades, as being the the famous Skumanich (1972) t1/2 law (i.e $\omega \sim t^{1/2}$).

Several models including stellar rotation are presented in literature. After the pioneering work by (Endal and Sofia, 1978, Pinsonneault et al., 1989), we quote among the others (Irwin et al., 2007), (Ekström et al., 2012). Recently the large amount of data on $Vsini$ and rotation periods of the stars are given the possibility to test the stellar models. Vega is probably the best example: its rotational velocity has been ignored during all the 20th centuries, until recent interferometric measurements revealing its oblateness and its V_{rot} estimate with very high resolved spectrograph (Aufdenberg et al., 2006). Nonetheless, it is particularly crucial to take into account the rotation of the stars to study the HR diagram of a population like those of open clusters, the effect of the rotation on the mixing and the luminosity of stars being significant for low mass stars masses in the determination of ages and masses on the HR diagram (Maeder, 1998).

2.2 Rotation in the stellar models

The role of rotation has an important role in the theory of stellar structure and evolution. (von Zeipel, 1924) first discussed the importance of the rotation on the evolution of a star. (Kraft, 1965) presents the effect of the rotation on the HR diagram of c_1, the Balmer discontinuity index as a function of the b-y Strömgrem index (2.1). The differences between

the case of non-rotating star and the case of pole-on rotation, edge-on rotation and extreme rotation are greater in the region of greater c_1. The different view angle of the stars results in a different location in the HR diagram. A spread in the view angle of the stars produces a broadening of the MS.

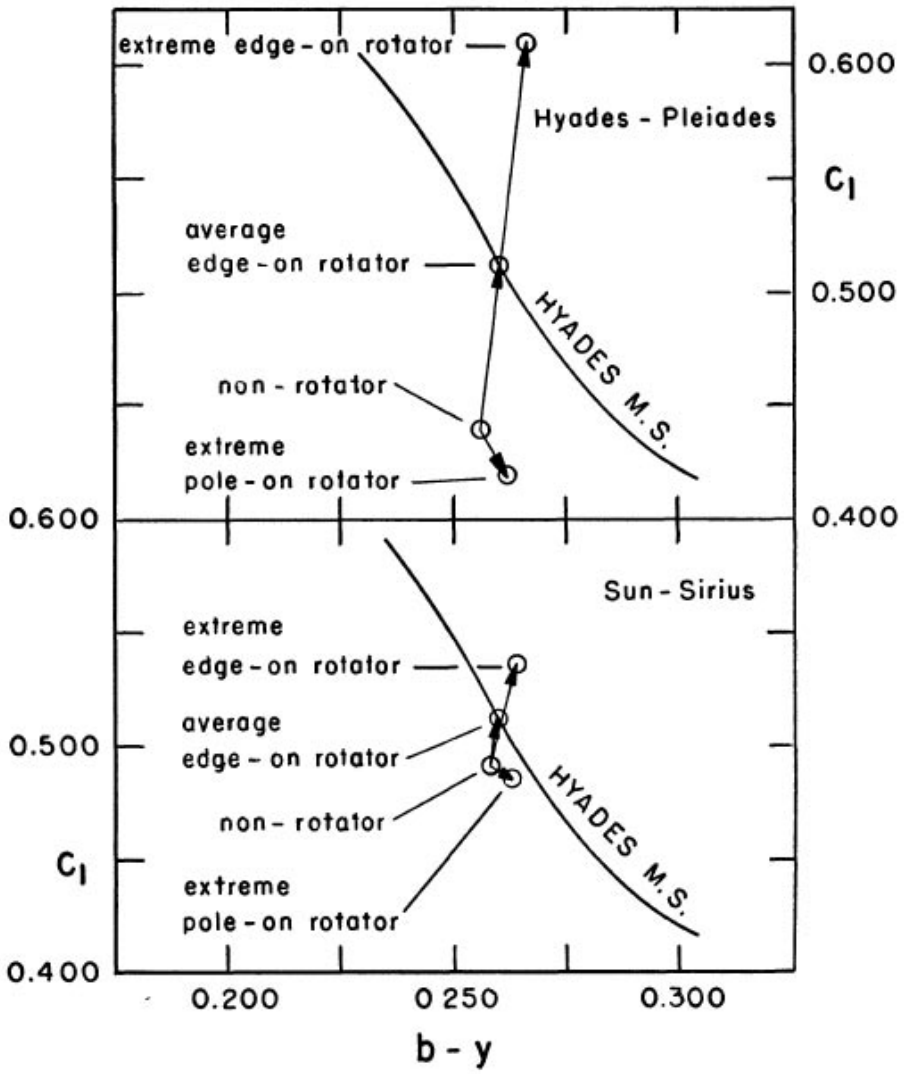

Figure 2.1: In this graphic c_1, the Balmer discontinuity index, b-y, the Strömgrem-Crawford colour index, made a first reflection on the braodening due to the inclination of rotation angle, non-rotation case and extreme rotation case. The different view angles of the stars result in a different position in the HR diagram. The main sequence location is compared with the observational MS of the Hyades.

Due to the increase in spatial resolution and photometric accuracy, colour-magnitude diagrams (CMDs) of star clusters have become accutae in recent years and the broadening is more evident. In (Bastian and de Mink, 2009) we can see how the shape of the observed

CMD of an intermediate-age (around 1-2 Gyr) cluster is affected by rotation. As we can see in the figure (2.2), the isochrones don't fit the CMDs because the broadening due to the effect of rotation. The broadening can also arise from a bimodal velocity distribution, including the presence of slow and fast rotators in the same cluster.

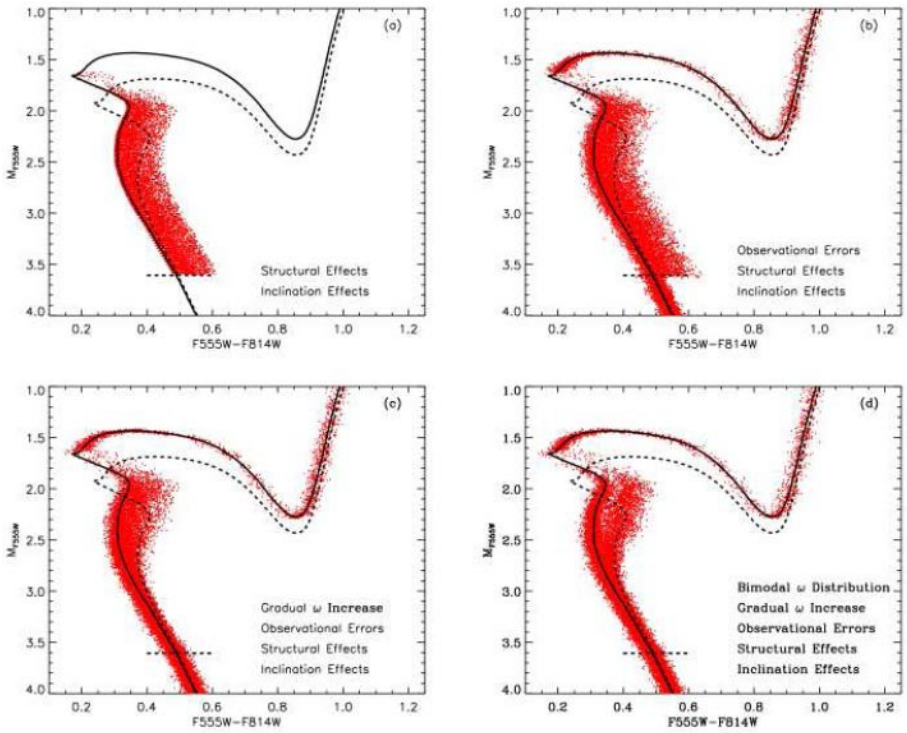

Figure 2.2: Simulated CMDs including the effects of rotation. The isochrone for an age of 1.25 Gyr is shown as a solid line. In each panel the effects that are included in the simulation are given. In the x axis there is F555W and F814W colour of HST and in the y axis there are the magnitude of these colour, assuming metallicity of Z=0.008.

This behavior is evident in the observational Hyades HR diagram of the Hyades(Gaige, 1993), figure (2.3) where two group of stars having low and rapid rotation are clearly separated in temperature

However, the rotational velocity has a critical value for each star mass listed in 2.1. This means that the broadening on the HR diagram is limited from 0 rotational velocity (the cooler part of the HR diagram) to the critial value (the hotter part of the HR diagram).

2.3 Rotational mixing

One of the effect of the rotation is a thermal imbalance that lead to a strong meridional circulation current (Sweet, 1950). The resulting turbolence leads to mixing of angular momentum and chemical composition. But the structure, mixing and angular momentum transport depends on the size of the different zone: convective and radiative zone. The

Initial M	v_{crit}
120	711
85	646
60	623
40	586
25	536
20	513
15	487
12	466
9	439
7	416
5	385
4	365
3	342
2.5	330
2	316
1.5	312

Table 2.1: List of the critical rotational velocity for each stellar mass calculated by Maeder 2009

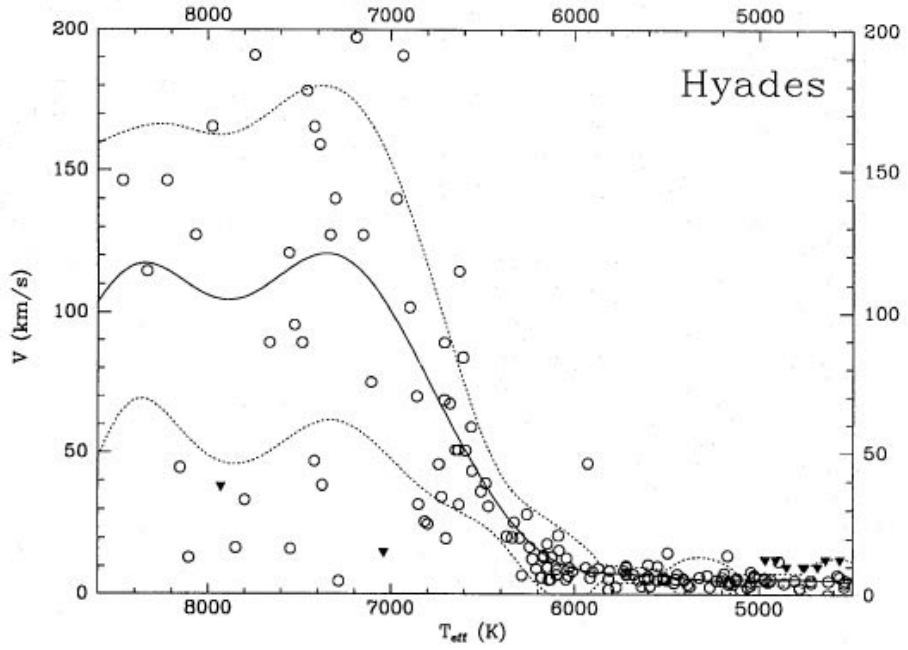

Figure 2.3: The observational Hyades velocity distribution (circles). Theoretical $\bar{v} \pm 1\sigma$ are given respectively by solid and dashed lines. The circles represent the observed $v \sin i$ multiplied by $4/\pi$.

size of those regions depends on the stellar mass and evolutionary status and the rotation rate affect a lot the evolution of a star.

Any model of stellar rotation have to be able to match the observed changes in chemical enrichment and structure. The treatment of rotation and its induced chemical mixing in stars has known many changes in last decades. The centrifugal force caused by rotation affects the hydrostatic balance of the star, effectively reducing the local gravity. On a surface of constant radius the centrifugal force acts more strongly at the equator than the poles. The resulting distortion of stars depends on co-latitude and our assumption of spherical symmetry is no longer valid (von Zeipel, 1924) (see following section). (Tassoul, 1978) shows that the effect of rotational deformation remains axially symmetric, except for stars close to the critical rotation. (Eddington, 1926) pointed out that some mixing occur in stellar radiation zones, in order to prevent the gravitational settling and thermal diffusion of heavier elements, which is not observed always. His suggestion was that the mixing was mediated through the meridian circulation caused by rotation and this remains the accepted explanation. In the standard formulation, (Sweet, 1950)(Mestel, 1953), the meridian flow is calculated assuming a uniform rotation for semplicity and Mestel argued that a weak magnetic field sufficies to keep the rotation nearly uniform. But in the absence of this field the flow advects angular momentum and induces differential rotation. The rotation state must result from the balance between meridian advection and turbolent stresses, since viscosity is far too weak to act on large scale flows (Zahn, 1992). Turbolent motions

are in the inviscid stellar material, due to various instabilities that are produced by differential rotation. The shear instability is invoked (Spiegel and Zahn, 1970)(Zahn, 1974) (Zahn, 1975).

2.4 Von Zeipel effect

The Von Zeipel theorem estabilishes a relation between the radiative flux at some colatidude ϑ on the surface of rotating star and the local effective gravity $g_{eff}(\Omega, \vartheta)$, as a function of the angular velocity Ω and ϑ. In a solid body rotating star, the equipotentials and isobars coincide: they are surfaces of constant T temperature and ϱ density. The formula giving the Von Zeipel effect for a star of total mass M and luminosity L is:

$$F(\Omega, \vartheta) = -\frac{L}{4\pi G M^*} g_{eff}(\Omega, \vartheta) \tag{2.1}$$

where

$$M^* = M(1 - \frac{\Omega^2}{2\pi G \bar{\varrho}_M}) \tag{2.2}$$

and

$$g_{eff} = [(-\frac{GM}{R^2(\vartheta)} + \Omega^2 R(\vartheta) \sin^2 \vartheta)^2 + \Omega^4 R^2 (\vartheta \sin^2 \vartheta \cos^2 \vartheta)]^{\frac{1}{2}} \tag{2.3}$$

in which ϱ_M is the average stellar density. The relation 2.1 shows that the radiative flux at the surface of a rotating star is proportional to the local effective gravity at the considered colatitude(Maeder, 2009). From the 2.3 and 2.1 it is possible to obtain the local effective temperature at this colatitude

$$T_{eff}(\Omega, \vartheta) = (\frac{L}{4\pi G M^*})^{\frac{1}{4}} [g_{eff}(\Omega, \vartheta)]^{\frac{1}{4}} \tag{2.4}$$

Both g_{eff} and T_{eff} vary over the surface of rotating star and influence the emergent spectrum. In the 2.4 we can see the differences between the case of non-rotating system (angular momentum $j = 0$) and the case of rotating star ($j \neq 0$): while the spherical simmetry is broken, the axial simmetry remains far to the critical velocity.

This effect was measured by means of interferometric observations for Vega. (Aufdenberg et al., 200 present the results from the analysis of CHARA infrared K' band (1.94-2.34 μm) on Vega. This star has been used like a photometric standard. But Vega show anomalous properties. The suggestion that Vega is rapidly rotating was first advanced by (Gray, 1985)(Gray, 1988), who noted that Vega is pole-on and rotating at 90 % of its angular break-up rate to account for its apparent luminosity.(Aufdenberg et al., 2006) measurements show that the Roche-von Zeipel model is in agreement with the observations and the equatorial velocity of Vega is 270 ± 15 km/s. Improvement on the Roche model for the flattening of star in critical rotation regime, like Achenar (αEri), are made in (Zahn et al., 2010). For this 7 $M_\odot$star, the data were simulated using a linear perturbation method treating the quadrupolar moment as a small quantity. This assumption is justified in the case of massive MS stars, because these are sufficiently centrally condensed.

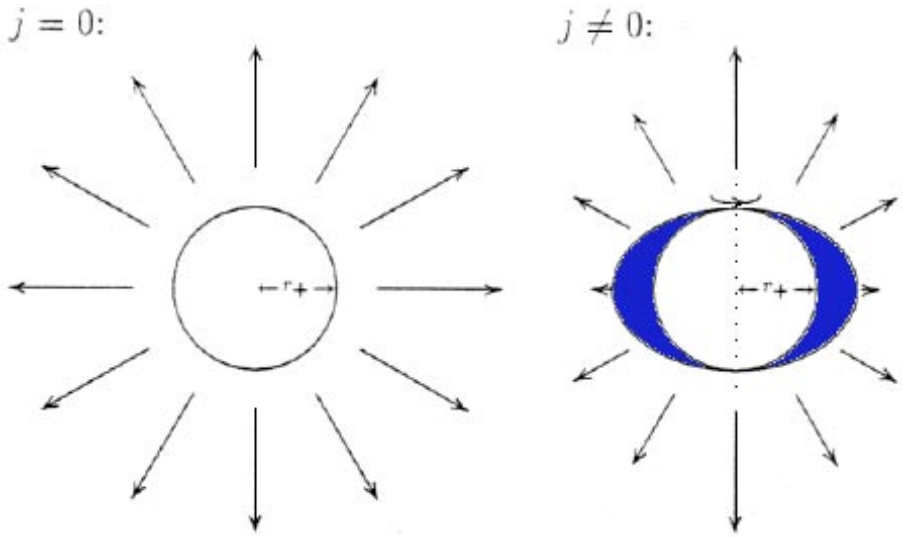

Figure 2.4: The case of non-rotating system (angular momentum $j = 0$) and the case of rotating star ($j \neq 0$). It is possible to see the flattening in the case of rotatinf star and the difference flux that go away from pole and the equator of the star.

Chapter 3

Rotation measurements

As we have seen in previous Chapters, the rotational velocity is a parameter that play a key role in the star evolution: it have influence on mixing, luminosity and temperature of a star. In this chapter we present the observational methods to measure the rotational velocity of a star.

These methods will be discussed in section 3.1 and 3.2. In section 3.3 we discuss the Chandrasekhar-Munch formula to statistical derive information on equatorial rotational velocity of a given cluster under the assumption that we know the distribution of projected rotational velocity. In Section 3.4 we discuss several functional forms of the distribution of projected rotational velocity that were presented in literature, and finally in the section 3.5 we present our choice of this distribution, the Tsallis distribution.

3.1 Rotation measurements

Presently, measurements of the surface rotation velocities or periods provide the best empirical constraints on stellar angular momentum models. Early studies in open clusters measured primarily $Vsini$, while recent determinations have focused on direct measurements of the stellar rotation period from brightness modulations by star spots.

3.2 Photometric measurement

Photometry can be used to measure the rotation period of a late type star. In the case that the star shows surface inhomogenities or hot spots, arising from magnetic activities, it is possible to detect the stellar rotation by analyzing the flux modulation (Messina et al., 2004), (Messina et al., 2010). These type of inhomogeneities are present in late-type stars (see 3.1).

The observed variability is dominated by phenomena that are manifested on different time scale. From the rotation period P we can know the star equatorial velocity V_{eq} from the relation

$$V_{eq} = 2\pi \frac{R}{P} \tag{3.1}$$

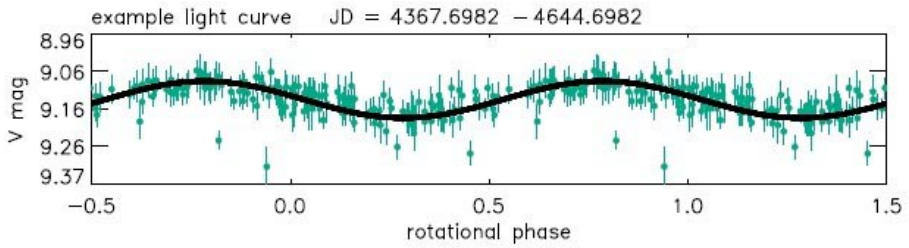

Figure 3.1: Example of light curve from HJD 2444367 with sinusoidal fit (solide line) taken from Messina et al. 2010

We have to know the radius R of star. From interferometry measurements or from theoretical study of colour-magnitude diagram (study of evolutionary tracks) we can have the information on the stellar radius and so the equatorial velocity.

This metod has been widely used in literature (e.g., (Prosser et al., 1995) (Krishnamurthi et al., 1998) (Barnes, 2003) (Irwin et al., 2007) (Meibom et al., 2009) (Hartman et al., 2010). The rotation period is independent of i and only slightly affected by latitudinal differential rotation. Its detection is limited to late type stars with variation of the brightness having amplitudes above a threshold set by the photometric precision and requires uninterrupted observations with a duration of at least twice the number of nights of the longest period one wants to measure. Recently dedicated time-series photometric surveys of cool stars in young open clusters have begun to give very interesting results, pointing in the direction of a mass and time dependences of the stellar rotation (e.g., (Barnes, 2003) (Meibom et al., 2009) (Hartman et al., 2010)).

3.3 Spectroscopic measurement

From the spectroscopy and the analysis of star line profile we can measure the rotational velocity $Vsini$ of each star. The Doppler effect between the various regions of the rotating stellar disk results in broadening of spectral lines. To derive the $Vsini$ the effect of other possible line broadening mechanisms like Zeeman splitting and turbolence need to be taken into account (Abney, 1877); (Benz and Mayor, 1984). $Vsini$ technique , requires a single measurement of the Doppler broadening of spectral lines to produce a result and is useful for stars that rotate faster than a threshold velocity set by the spectral resolution(see the example in 3.2). However, the result has a strong dependence on the unknown stellar radius (R) and spin-axis inclination (i). Direct measurements of the angle i can be derived only in rare case such as multiple system. In general, in a cluster ,statistical methods can be applied to get information about the distribution of i.

For young, magnetically active, spotted late-type stars it is possible to adopt both methods, measuring their period of rotation, P, from rotational modulation of their light curves and their projected equatorial velocity, $vsini$, from spectral line broadening. Using photometric data and an independent measure of distance, it is possible to derive sin i, the sine of the angle between the observer and the spin axis

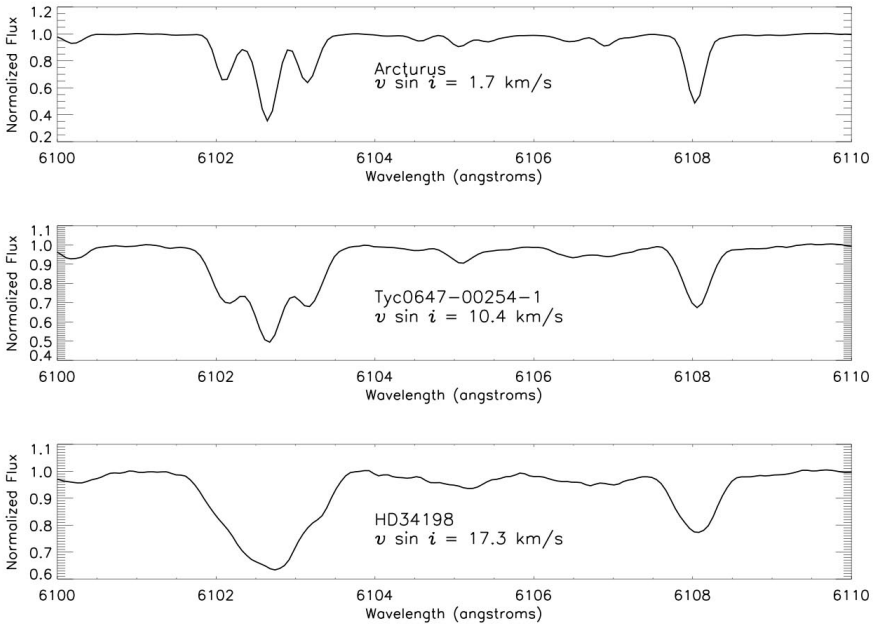

Figure 3.2: Here there is an example taken from Carlberg et al. 2011. The plot show the different line profile for the same range wavelengh for three different stars with projected rotational velocity different: Acturus ($Vsini = 1.7km/s$), Tyc0647-00254-1 ($Vsini = 10.4km/s$), HD34198 ($Vsini = 17.3km/s$).

$$sini = P/(2\pi R) \times (Vsini)$$

where the stellar radius R can be estimated from the surface brightness and distance. However, these observations give no information on the true azimuthal direction of the spin axis. On the other hand, assuming a random inclination of the spin axes, the measurements of $Vsini$ and rotation periods can be combined to determine the distances (Hendry et al., 1993) (Jeffries, 2007a) (Baxter et al., 2009), radii (Jackson et al., 2009) or star formation histories (Jeffries, 2007b) of young clusters.

3.4 Distributions of equatorial rotational velocities

In the following we discuss how a statistical analysis on the distribution of projected stellar rotation $Vsini$ can be used to infer an estimate of equatorial rotational velocity for stars in a cluster. To get information about the distribution of the equatorial velocities from the observational distribution of $Vsini$, we can make use of the the Probability Density Function of the $Vsini$ which is in general, the result of the convolution between the distribution of true equatorial velocities v, the distribution of inclination angles i, and the observational error law.

Under the hypothesis of random i alignment, the relation between the projected rotational velocity y and the true one x (equatorial velocity of star) is

$$y = \frac{x}{\sin i} \tag{3.2}$$

The probability of occurrence of inclination i between i and $i+di$ is $\sin i di$. If we denote $\Phi(y)$ the frequency function of y, it follows that $\Phi(y)dy$ is the surface integral of $f(x)\sin i$ over the area included between the curves (see 3.3) $y = x\sin i$ and $y + ydy = x\sin i$

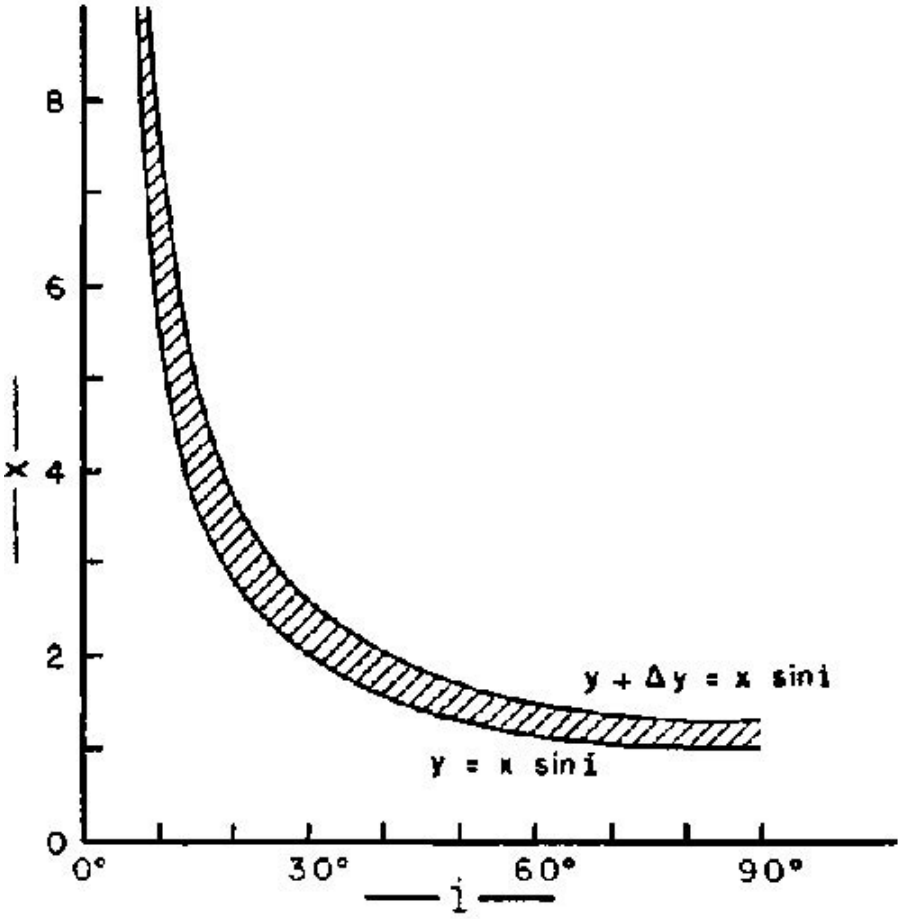

Figure 3.3: The area in the plane x,i where is integrated $f(x)sini$, taken from Chandrasekar & Munch 1950.

Thus we have to resolve the integral

$$\Phi(y)dy = \iint_{\Delta S} f(x)\sin i dx di \tag{3.3}$$

With some algebraic passage, we have the following integral relation

$$\Phi(y) = y\int_y^\infty \frac{f(x)}{x(x^2-y^2)^{1/2}}dx \tag{3.4}$$

We can invert the relation, because we can observe the $\Phi(y)$ from the $V \sin i$ measurement, and we obtain

$$f(y) = -\frac{2}{\pi} x^2 \frac{\delta}{\delta x} x \int_x^\infty \frac{\Phi(x)}{y(y^2 - x^2)^{1/2}} dy \tag{3.5}$$

That is the Chandrasekhar-Munch formula that relates the observational distributions of projected rotational velocity, and the true distribution of the equatorial velocity. This formula is widely used in literature to infer the rotational properties of the stars, and depend on the adopted functional form of $\Phi(y)$.

3.4.1 Rotational axes Distribution

The previous formulation was derived under the assumption of a random distribution of $sini$. In general, the distribution of the rotational axes arises from the fragmentation of the angular momentum of the primordial cloud. It is generally assumed that angular momentum vectors are randomly orientated in a star forming cloud (Struve, 1945). On a theoretical ground , it is not possible to rule out that the star formation leads to a preferred axis of rotation over the scale of a star forming region. This might arise if the gas is forced to collapse along strong, large-scale magnetic fields. This would require a relatively undisturbed collapse, where the effect of the disruption from turbulence or dynamical interactions is not relevant (e.g. (Shu et al., 1987)). There is no clear observational evidence of either process: some studies have suggested preferential spin alignment with the ambient magnetic field (e.g. (Vink et al., 2005)), while others have found no evidence of it (Ménard and Duchêne, 2004). Recently (Jackson and Jeffries, 2010) made an analysis on the Pleides and α Persei cluster, using a Monte Carlo method to simulate the spin-axis alignment. Their result points in the direction of a random distribution of the alignments.

3.4.2 $\Phi(y)$ distribution

The aim of this Section is to derive the functional form of $\Phi(y)$. The distribution of projected rotational velocity cannot be easily derived. The observational $Vsini$ distribution depends both on the true distribution and on the uncertainties and limits that apply to measurements. Many authors proposed analytical description of this distribution. Early observations (Kraft, 1965) are only for fast rotators, stars having $Vsini$ of order 100-200 km/s and only for bright stars. The objects were mainly field stars and the discussions were limited on 30-40 measurements. A better definition of the $Vsini$ distribution is now possible due to better statistics and improved techniques. The pioneering work was made by (Chandrasekhar and Münch, 1950). The authors made the hypothesis that function $\Phi(y)$ is Gaussian and found an analytical solution (see 3.4).

3.4.3 Tsallis distribution

An analysis on OC rotational velocity distribution (Gaige, 1993) leaded the author to the idea of a non-uniform distribution. (Soares et al., 2006) find a uniform distribution

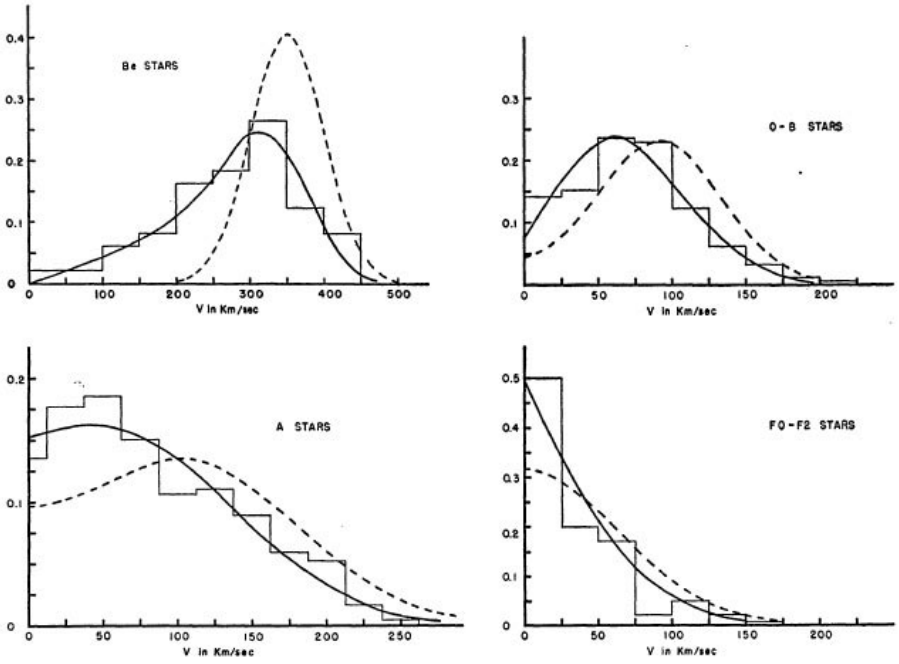

Figure 3.4: Here there is the comparison of the observed distributions of rotational velocity of stars with different spectral type, taken from Chandrasekar & Munch 1950.

that fit very well the observed distribution for the Pleiades cluster, the so-called Tsallis maximum entropy distribution. (Tsallis, 1988) proposes a non-Maxwellian (powerlaw) distribution function associated with the thermostatistical description (see 3.6). The question of the nature of the distribution of stellar rotational velocity is not simply a question of which mathematical function model is used, but it depends primarily on the statistical mechanics applied, which should be general enough to take into account the changes in rotation with time. This new distribution function generalizes the MaxwellBoltzmann function (Silva et al., 1998), and comes from the non-extensive statistical framework first proposed by Tsallis and applied successfully to different astrophysical problems, like matter distribution of self-gravitating system (Hamity and Barraco, 1996); (Rajagopal, 1996); (Lavagno et al., 1998), stellar polytropes (Taruya and Sakagami, 2002). The study of (Soares et al., 2006) is focused on the Pleiades. They use the distribution function:

$$\Phi_q(y) = B_q y\left[1-(1-q)\frac{y^2}{\sigma^2}\right]^{\frac{1}{1-q}} \tag{3.6}$$

When q =1, this distribution becomes a Maxwellian distribution. This distribution descend from non-extensive statistical mechanics, where the q-exponentials play a fundamental role. This observation enabled the establishment of the q-generalized classical energy equipartition theorem (Lima and Plastino, 2000) yielding also a power law type distribution in which the variable parameter is the kinetic energy. On the other hand,(Latora et al., 2002) have used the rotational velocity as the variable parameter in his work on the dynamics of a Hamiltonian system of N planar classical spins, whereas

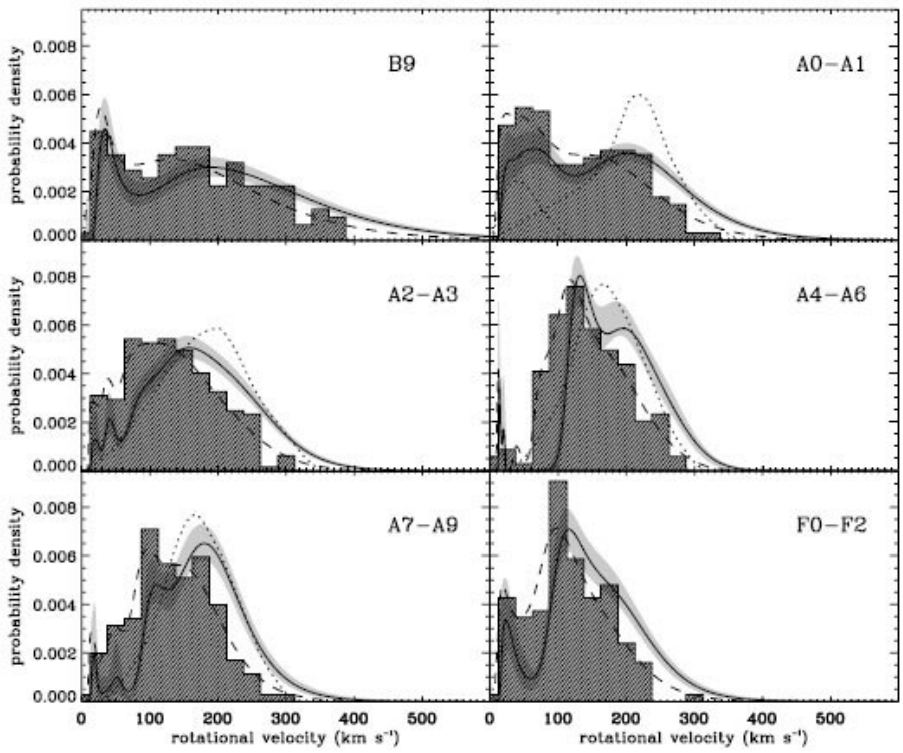

Figure 3.5: Here there is the plot taken from Royer et al. 2007: distributions of rotational velocities for observed samples. Histograms are the observed $V sini$, dashed lines are the distributions of projected rotational velocities, solid lines are the distributions of true equatorial velocities.

(Campa et al., 2001) have used the same framework in the study of rotators interacting through an infinite range potential.

3.5 Observational framework

Early data on star rotational velocities, that were mainly on fast rotators, are well fitted by Gaussian distribution.

However, when data on low rotators appeared, the Gaussian form distribution failed to fit the data. (Deutsch, 1970) claimed that the distribution of stellar rotational velocities should have the form of a Maxwellian-Boltzmann law. (Dufton et al., 2006) find that Maxwellian or Gaussian distribution can fit the distribution of fast rotators (OB stars) in the Magellanic Clouds and in the Galaxy. However, a number of studies have shown a clear discrepancy between theory and observations, where observed distributions are not fitted by a Gaussian or Maxwellian function with a good level of significance. A Gaussian or Maxwellian distribution that fits the fast rotators fails to account for low rotation rates. On the other hand, a fit to slow rotators fails to explain the rapidly rotating stars. The amount of angular momentum stored by a star before it reaches the

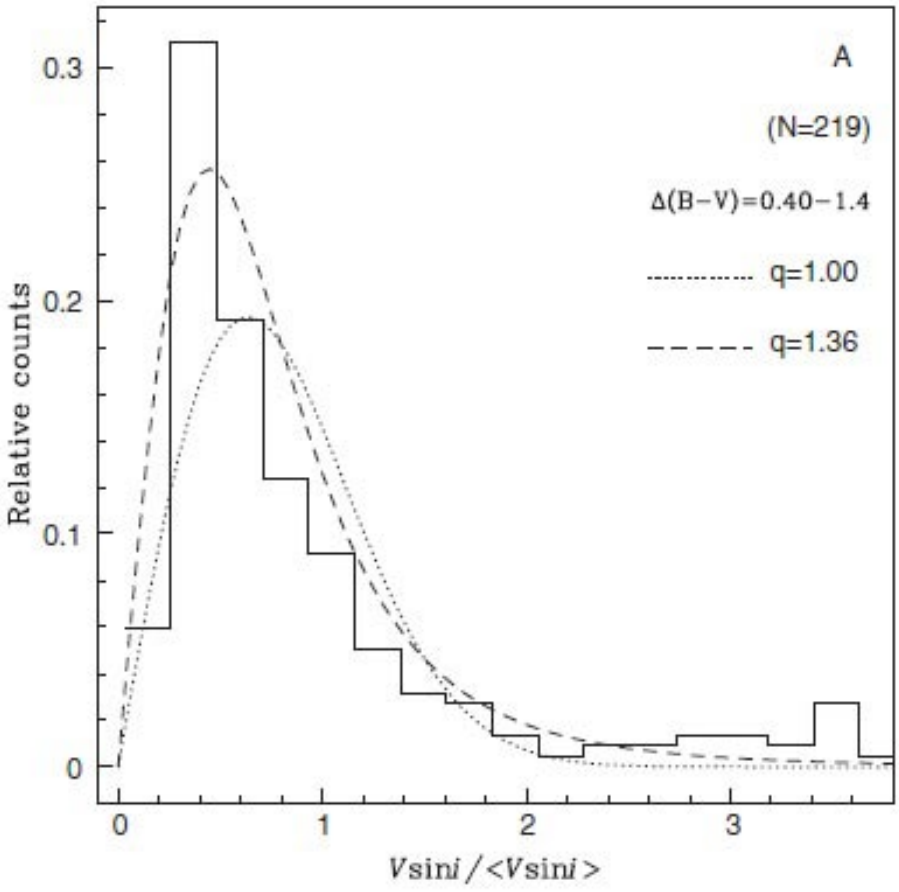

Figure 3.6: This plot is taken from Soares et al. 2006. here is plotted the distribution of rotational velocities for Pleiades cluster. The histogram is the observed $Vsini$, dashed line is the distribution calculated from Tsallis distribution, dotted line is the standard Maxwellian distribution.

zero-age main sequence can be depending on the accretion, winds (Schatzman, 1962), and magnetic fields ((Koenigl, 1991); (Edwards et al., 1993)). If such processes would produce only the rigid rotation profile in stars, the distributions of angular velocity rates would probably be unimodal and Maxwellian (Deutsch, 1970). However, due to differences in the initial chemical composition and other conditions multimodal distributions are not unexpected. Recently, the bimodality of the data of Ocs, suggests that there are two different rotational projected velocity distributions, one for the low rotators and the other one for the fast rotators: (Royer et al., 2007) showed that late B and early A-type MS stars have bimodal distribution (see3.5), while late type A-stars show a lack of slow rotators. The bimodality is observed among young solar mass stars in Orion ((Attridge and Herbst, 1992); (Choi and Herbst, 1996); (Herbst et al., 2001); (Barnes, 2003)) and is present also among the A-F stars of the main sequence (hereafter MS). Because these groups have different

average ages, the question is raised whether this can be due to difference in the evolution of the rotation according to the stellar mass, as suggested recently (Zorec and Royer, 2012). In the following we will derive the rotational velocity distribution in a sample of OCs, to derive the rotational properties of intermediate mass stars in OCs as a function of age.

Chapter 4

Clusters data

In this Chapter we present the compilation of data of $Vsini$ and rotational periods of a sample of open clusters. Those data will be compared with the new stellar models including rotation calculated with CESAM.

4.1 Introduction

The distributions of stars from a single open, or galactic cluster in the HR diagram tend to be very narrow, contrary to the distribution of field stars. This most likely reflects the homogeneity in age and chemical composition for stars in a cluster. Thus, clusters can in principle provide the means to empirically resolve the HR diagram. In spite of the progresses of the stellar evolution in the recent past still several open problems in the stellar evolution remain. In particular we can mention the mixing in the stellar interiors, the rotation, the magnetic fields. All those effects significantly influence the stellar magnitudes, lifetimes, burning phase duration and need to be calibrated comparing models with observations. OCs give the opportunity to study large numbers of stars spanning a broad range of masses and evolutionary stages. Stars in OCs can be assumed to have similar age and chemical composition. Observations may give the position of the main sequence in the HR diagram, the density of stars along that sequence, the M-L relation if the masses of some binary stars can be derived from the observations. The analysis of the observational features of a given cluster by means of internal structure models allows estimating characteristics not directly accessible through observation, such as the age or helium content of the members. Furthermore, if the observational data are accurate enough, constraints on the physical processes at work in the stellar interiors, for instance the various transport processes, can be inferred.

Here we concentrate on the study of OCs to test the stellar evolution models including the effect of the rotation. In this Chapter we present the observational data which will be analyzed in the following. The target clusters are selected in the age range 100 - 800 Myr in order to have rapidly rotating stars at the turnoff with masses in the range 2-3 to $0.8 M_{\odot}$with well determined velocities and clear membership of the stars to properly derive the age and test the effect of the rotation on CESAM stellar models of intermediate masses. We select the Hyades, Alpha Persei, Praesepe, Blanco 1.

4.2 Hyades

For most of the past century, the Hyades has been an important calibrator of many astrophysical relations. The nearest moderately rich cluster, with ∼400 known members, among which are white dwarfs, red giants, mid-A stars in the turn-off region, and numerous main sequence stars, at least down to ∼0.10 $M_{\odot}$M dwarfs. Its total mass is of the order of 300-400 $M_{\odot}$, and its age is around 600-700 Myr (Perryman et al., 1998, Lebreton et al., 1997). Recently, high-quality observations of the Hyades stars have been obtained. Hipparcos data combined with ground-based photometric or spectroscopic observations provided a more precise HR diagram of the cluster (Perryman et al., 1998, Dravins et al., 1997, de Bruijne et al., 2001). The Hyades has been used for detailed astrophysical studies because of its proximity (mean distance around ∼ 45 pc), also giving rise to several other advantages such as relatively bright stars and negligible interstellar reddening and extinction, large proper motion ($\mu \sim 111$ mas yr1) and peculiar space motion (∼35 km s1 with respect to its own local standard of rest), greatly facilitating both proper motion- and radial velocity-based membership determinations. Its proximity, however, has also always complicated astrophysical research: the tidal radius of ∼10 pc results in a significant extension of the cluster on the sky (∼20°) and a significant depth along the line of sight. The precise definition and location of the main sequence and turn-off region in the HertzsprungRussell diagram, and thereby, accurate knowledge of the Helium content and age of the cluster, has always been limited by the accuracy and reliability of distances to individual stars. The metallicity content of the cluster is derived by (Cayrel de Strobel et al., 1997) and confirmed by recent work (Carrera and Pancino, 2011). We adopt the value of $[Fe/H] = 0.14dex$ used in previous work (Lebreton et al., 2001), (de Bruijne et al., 2001) as a input parameter for analysis presented in the next chapter. Observations of several binary systems in the Hyades yield an improved M-L relation (Torres et al., 1997b, Torres et al., 1997c, Torres et al., 1997a). The excellent accuracies on the masses and luminosities reached for the Hyades binaries provide rather severe constraints on the helium content of the cluster, refining of the helium value previously inferred from the analysis of the HR diagram (Perryman et al., 1998, Cayrel de Strobel et al., 1997, Lebreton et al., 1997, Lebreton et al., 2001). These studies derive an helium content of $Y = 0.255 \pm 0.009$ which will be used for our analysis. The study of the membership of the Hyades stars are taken by the study on the Hipparcos observation as derived by (Perryman et al., 1998), then as refined by (de Bruijne et al., 2001). The latter also derive the surface gravity of the selected members (log g) with (Beck, 2008) for HD 20894. The most recent determinations are by (van Leeuwen, 2009) who re-reduced the Hipparcos data, and by (Röser et al., 2011). We adopt these membership and parallax determinations to select the cluster stars. The photometric information, m_V, $(B-V)$, the surface gravity *logg* to built colour-magnitude diagram in the figure (4.1 and 4.2) and the error bar is given by the catalogue of (Röser et al., 2011). Rotational velocities $Vsini$ for stars of spectral type hotter than F,K are derived from the catalogue of (Mermilliod et al., 2009). This is an homogeneous Catalog including the results of a long-term monitoring of solar-type dwarfs in 13 nearby open clusters having distances $<$ 500 pc. This monitoring has allowed to detect membership and duplicity, and to

search for new cluster members. The observations were collected at the Haute-Provence Observatory (France) and at ESO La Silla (Chile). Rotational periods are derived by (Radick et al., 1987),(Prosser et al., 1995), (Delorme et al., 2011) for solar type stars, for the very low-mass regime (M-type and below) from(Reid and Mahoney, 2000).

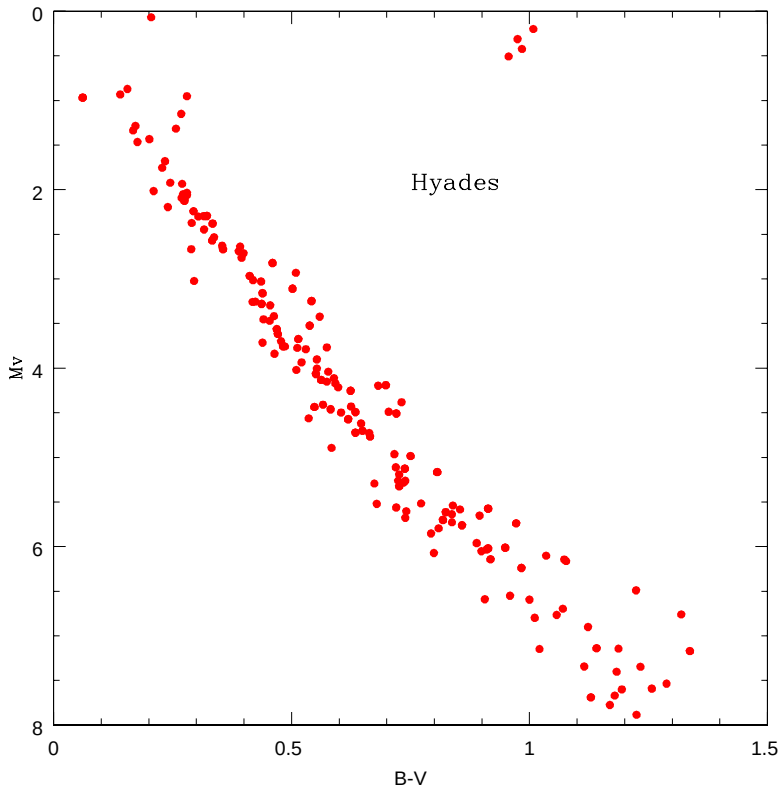

Figure 4.1: HR diagram built for Hyades cluster. The selected stars have information on magnitude, (B-V) colour and projected rotation velocity $V \sin i$.

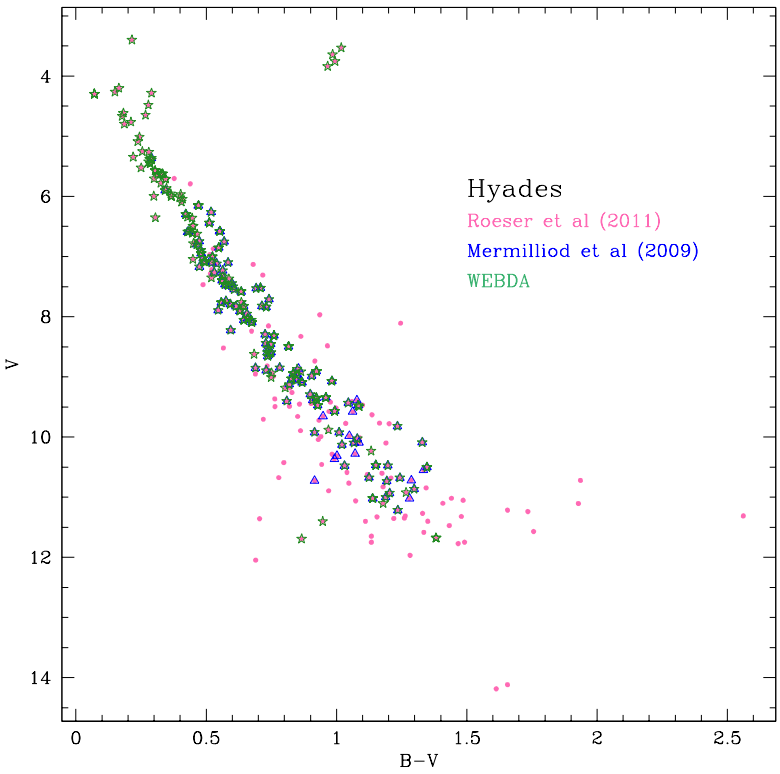

Figure 4.2: Colour-Magnitude diagram for Hyades cluster. Cluster stars are plotted in different colour: red for the catalogue of Roeser et al. 2011, for membership, magnitude and colour index; blue for the catalogue of Mermilliod et al. 2009 for the Vsini data; green for the WEBDA database for the other Vsini that there aren't in the Mermilliod catalogue.

4.3 Alpha Persei

Alpha Persei is unusual in some respects when compared with the Pleiades and the Hyades with a metallicity of $[Fe/H] = -0.13dex$ (Balachandran et al., 2011). Being somewhat more distant and considerably younger, this cluster possesses a number of features that

differentiate it from the older, better studied counterparts. The most obvious feature is its large size and low number density (Artyukhina, 1972), especially of stars more massive than the Sun. The only star evolved off the main sequence is αPer. The estimated velocity dispersions inside the Hyades and the Pleiades are roughly in agreement with theoretical expectations for a dynamically steady and uniform cluster. This has not yet been shown unequivocally for younger and more distant clusters, such as $\alpha Persei$ (age $\sim$ 50 Myr), mostly due to the paucity of accurate proper motions and radial velocities, but also because of difficulties with membership determination (Makarov, 2006). Fairly massive probable members of the cluster can be found at 20 pc and farther out (Artyukhina, 1972). It appears that the cluster is engulfed by a spacious moving group, or halo (Shatsova, 1981), which has very similar kinematics and photometric properties and was probably formed along with it. (Mermilliod et al., 2008b) undertook a radial velocity program to check for spectroscopic binaries in the cluster. Their criteria for membership were three-fold: proper motions (from the Second USNO CCD Astrometric Catalog UCAC2), radial velocity and location in the colormagnitude diagram. These criteria were applied independently of (Prosser, 1992) and (Makarov, 2006) efforts at membership determination. Makarov et al work is based on the astrometric proper motions and positions in the Tycho-2 catalog and Second USNO CCD Astrographic Catalog (UCAC2). Using the astrometric data and photometry from the Tycho-2 and ground-based catalogs, 139 probable members of the cluster are selected, 18 of them new. 54 of 86 stars accepted as members by (Makarov, 2006) were in (Mermilliod et al., 2008b) program. Inside Mermilliod sample, we select stars having membership probability higher than 50%. Photometry is derived by Kharchenko et al. (2004)(see fig. 4.3 and 4.4) . The uncertainty on the B magnitude is of the order of 0.05 at B=11, rapidly increasing toward fainter magnitudes (see fig. 4.5). We limit our analysis to stars brighter than B=11 mag.

4.4 Praesepe

Praesepe is a rich ($N \sim 1000$ known or suspected members), intermediate-age ($\sim$ 600 Myr) cluster at a distance of $\sim$ 180 pc (van Leeuwen, 2009) with a total mass of $M \sim 500$ $M_{\odot}$(Kraus and Hillenbrand, 2007),Praesepe has been the target of numerous photometric and astrometric membership surveys over the past century. Part of the reason for its popularity is that its proper motion is relatively distinct from that of field stars (-36.5, -13.5 mas yr^{-1}), simplifying the identification of new members. Its high-mass stellar population was identified early in the last century by Klein-Wassink (1927), and subsequent surveys extended the cluster census to intermediate-mass stars (Jones and Cudworth, 1983). The M dwarf stellar population was first identified by (Jones and Stauffer, 1991). A later survey by (Hambly et al., 1995) extended this work to a fainter limit and a larger fraction of the cluster, producing a cluster census that is still used for most applications (Allen and Strom, 1995, Holland et al., 2000, Kafka and Honeycutt, 2006). The area covered by the cluster is about 4.5 °in diameter. The distance modulus as derived from the new Hipparcos reduction is, at 6.30 ± 0.07 effectively identical to one determined by (An et al., 2007) (6.33±0.04) and fully consistent with the value derived by (Percival et al., 2003) (6.24 ± 0.04, using $(VI)_C$data). It is larger, but not significantly, than the value of 6.15

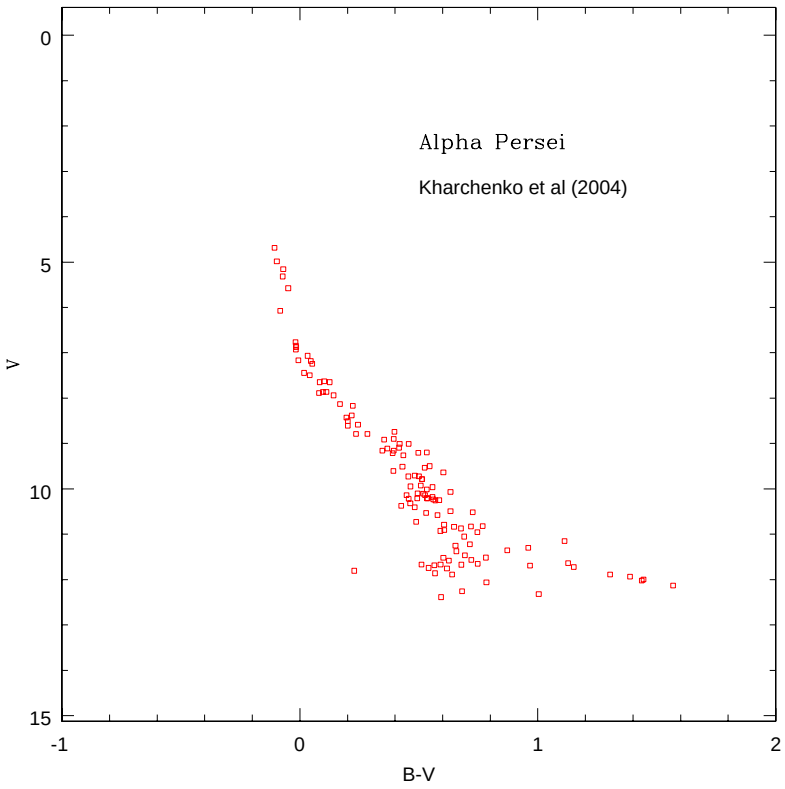

Figure 4.3: Colour magnitude diagram built for Alpha Persei cluster. The selected stars from Kharchenko et al. (2004) have the information on magnitude in V band, B-V colour. We select stars having membership kinematic probability greater than 0.5.

derived by (Cameron, 1985) from UBV data, and the value of 6.10 ± 0.18 derived by (Nicolet, 1981) using photometric boxes. Also within the same range is the value derived from differential parallax measurements by (Gatewood and de Jonge, 1994), 6.42 ± 0.33. These results, in a way, mostly reflect the very strong similarity between the Hyades and Praesepe clusters. The magnitudes and colors, together with the membership information are given in the (Kharchenko et al., 2004) Catalog. In the following we analyze the

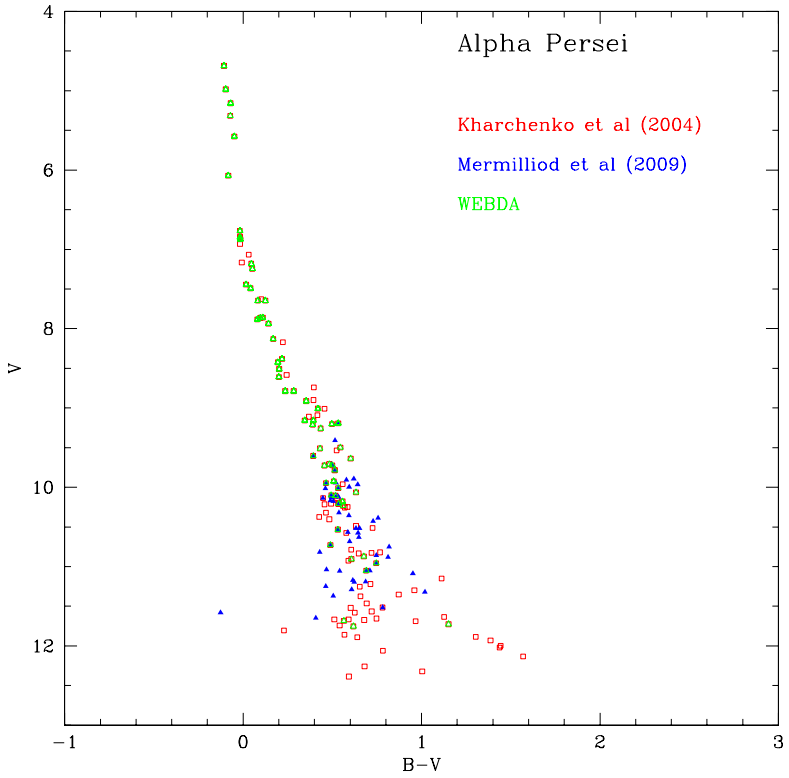

Figure 4.4: Colour-Magnitude diagram for Alpha Persei cluster. Cluster stars in different colour: red for the catalogue of Kharchenko et al. 2004, for membership, magnitude and colour index; blue for the catalogue of Mermilliod et al. 2009 for the Vsini data; green for the WEBDA database for the other Vsini that there aren't in the Mermilliod catalogue.

stars having a membership probability higher than 50% in the (Mermilliod et al., 2009) Catalog (see fig. 4.6 and 4.7). For the surface gravity we adopt the information give in (Fossati et al., 2008), that are only for star in turn-off zone of Praesepe cluster (A-type stars).

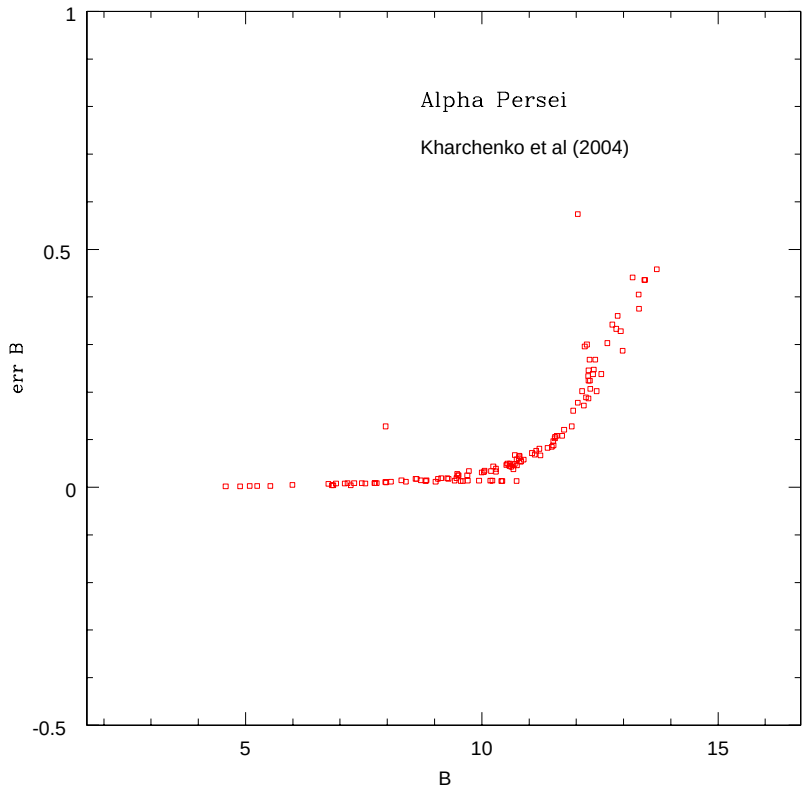

Figure 4.5: In this figure we show the trend of the error bar for magnitude.

4.5 Pleiades

The Pleiades cluster covers an area on the sky of about 9 to 10 degrees in diameter (van Leeuwen, 1980), which is, contrary to statements made by (An et al., 2007), much larger than the error-correlation scale length for the 1997 Hipparcos catalogue(van Leeuwen, 1999). In that area, the Hipparcos catalogue contains about 57 members of the cluster. For Pleiades cluster the distance modulus is 5.40±0.03 (van Leeuwen, 2009). It has been stated by (Soderblom et al., 1998), and re-iterated by (Stello and Nissen, 2001) and (An et al., 2007), that at the parallax found from the Hipparcos data for the Pleiades cluster, the clus-

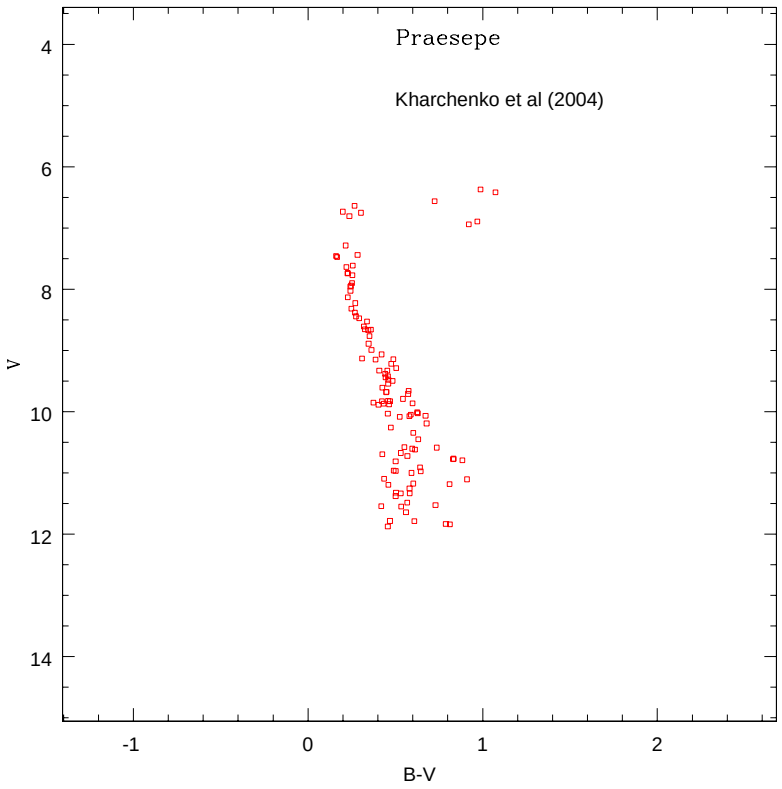

Figure 4.6: Colour magnitude diagram for Praesepe cluster (Kharchenko et al. 2004) for stars having a membership probability higher than 50% in Mermilliod et al (2009) Catalog

ter members will occupy an area of the HR diagram in which no field stars, or more specifically no field stars that are assumed to be young, are found. This is not the case, as field stars contained in the Hipparcos catalogue are observed in the area occupied by the Pleiades. Pleiades metallicity that we use as reference is taken from (Soderblom et al., 2009) and it is $[Fe/H] = 0.03dex$. The cluster has an age of ~ 125 Myr (Converse and Stahler, 2008) (Stauffer et al., 1998). Also for this cluster we derive the photometry from (Kharchenko et al., 2004), and the membership from (Mermilliod et al., 2009)

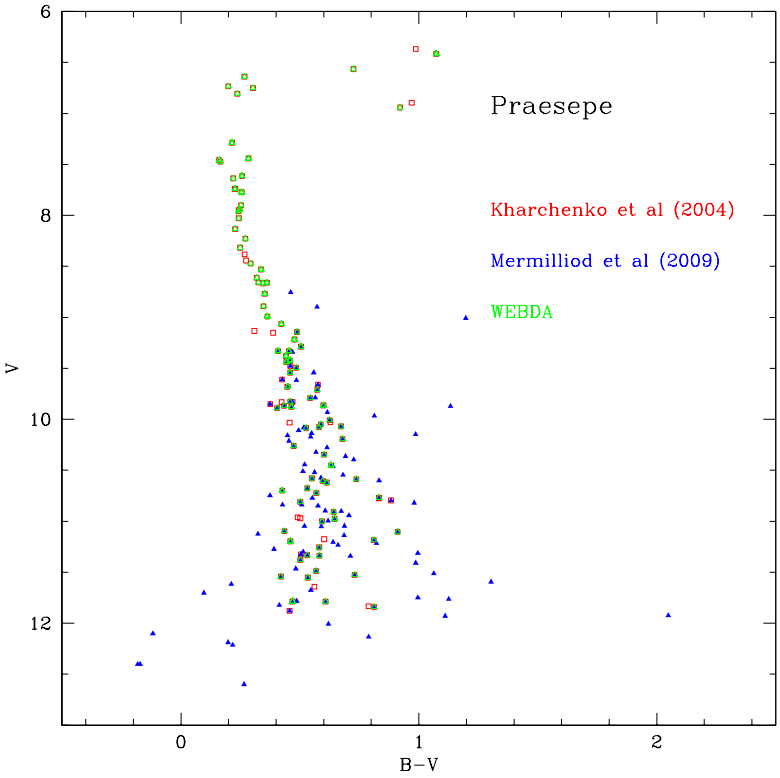

Figure 4.7: Colour-Magnitude diagram for Pleiades cluster. Cluster stars are plotted in different colour: red for the catalogue of Kharchenko et al. 2004, for membership, magnitude and colour index; blue for the catalogue of Mermilliod et al. 2009 for the Vsini data; green for the WEBDA database for the other Vsini that there aren't in the Mermilliod catalogue.

Catalog (see Fig. 4.8 and 4.9).

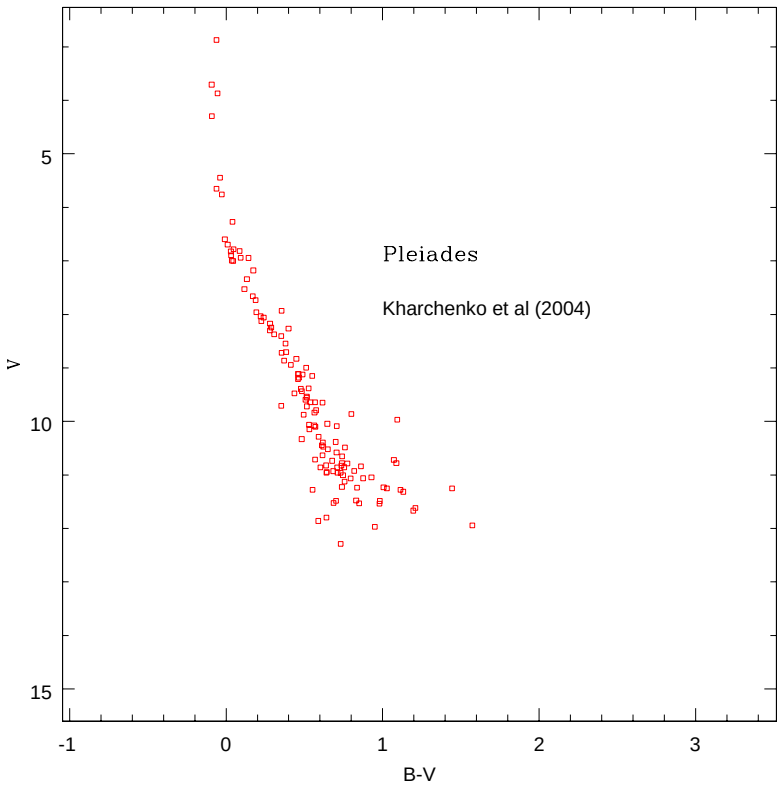

Figure 4.8: Colour magnitude diagram of the Pleiades cluster. The photometry is from Kharchenko et al. (2004). Only stars having membership probability higher than 50% are plotted.

4.6 Blanco1

Blanco 1 is a nearby, young open cluster seen in the direction of the south Galactic pole with a metallicity of $[Fe/H] = 0.04dex$ (Ford et al., 2005) and with a distance of 207 ± 12 pc (van Leeuwen, 2009). It is difficult to estimate precisely the age of Blanco 1 by the usual method of isochrone fitting because of the lack of evolved stars on the upper main sequence. However, the comparison of $H\alpha$ emitters, the lithium trend as a function of B -

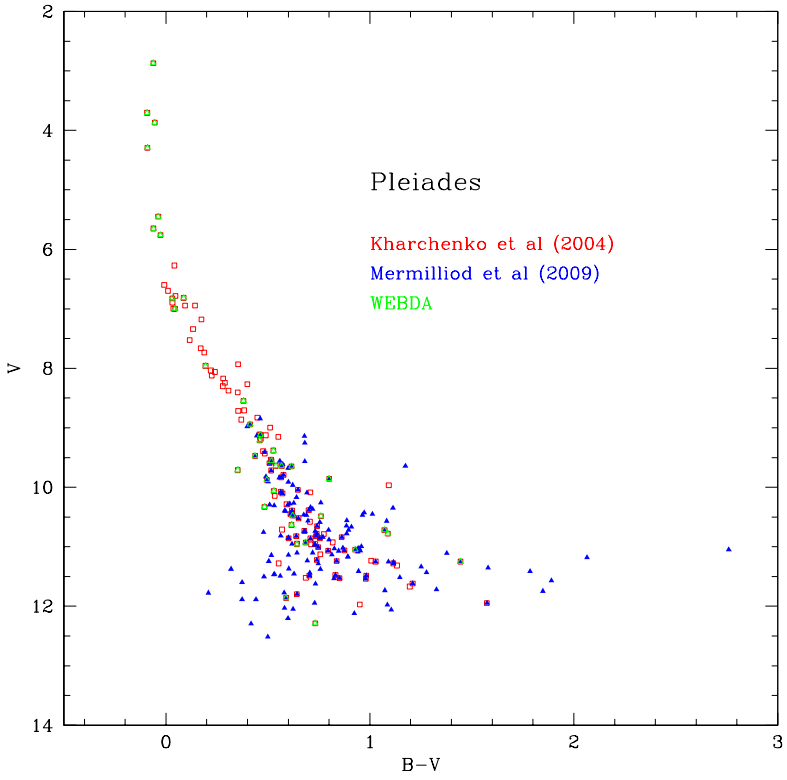

Figure 4.9: Colour-Magnitude diagram for Pleiades cluster. Cluster stars are plotted in different colour: red for the catalogue of Kharchenko et al. 2004, for membership, magnitude and colour index; blue for the catalogue of Mermilliod et al. 2009 for the Vsini data; green for the WEBDA database for the other Vsini that there aren't in the Mermilliod catalogue.

V, and the X-ray luminosity distribution for the Pleiades and Blanco 1 indicate that both clusters are about the same age (Ford et al., 2005). An attempt to estimate the cluster age is done by (Cargile et al., 2010) with an analysis on lithium abudance on cluster stars and they found 132 ± 24 Myr. The problem of this cluster is the difficulty in the member-

ship determination. Many attempt were done in this direction with different strategies. The membership of 68 stars is confirmed on the basis of proper motion, radial velocity, and photometric criteria by (Mermilliod et al., 2008a). (Baumgardt et al., 2000) combine Hipparcos data with information provided by ground based studies. (Pillitteri et al., 2003) make use of the astrometric-photometric membership obtained from the GSC-II project confirming membership probability higher than 80% for 93 stars. The first extensive investigations were photometric (de Epstein and Epstein, 1985) published photographic uvby data and B V indices computed from uvby for 261 stars. (Westerlund et al., 1988) obtained photoelectric observations for 130 stars, mostly brighter than $V = 12$, on the $UBV\beta$ system, although nearly a half of their observed stars also have uvby data. Photometry and memberships are taken from Kharchenko et al. (2004), (see Fig.4.10). $V sini$ for about 200 stars is derived by (Mermilliod et al., 2008a), (Ford et al., 2005).

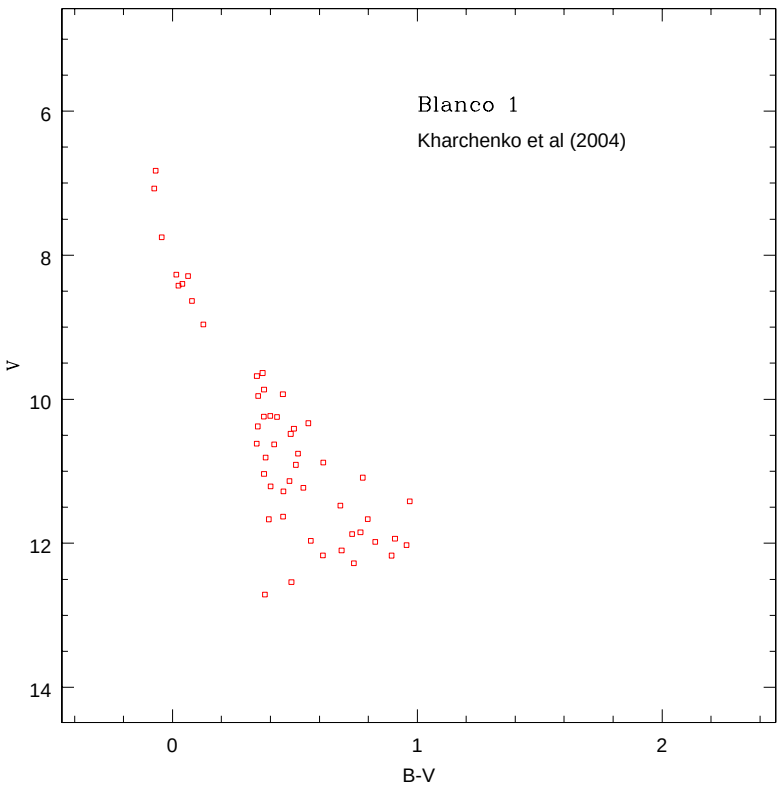

Figure 4.10: Colour magnitude diagram for Blanco 1 (see text for details).

Chapter 5

CESAM code for stellar evolution

5.1 Introduction

In this Chapter, we present the stellar code Cesam used in this Thesis to calculate evolutionary tracks and isochrones for different metallicity and rotational velocities. We will paid particular attention to the treatment of the rotation in low mass stars. CESAM, an acronym for "Code d'Evolution Stellaire Adaptatif et Modulaire" (in English for an Adaptative and Modular Code for Stellar structure and Evolution), is a stellar evolutionary code that allows the computation of the quasi-static evolution of stellar models as long as the assumption of quasi-static equilibrium remains valid in the core (Morel and Lebreton, 2008). The Cesam code is a consistent set of programs and routines which perform calculations of 1D quasi-hydrostatic stellar evolution including microscopic diffusion of chemical species and diffusion of angular momentum. The solution of the quasi-static equilibrium is performed by a collocation method based on piecewise polynomials approximations projected on a B-spline basis, that allows the exact restitution of the solution, not only at grid points. Another advantage is the monitoring by only one parameter of the accuracy. An automatic mesh refinement has been designed for adjusting the localisations of grid points according to the changes of unknowns. The code solves the evolutionary equations for each time step in iterative way. It consist on decoupling two problem: initial conditions (Cauchy problem) and limit conditions (Dirichlet problem). It is solve with Newton - Raphson iteration method. The CESAM story begins in 1987. Bernard Pichon wrote a totally new version in 2001: Cesam2k was rewritten in Fortran 90/95 with many important new features. The run is interactive. Messages displayed in French, or in English, allow the control of calculations. The extent of convection zones, a HR diagram, and the profiles of temperature, pressure, luminosity and abundances are displayed on line using PGPLOT package. Its overall structure is separated in two spaces: 1. A physical space where the coefficients of the differential equations are written in a form close to their physical formalism. 2. A numerical space where the differential equations are formally solved. Therefore Cesam allows to implement physical processes, and physical data, without any knowledge of numerical methods involved for the solution of the equations. To start the evolution is need only the input file. In this file we give all the "ingredients" for the models: the theory we want to use for diffusion, convection, atmosphere, the chemical

abundances and all the parameters for the control of the models.

5.1.1 Stellar Atmospheres

The atmosphere connects the convective optically thick outer part of the envelope to the optically thin interstellar medium. The radiative transfer calculation in the atmosphere is a complex problem that is not possible to solve in same time with the transfer in the innner structure. One problem is that the radiation pass through an isotropic opaque medium inside the star to the anisotropic interstellar medium. There is the possibility to use Kuructz and MARCS atmosphere models (Gustafsson et al., 2008) to do very realistic simulations.

5.1.2 Convection

Two formalisms for the computation of the temperature gradient in the convection zones are available: the standard (Böhm-Vitense, 1958) mixing-length (MLT) formalism is considered with the optical thickness of the convective bubble, and the (Canuto and Mazzitelli, 1991) formalism. Overshooting beneath and/or above the convection zones can be accounted for. The mixing length parameter and the overshooting parameter are read as an input to build the models.

5.1.3 Diffusion

The diffusion implemented in Cesam2k is of three types: turbolent, microscopic and the radiative acceleration. The turbolent diffusion is essentially based on the calculus of the coefficients named D that govern the diffusion. This coefficients are calculated in two different way that the user of Cesam can choose. One according to (Michaud and Proffitt, 1993), but this formalism is only valid for the main sequence. A second choice is the according to (Burgers, 1969). For boundary conditions is assumed at the outermost limit that there is neither input nor output of matter. At centre M = 0, because of the spherical symmetry. The microscopic diffusion is also included following the study of (Morel and Thévenin, 2002). The physical meaning of this, as efficient as simple source of turbulent mixing, has been questioned by (Alecian and Michaud, 2005). Radiative acceleration is still under test.

5.1.4 The nuclear networks

The nuclear reaction rates are tabulated on relevant intervals of temperatures. The rates are computed using the formulas of (Caughlan and Fowler, 1988) or of NACRE compilations (Angulo et al., 1999). For solar models, the improved rates of (Adelberger et al., 1998) are available.

5.1.5 Equation of state and opacity

Equation of state (EOS): the CEFF EOS (Eggleton et al., 1973) (Christensen-Dalsgaard and Daeppen, 1992) has mostly been used have been designed to study the Sun (MHD EOS,(Mihalas et al., 1988)

and very-low mass stars; it includes the Debye-H$\acute{}$uckel corrections for pressure. The OPAL EOS (Rogers et al., 1996) that includes collective effects has been used at low mass for the purpose of comparison. Opacities: we used OPAL (Iglesias and Rogers, 1996) complemented by (Alexander and Ferguson, 1994) data for $T \leq 10^4 K$, both being for (Grevesse and Noels, 1993) solar mixture.

5.1.6 Rotation

Rotation is considered in CESAM under the assumption of spherical symmetry. As we have seen, this is not true, but this is a reasonable first-order approximation usually adopted for slow rotators, for instance the Sun. However, departure of the spherical symmetry in the Sun can be measured and are significant (Lydon and Sofia, 1995). These departures are sufficient for rotation to induce large-scale circulations in the radiative and convective interior, transporting angular momentum, and chemical species (Busse, 1982) (Zahn, 1992). Moreover, in case of radial differential rotation, which could be the case in the solar deepest interior, different hydrodynamical instabilities may develop that will generate hydrodynamical turbulence in the radiative regions. With non zero angular velocity, the mean centrifugal acceleration affects the local gravity. In the initial model, rigid rotation is assumed. The initial angular velocity can be read from input file in radians, in km/s, that is the rotational velocity in the star outer part, or in days, that corresponds to the rotation period. It is possible to have a simulation without the diffusion of angular momentum. These options are available:

- no rotation, the angular velocity is zero;
- solid-body rotation, the angular velocity has his initial value;
- solid rotation, angular momentum globally conserved, but the angular velocity changes in time;
- The rotation is not solid, angular velocity changes according to the conservation of the local angular momentum

It also possible do simulations with diffusion of angular momentum and in Cesam2k there are two different choice. The first one follow the work (Talon et al., 1997) and the second one possibility is to use the formalism that follows the theory of (Mathis and Zahn, 2004). The first one present a simplified treatment of the gravitational potential fluctuations, while the second one allow a more sophisticated description of rotational mixing in stellar radiation zone . In rotating stars the centrifugal force breaks the radiative equilibrium, producing a large-scale circulation, which transports matter and angular momentum. A similar circulation is induced locally in the vicinity of a differentially rotating convection zone, in the so-called tachocline. As a result, radiation zones rotate non-uniformly, and therefore they are liable to various instabilities which may generate turbulence which in turn transport matter and angular momentum .(Mathis and Zahn, 2004) prescriptions for the turbulent transport result in an enhanced mixing even in low mass stars. Diffusion coefficients are according to (Palacios et al., 2003) and to (Mathis et al., 2004). We have

adopted the (Mathis et al., 2004) and the vertical component of the turbulent diffusivity is from Talon & Zahn.

In this Thesis we calculate stellar models using two of the above schemes: first, the differential rotation by (Zahn, 1992) and (Maeder and Zahn, 1998), including a self-consistent picture of the transport of the chemical elements and of the angular momentum in stellar interiors. The rotation rate and the turbolent transport are not postulated, but will be adjusted interactively. When applied to massive stars, which are fast rotators, such mixing yields much better agreement between models and observations, as discussed by (Meynet and Maeder, 2000). However numerical problems arise during the advanced stages of evolution, when steep gradients of composition and rotation develop. In addition (Mathis and Zahn, 2004) description is used to increase the accuracy of the modelization in latitude by adding higher order terms to the expansion in spherical harmonics, and also to better resolve the phases of rapid evolution by retaining all time derivatives, except those related to the dynamical relaxation.

5.2 Cesam: abundances with diffusive mixing

In the work of (Morel and Thévenin, 2002) the authors use Cesam models for another type of analysis. They focus on the role of the radiative diffusivity generated by the photon-ion collisions that is not presently taken into account in the microscopic diffusion coefficients. The photon-ion collisions are an efficient physical process that inhibits the large sedimentation of helium and heavy elements in outer layers of main sequence star models. The ingredients for their model are taken from (Lebreton et al., 2001) and they don't use the overshooting. The cluster system that they use like a laboratory is Hyades cluster. The results for the colour-magnitude diagram is plotted in figure 8.5.

In (Lebreton et al., 2001) the isochrones calculated without overshooting lead to an age estimated of 550 Myr, the inclusion of elemental diffusion in (Morel and Thévenin, 2002) leads to the age of 570 ± 15 Myr. This means the effect of elemental diffusion increase the age estimation of 3%. Diffusion has visible impact also on the abundances 5.2 where surface abundances of several elements calculated without rottaion, but with diffusion are comapred to the observational data.

The models are in good agreement with the observations, but for oxygen where the distribution of the observed abundances are rather scattered. In addition non-LTE effects or 3D temperature inhomogeneities in the atmosphere (Asplund et al., 2000) can play a role. The open questions of element depletion in stellar models is not solved by the radiative diffusivity (Balachandran, 1995) (Sills and Deliyannis, 2000). This type of diffusivity simply acts together with other mechanism such as the mixing induced by rotation (Zahn, 1992), the mass-loss (Chaboyer et al., 1999), the turbulent mixing (Schatzman, 1969) and the radiative accelerations (Alecian et al., 1993) to inhibit the large element diffusion.

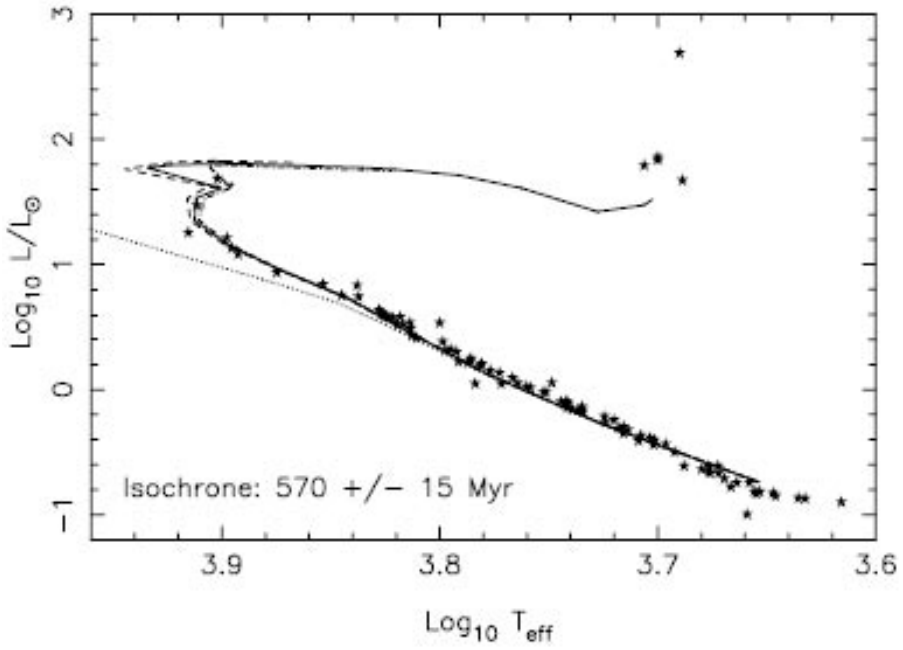

Figure 5.1: This graphic is taken from Morel & Thévenin 2002. It shows the results on Luminosity - effective Temperature diagram of age estimate for Hyades cluster with Cesam code with the inclusion of elemental diffusion.

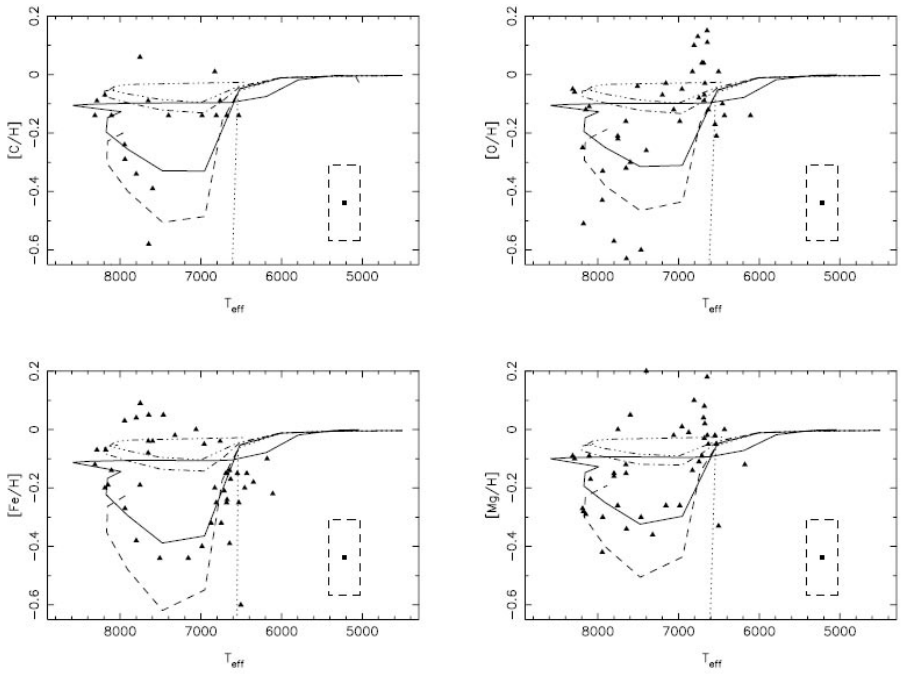

Figure 5.2: The graphic shows the surface abundances of C, O, Mg, and Fe with respect to effective temperature in models computed for Vsin=0, with D_R = 0.0 (dotted), 0.5 (dashed), 1.0 (full), 5.0(dash-dot), 9.0 (dash-dot-dot-dot), together with the observations of Varenne & Monier (1999).

Chapter 6

Stellar models

6.1 Introduction

In this chapter we present the stellar models including the effect of the rotation. To derive the age of the clusters (see following Chapters) we calculate several sets of evolutionary tracks at changing masses and V_{rot}. No overshoot is included in the calculations. We first present the models on the Luminosity-Temperature diagram and then we discuss the effect of the rotation on the chemical abundances.

6.2 CESAM models with rotation

Here we show the series of models built with Cesam2k to see the results in the diagram Luminosity-Temperature and colour-magnitude. Different physics give us different evolutionary tracks and we comment the solid and differential rotation in comparison to the no rotation also for the diffusion of chemical elements. In the Chapter before we describe in general on the code Cesam2k, but for the final set of models that we use for age estimation we use the following physics: the theory of (Canuto and Mazzitelli, 1991) for the convection, (Burgers, 1969) for the diffusion, MARCS atmophere from (Gustafsson et al., 2008) when it is possible, NACRE compilations from (Angulo et al., 1999) for the nuclear frameworks, OPAL EOS (Rogers et al., 1996) and (Iglesias and Rogers, 1996) for the equation of state and opacity, without overshooting because doesn't work at the same time with rotation, and for rotation we use the formalism from (Mathis et al., 2004). We built set of models for Hyades, Praesepe, Pleiades and Alpha Persei metallicities and for different set of rotational velocities from 0 km/s to 250 km/s in order to have different evolutionary tracks that have the rotational velocity observed. All this set are done for different mass at the turn off of the open clusters: for the Hyades and Praesepe clusters we do a set of stellar mass from 1.85 $M_{\odot}$to 2.8 $M_{\odot}$; for Pleiades and Alpha Persei clusters we do a set of stellar mass from 1.85 $M_{\odot}$to 6 $M_{\odot}$. In the fig. 6.1 we show only a set of evolutionary tracks with rotational velocity of 50 km/s. We adopted the transformation of BaSeL (Lejeune, 2002) to pass from the plane Luminosity-Temperature to the observational plane Magnitude-colour index.

In figure 6.3 we compare the models without rotation with models with solid rotation

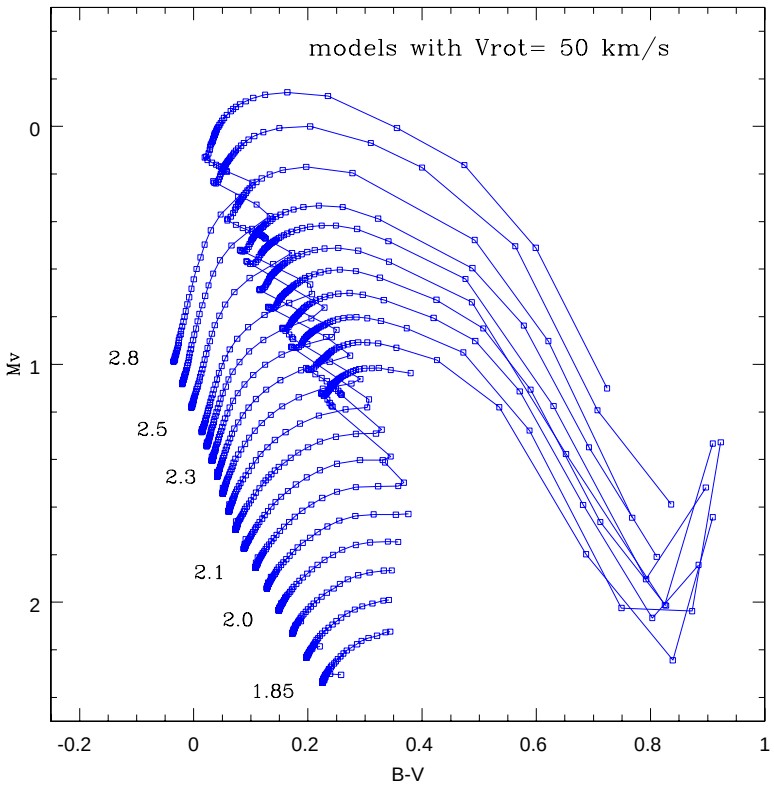

Figure 6.1: CESAM evolutionary tracks in blue the models with differential MS rotation of 50 km/s for the 1.85 $M_{\odot}$to 2.8 $M_{\odot}$masses, not all the mass are marked out, only few masses to guide the eyes of reader.

V_{rot}= 130 Km/s for stars of 2 and 2.8 $M_{\odot}$. Rigid rotation means that the angular velocity is constant during the evolution, differential rotation means that we adopt the theory of (Maeder and Zahn, 1998). In this mass range, models with rotation are significantly redder, while a minor effect is visible on the luminosity. Fig.6.3 is the analogous where models without rotation and with differential rotation are compared. Rotation affects luminosity and color of the models. This means that the estimate of the masses for the

single stars is different and also the age determination.

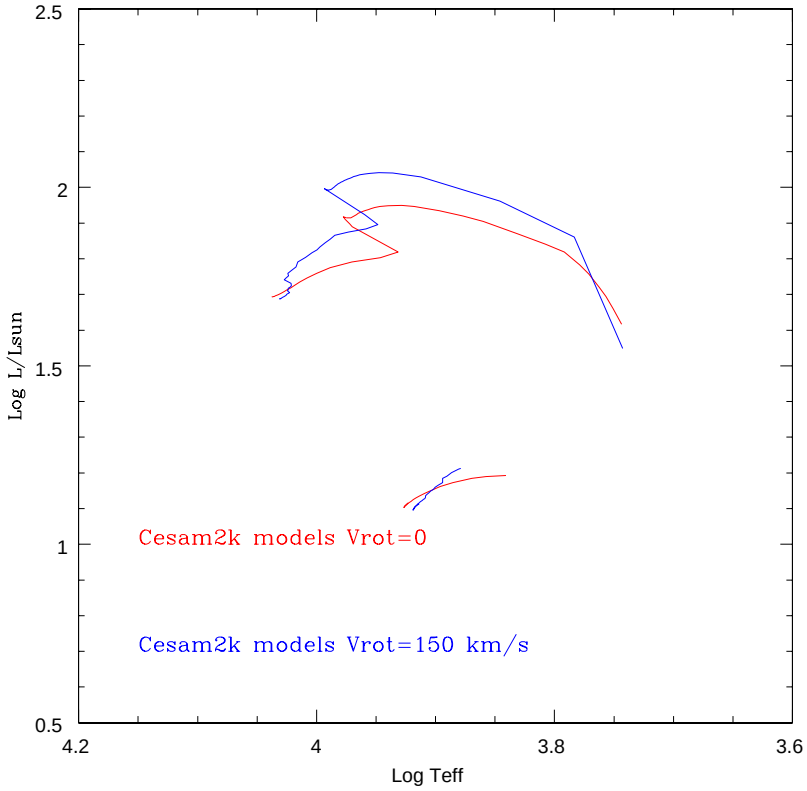

Figure 6.2: CESAM evolutionary tracks: in red the models without rotation for stars of 2 and 2.8 $M_{\odot}$; in blue the models with differential MS rotation of 130 km/s for the same masses.

Fig.6.4 presents the evolutionary tracks for the same masses as in Fig.6.3 for models with rigid rotation and with differential rotation.

The differences between this two type of models are evident: the models with differential rotation are hotter and more luminous than the other one. In fig.6.5 we show evolutionary tracks with differential rotation at changing V_{rot}.

Stars which are faster rotating are more luminous and hotter. This effect is very im-

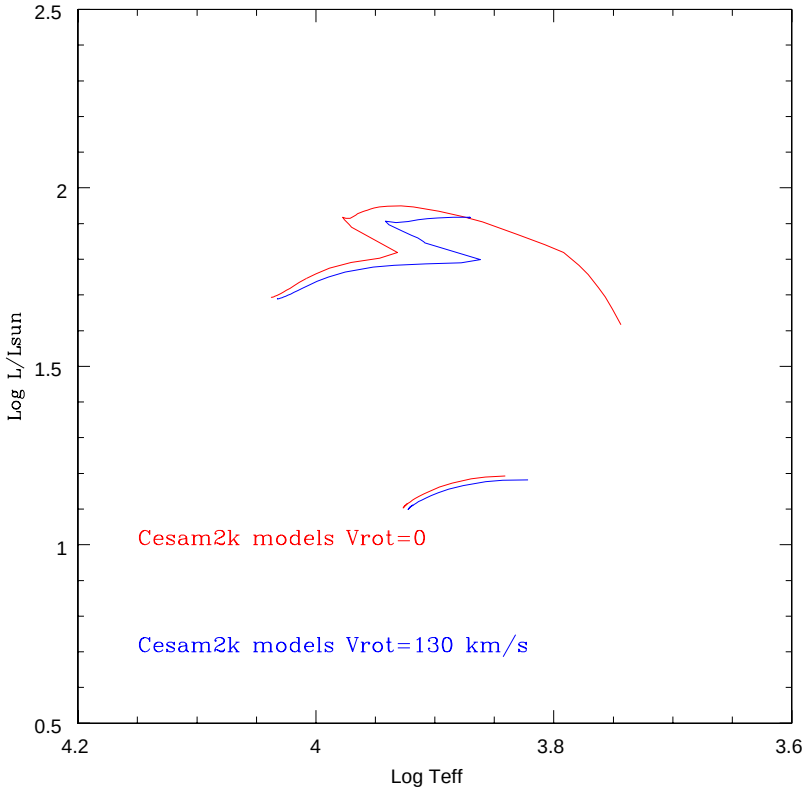

Figure 6.3: CESAM stellar models: in red models without rotation for mass of 2 and 2.8 $M_{\odot}$and the blue models with solid rotation for the same masses with rotation in the MS of 150 km/s.

portant to derive the age of a young cluster where stars having different rotation velocities are found. As we discussed in previous Chapters, in young clusters there are stars with same luminosity but with different rotational velocity with a difference of the order of 100 km/s.

Finally, in fig. 6.6, we present the effect of the rotation on the age determination for the cases of solid body rotation, differential rotation, and no rotation. The values

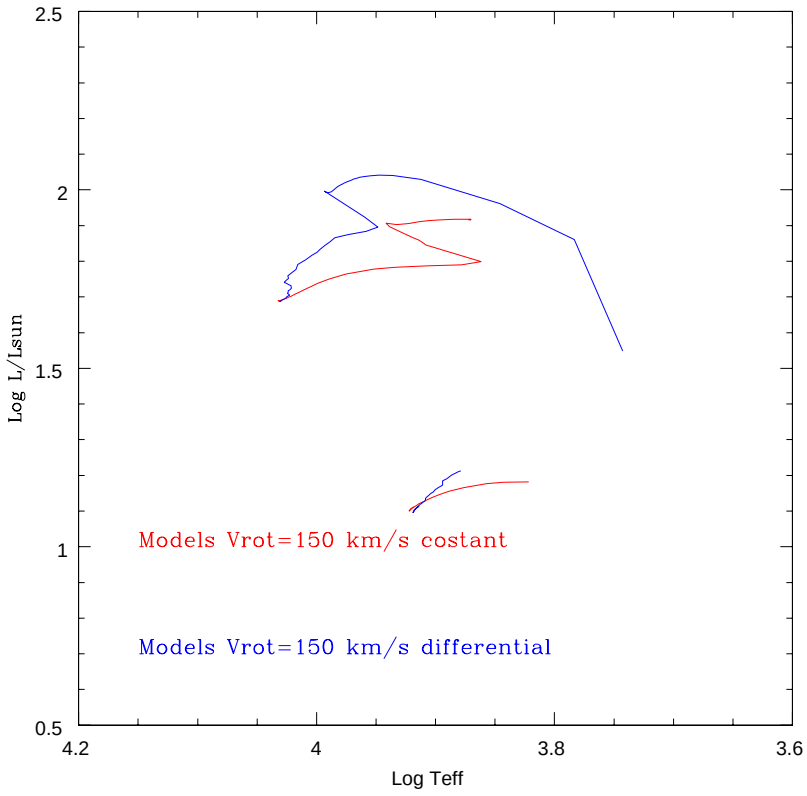

Figure 6.4: Stellar models with CESAM: in red models with rigid rotation for V_{rot} 150 km/s for mass of 2 and 2.8 $M_{\odot}$and in blue models with differential rotation for the same masses and same V_{rot}.

of rotational velocity are similar to the rotational velocities of Hyades stars. The major effect is on the effective temperature at higher mass. The effect on the luminosity is lower, but is detectable on the higher mass. The three type of evolutionary tracks are evolved until they reach the same age, 700 Myr. Models with differential rotation have longer lifetimes on the MS phase. This means the age determination change with the addition of rotational effect in a range of masses important for the study of open cluster like Hyades,

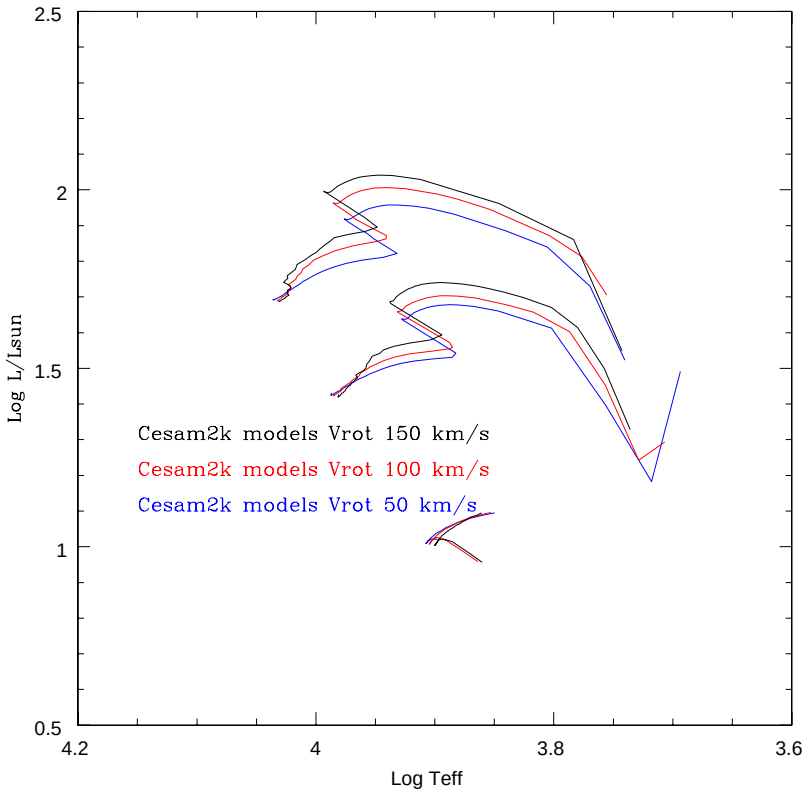

Figure 6.5: CESAM evolutionary tracks for 2.8 , 2.4 and 1.9 $M_{\odot}$. The black evolutionary tracks are calculated with differential rotation with rotational velocity of 150 km/s. The red ones with rotational velocity of 100 km/s and the blue ones with rotational velocity of 50 km/s.

Pleiades.

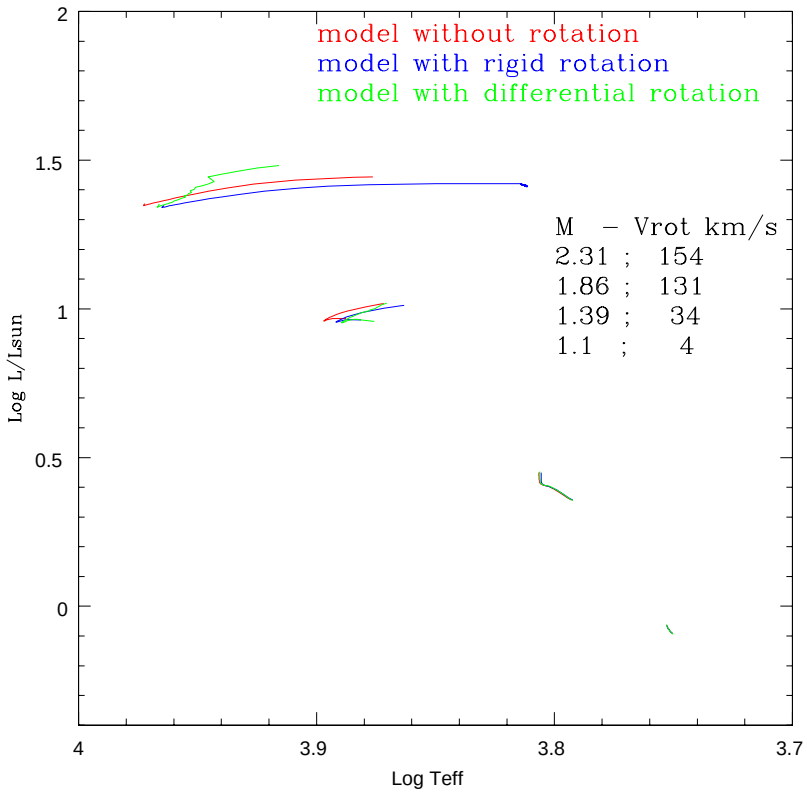

Figure 6.6: Evolutionary tracks for star mass of 1.1, 1.39, 1.86, 2.31 $M_{\odot}$with rotational velocity of 4, 34, 131, 154 km/s for rigid rotation in blue, differential rotation in green and without rotation in red in the Luminosity Temperature diagram. The tracks stops at an age of 700 Myr.

6.3 Rotation and Chemical abundances

It is well known that rotation has an influence on the surface chemical abundances. The theory of (Maeder and Zahn, 1998) is implemented in Cesam2k code, as we explained above, and here we present some models to show the effect of the rotation on chemical abundances. In 6.7, 6.8 and 6.9 and in Tables 6.1,6.2,6.2 we give the surface abundances

of ^{12}C, Fe, Mg as a function of the effective temperature for stellar mass of 0.8, 0.9, 1.0, 1.1, 1.25, 1.35, 1.5, 1.7, 2.0, 2.5 with 50 km/s rotational velocity on the main sequence for three different models: models without rotation, with rigid rotation and with differential rotation. While it is clear that the effects of the rotation are stronger for higher masses, the rotationally induced mixing is significant also in the mass regime discussed in this Thesis.

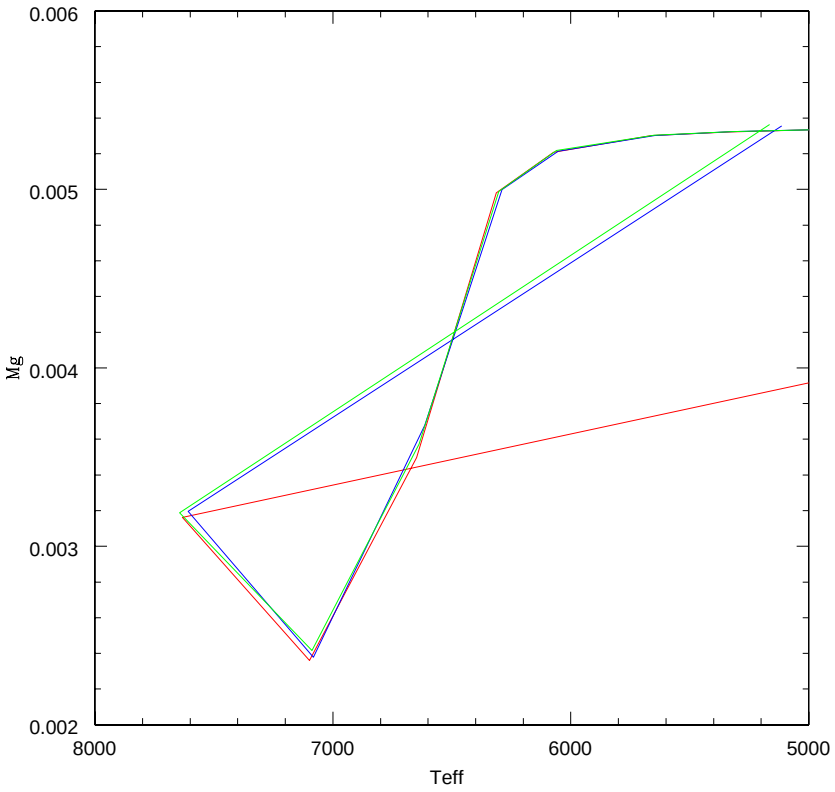

Figure 6.7: Effective temperature vs magnesium abundance in three type of models: in blue without rotation, in green with rigid rotation and in red with differential rotation. The models are done for 0.8, 0.9, 1.0, 1.1, 1.25, 1.35, 1.5, 1.7, 2.0, 2.5 $M_{\odot}$and for 50 km/s rotational velocity.

Stellar mass	without rotation	with solid rotation	with differential rotation
0.8	$5.345 \cdot 10^{-3}$	$5.343 \cdot 10^{-3}$	$5.344 \cdot 10^{-3}$
0.9	$5.334 \cdot 10^{-3}$	$5.335 \cdot 10^{-3}$	$5.336 \cdot 10^{-3}$
1.0	$5.322 \cdot 10^{-3}$	$5.323 \cdot 10^{-3}$	$5.324 \cdot 10^{-3}$
1.1	$5.301 \cdot 10^{-3}$	$5.302 \cdot 10^{-3}$	$5.305 \cdot 10^{-3}$
1.25	$5.208 \cdot 10^{-3}$	$5.215 \cdot 10^{-3}$	$5.218 \cdot 10^{-3}$
1.35	$4.980 \cdot 10^{-3}$	$4.998 \cdot 10^{-3}$	$4.989 \cdot 10^{-3}$
1.5	$3.497 \cdot 10^{-3}$	$3.679 \cdot 10^{-3}$	$3.573 \cdot 10^{-3}$
1.7	$2.359 \cdot 10^{-3}$	$2.379 \cdot 10^{-3}$	$2.415 \cdot 10^{-3}$
2.0	$3.161 \cdot 10^{-3}$	$3.195 \cdot 10^{-3}$	$3.188 \cdot 10^{-3}$
2.5	$5.350 \cdot 10^{-3}$	$5.355 \cdot 10^{-3}$	$5.363 \cdot 10^{-3}$

Table 6.1: Abundance of Magnesium for the three type of evolutionary models: without the rotation, solid rotation and differential rotation in mass unity for stellar mass (in unity of solar mass) in first column

6.4 Comparison with Geneva code

In this last years many efforts are done to understand the impact of rotational velocity on the evolution of a star. Several models were developed, involving different treatment of the 2D effects /such as the von Zeipel effect), and different physical prescriptions (magnetic field, overshoot, diffusion). Here we compare the CESAM evolutionary tracks with the Geneva stellar models with rotation, in the most recent version by (Ekström et al., 2012). This latter uses $v_{ini}/v_{crit} = 0.4$, that means at fixed star mass the rotational velocity is the 40 % of the critical one..

The comparison is shown in fig. 6.10 where we plot the evolutionary tracks for star masses of 0.8, 1.0, 2.0 and 3.0 sun mass, in red the models built with Cesam2k code and in blue the models of Geneva code (Ekström et al., 2012). We can see a significant difference in the result of the evolutionary tracks in the 2 code. This difference in luminosity and in the temperature probably is due to different physics mechanism used in the two code. The main differences among the two codes are the use of a mechanism to slow down the rotational velocity from the PMS to the ZAMS (magnetic field), the presence of 2D effects, and of overshhot implemented in the Geneva code. In Cesam2k code the models are built with rotation but without overshooting, without Von Zeipel effect and without magnetic field.

Stellar mass	without rotation	with solid rotation	with differential rotation
0.8	$1.746 \cdot 10^{-3}$	$1.746 \cdot 10^{-3}$	$1.746 \cdot 10^{-3}$
0.9	$1.743 \cdot 10^{-3}$	$1.743 \cdot 10^{-3}$	$1.743 \cdot 10^{-3}$
1.0	$1.738 \cdot 10^{-3}$	$1.739 \cdot 10^{-3}$	$1.739 \cdot 10^{-3}$
1.1	$1.731 \cdot 10^{-3}$	$1.731 \cdot 10^{-3}$	$1.732 \cdot 10^{-3}$
1.25	$1.695 \cdot 10^{-3}$	$1.698 \cdot 10^{-3}$	$1.699 \cdot 10^{-3}$
1.35	$1.609 \cdot 10^{-3}$	$1.616 \cdot 10^{-3}$	$1.612 \cdot 10^{-3}$
1.5	$0.998 \cdot 10^{-3}$	$1.068 \cdot 10^{-3}$	$1.029 \cdot 10^{-3}$
1.7	$0.637 \cdot 10^{-3}$	$0.643 \cdot 10^{-3}$	$0.656 \cdot 10^{-3}$
2.0	$0.920 \cdot 10^{-3}$	$0.932 \cdot 10^{-3}$	$0.930 \cdot 10^{-3}$
2.5	$1.751 \cdot 10^{-3}$	$1.753 \cdot 10^{-3}$	$1.755 \cdot 10^{-3}$

Table 6.2: Abundance of Iron for the three type of evolutionary models: without the rotation, solid rotation and differential rotation in mass unity for stellar mass (in unity of solar mass) in first column

Stellar mass	without rotation	with solid rotation	with differential rotation
0.8	$4.168 \cdot 10^{-3}$	$4.169 \cdot 10^{-3}$	$4.169 \cdot 10^{-3}$
0.9	$4.162 \cdot 10^{-3}$	$4.162 \cdot 10^{-3}$	$4.163 \cdot 10^{-3}$
1.0	$4.153 \cdot 10^{-3}$	$4.153 \cdot 10^{-3}$	$4.154 \cdot 10^{-3}$
1.1	$4.136 \cdot 10^{-3}$	$4.137 \cdot 10^{-3}$	$4.139 \cdot 10^{-3}$
1.25	$4.064 \cdot 10^{-3}$	$4.069 \cdot 10^{-3}$	$4.072 \cdot 10^{-3}$
1.35	$3.879 \cdot 10^{-3}$	$3.893 \cdot 10^{-3}$	$3.886 \cdot 10^{-3}$
1.5	$2.516 \cdot 10^{-3}$	$2.673 \cdot 10^{-3}$	$2.585 \cdot 10^{-3}$
1.7	$1.956 \cdot 10^{-3}$	$1.973 \cdot 10^{-3}$	$2.005 \cdot 10^{-3}$
2.0	$2.559 \cdot 10^{-3}$	$2.584 \cdot 10^{-3}$	$2.582 \cdot 10^{-3}$
2.5	$4.171 \cdot 10^{-3}$	$4.175 \cdot 10^{-3}$	$3.561 \cdot 10^{-3}$

Table 6.3: Abundance of Carbon 12 for the three type of evolutionary models: without the rotation, solid rotation and differential rotation in mass unity for stellar mass (in unity of solar mass) in first column

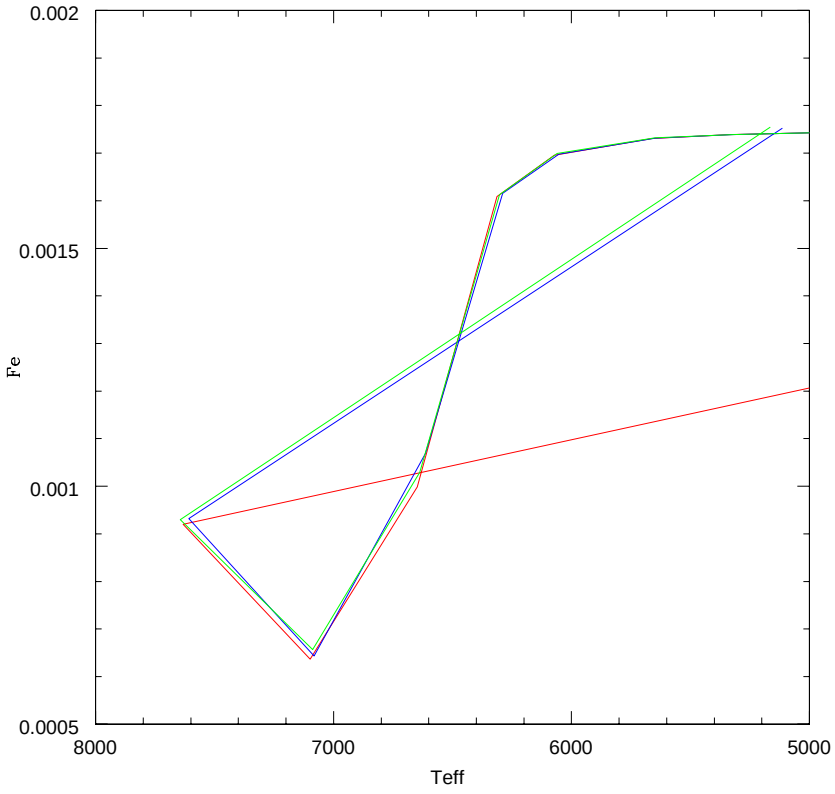

Figure 6.8: In this graphic are plotted effective temperature vs iron abudance in three type of models: in blue without rotation, in green with rigid rotation and in red with differential rotation. The models are done for 0.8, 0.9, 1.0, 1.1, 1.25, 1.35, 1.5, 1.7, 2.0, 2.5 $M_{\odot}$and for 50 km/s rotational velocity.

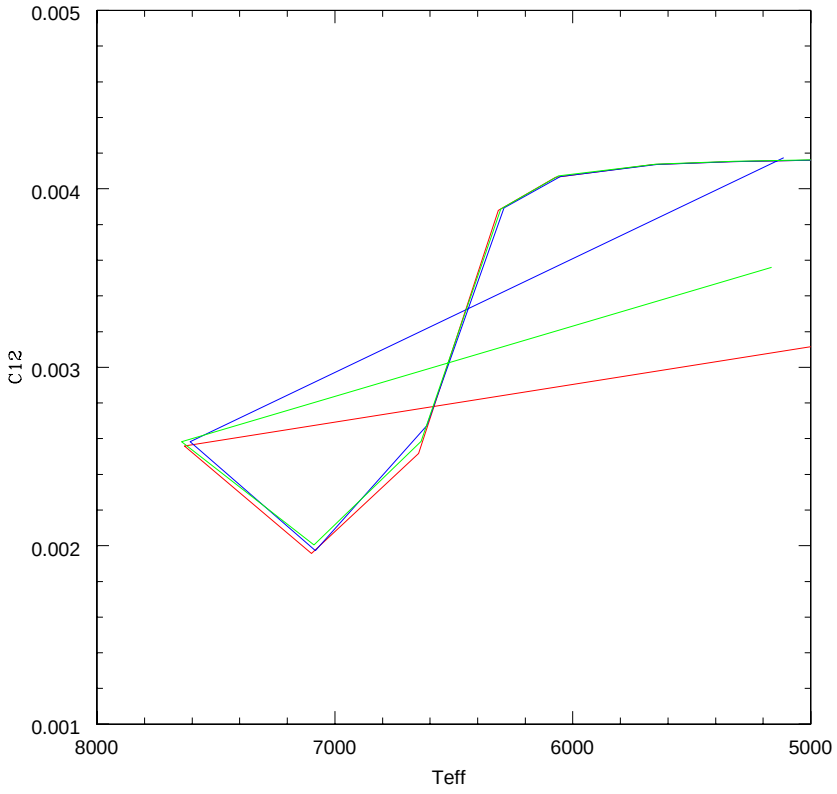

Figure 6.9: In this graphic are plotted effective temperature vs carbon 12 abudance in three type of models: in blue without rotation, in green with rigid rotation and in red with differential rotation. The models are done for 0.8, 0.9, 1.0, 1.1, 1.25, 1.35, 1.5, 1.7, 2.0, 2.5 $M_{\odot}$and for 50 km/s rotational velocity.

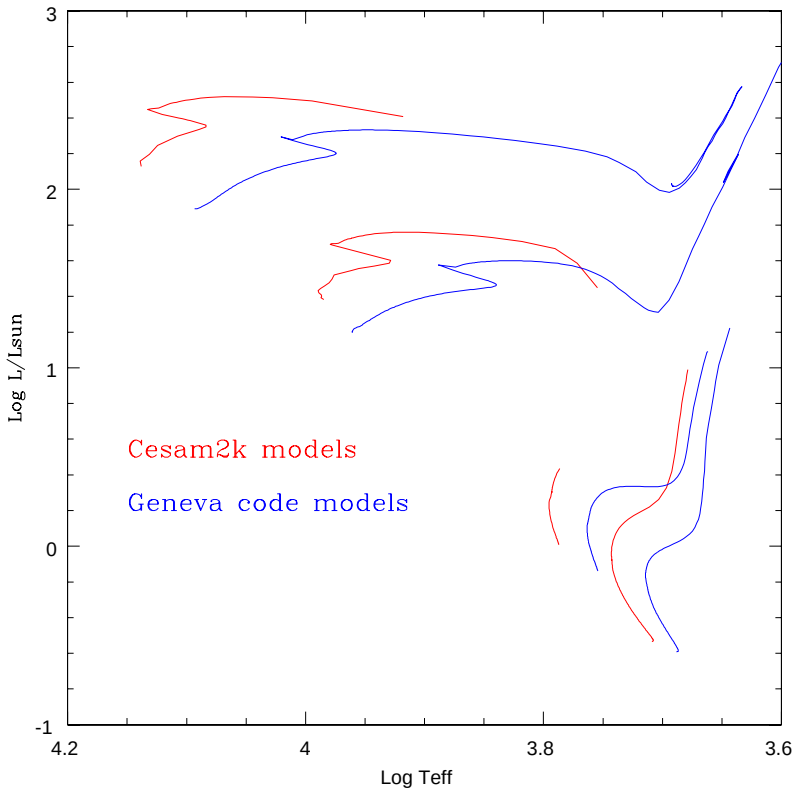

Figure 6.10: Evolutionary tracks calculated using Cesam2k code in red and using Geneva code in blue for stellar mass of 0.8, 1.0, 2.0 and 3.0$M_{\odot}$.

Chapter 7

Statistical inversion

7.1 Introduction

In this chapter we will first apply the Chandrasekar-Munch formula to derive the equatorial rotational velocity for the stars in the open clusters. The procedure will be tested on binary stars and on stars having known rotational periods and $Vsini$.

7.2 Rotational velocity estimate

As we have discussed in the chapter 3, the Chandrasekar-Munch formula give us a powerful instrument to statistically relate the observational distribution of $V_{rot}sini$ with V_{rot} under the condition we know the function describing the distribution of the projected rotational velocity. In the same chapter we show that the Tsallis distribution gives the most suitable description of the rotational velocity distribution of the Pleiades cluster. In the chapter 4 we present the data for a set of young clusters. Here we apply the Chandrasekar-Munch formula to these clusters to derive the rotational velocity distribution. To built the distributions we choose a velocity bin width related to the observational errors. The data have a typical error bar of 2-3 km/s. So we decide to adopt a bin width of 2.5 km/s. First, we built the $Vsini$ distribution histogram for the studied clusters(see 7.1 7.2 7.3 7.4 7.5).

We make use of the Tsallis distribution 3.6 for the statistical inversion of the C-M formula. We first have to derive the two parameter that characterize the distribution: σ and q. We assume normalization constant $B_q = 1$:

$$B_q = \int_0^\infty y\left[1-(1-q)\frac{y^2}{\sigma^2}\right]^{\frac{1}{1-q}} \qquad B_q = \frac{\sigma^2}{4-2q} \tag{7.1}$$

It is evident that for the computation of the constant B_q is necessary to know the two paramenters σ and q. To derive them, we fit the cumulative Tsallis distribution of our data set 7.2 using a χ^2 test:

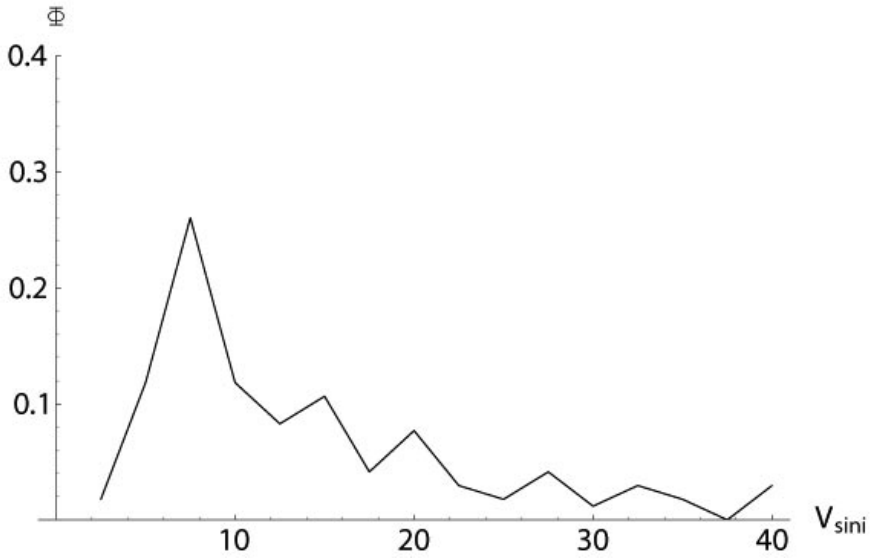

Figure 7.1: The plot represents the histogram of rotational velocity projected for the Pleiades. In the abscissa axis there is the rotational projected velocity in km/s and in the ordinate there is the number of stars per bin.

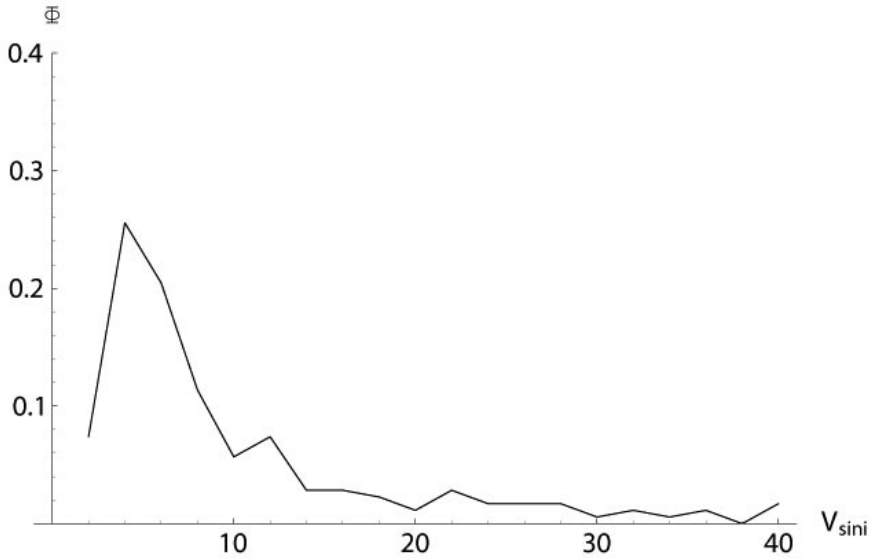

Figure 7.2: The analogous of fig. 7.1 for the Hyades

$$\Phi_q(y) = \frac{\int_0^y y\left[1-(1-q)\frac{y^2}{\sigma^2}\right]^{\frac{1}{1-q}}}{\int_0^\infty y\left[1-(1-q)\frac{y^2}{\sigma^2}\right]^{\frac{1}{1-q}}} \tag{7.2}$$

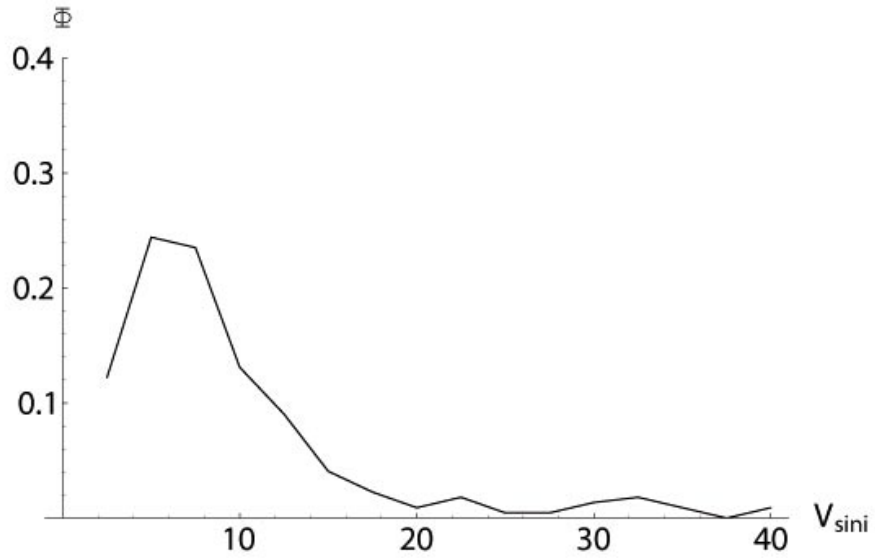

Figure 7.3: The analogous of fig. 7.1 for the Praesepe

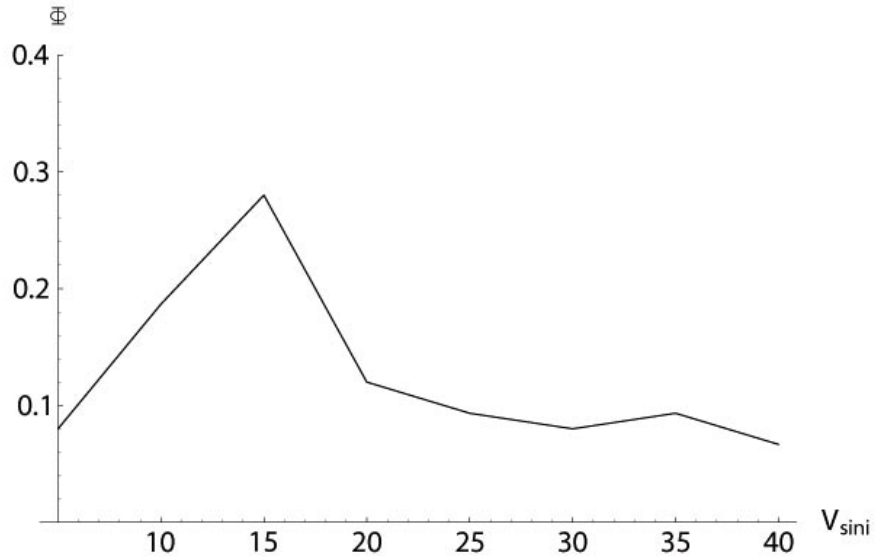

Figure 7.4: The analogous of fig. 7.1 for the Alpha Persei

Figs 7.6 7.7 7.8 7.9 7.10 show the cumulative distributions obtained from the data sets (dot points) and the best fit for the cumulative distributions of the Tsallis distributions.

The best fit parameters for all the clusters are given in table 7.2 together with the values of the peak of the distribution (see 3.5).

This statistical results are obviously affected by uncertainties. To derive the uncertainties on the parameters, we make use of a Montecarlo simulation, where about 30% of the data are substituted generating new values with a gaussian distribution inside the

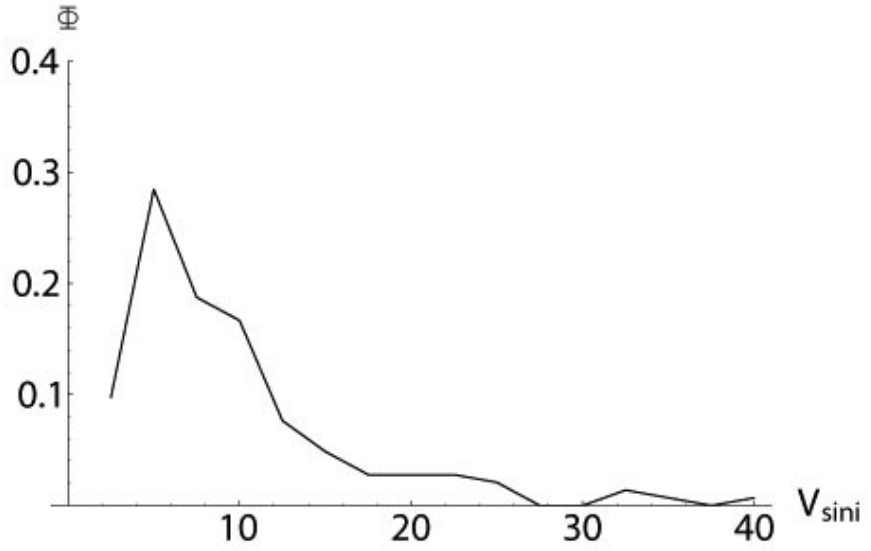

Figure 7.5: The analogous of fig. 7.1 for the Blanco 1

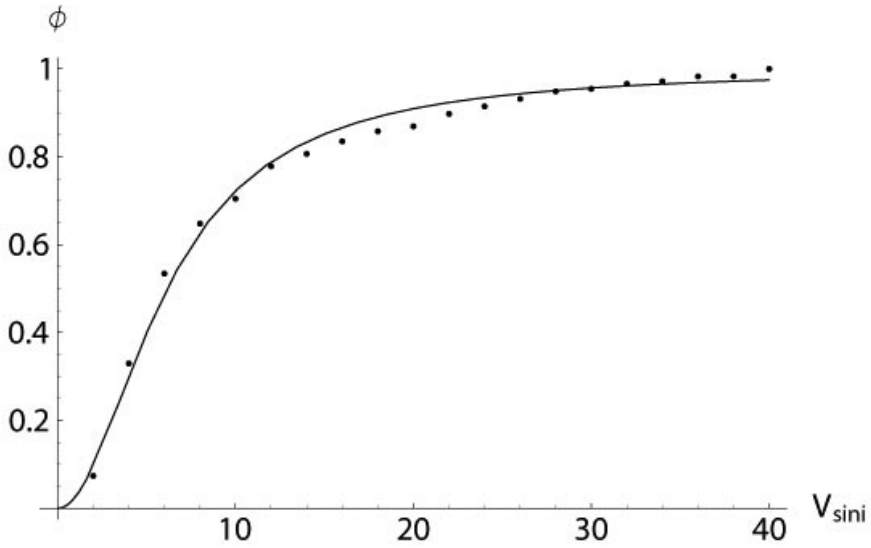

Figure 7.6: Cumulative distribution of data set for Hyades cluster (dots) and the cumulative distribution of Tsallis with the best fit parameter. In the abscissa axis there is the rotational projected velocity in km/s and in the ordinate axis there is the count of cumulative distribution Φ.

expected uncertainties. About 100 simulations are generated in that way for each cluster, and the parameters of the Tsallis distribution are re-derived following the same fitting procedure applied to the data. Finally the derived values are averaged and the stanadard deviation is assumed as uncertainty on the fit. The results are summarized in Table 7.2.

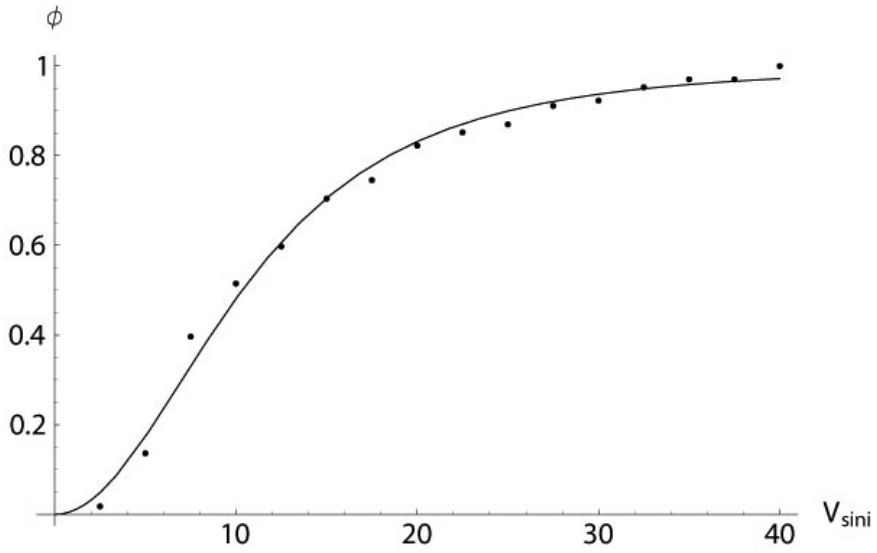

Figure 7.7: The analogous of Fig 7.6 for the Pleiades

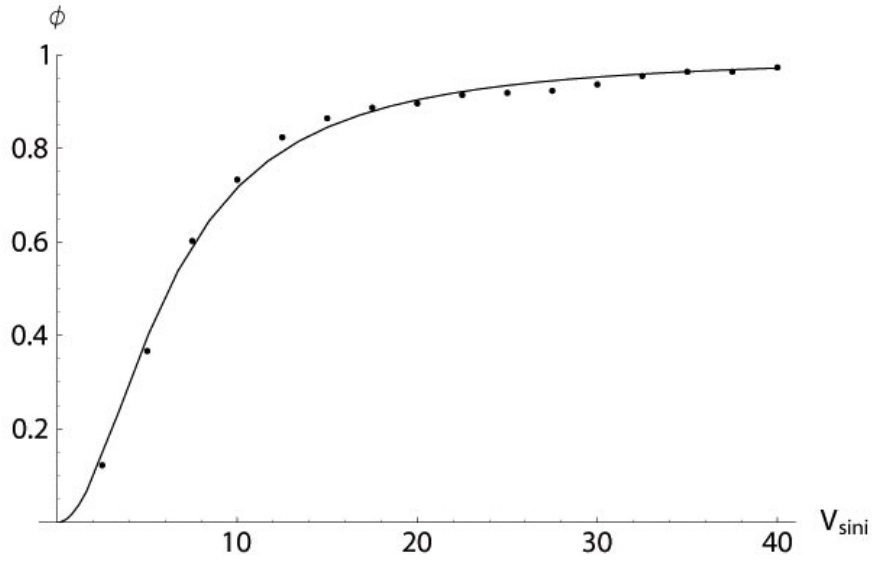

Figure 7.8: The analogous of Fig 7.6 for Praesepe.

7.3 Statistical inversion and test

In the following Chapter we will use the the Tsallis distribution 3.6 with the parameters derived above to solve the integral-derivative equation 3.3 to estimate the true rotational velocity for each cluster star. In turn, the derived velocity will be used to estimate the age of the clusters by means of a comparison with the stellar models calculated with Cesam2k code. This will be the discussed in the next Chapter. Here we test the procedure using

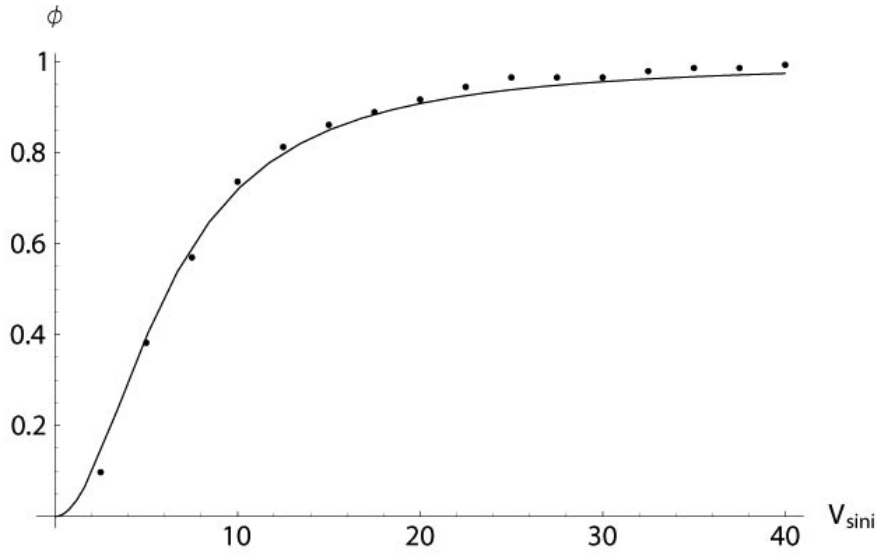

Figure 7.9: The analogous of Fig 7.6 for Blanco1.

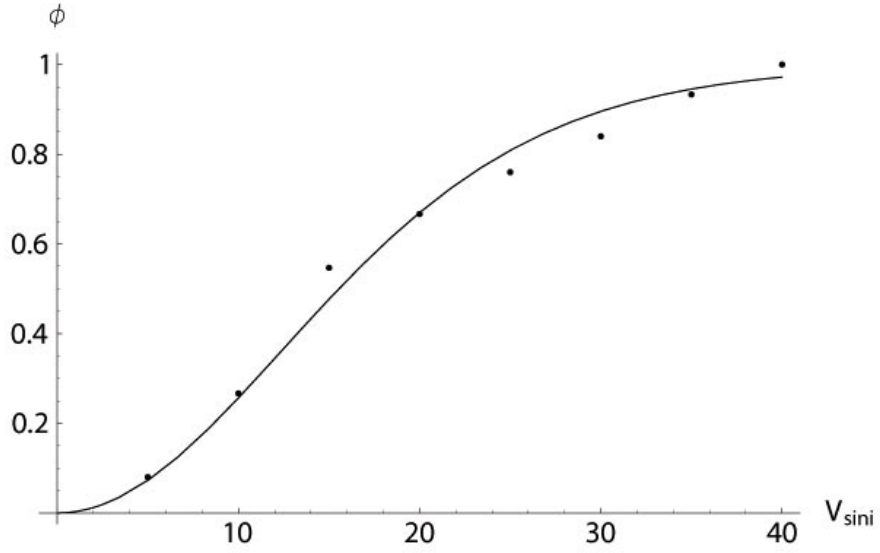

Figure 7.10: analogous of Fig 7.6 for Alpha Persei.

a) binaries with well derived stellar parameters and inclination; b) a small sample of stars having observationally derived rotational periods and $V sini$.

7.3.1 Testing the method using Hyades wide binaries

In an eclipsing binary system we know all the orbital parameters. In the Hyades, 5 binary systems have known orbital parameters and projected rotational velocity of the primary

Parameter	Alpha Persei	Pleiades	Blanco 1	Hyades	Praesepe
q	1.14	1.38	1.51	1.51	1.54
σ	16.83	8.75	4.27	4.27	4.02
y_{peak}	12.34	6.91	3.5	3.5	3.34

Table 7.1: Parameters of the Tsallis distribution, namely q and σ calculated via χ^2 test and the peak position of the distribution for each cluster.

Parameter	Alpha Persei	Pleiades	Blanco 1	Hyades	Praesepe
q	1.14 ± 0.04	1.38 ± 0.02	1.51 ± 0.02	1.51 ± 0.03	1.54 ± 0.02
σ	16.83 ± 0.03	8.75± 0.02	4.27± 0.01	4.27 ± 0.01	4.02± 0.01

Table 7.2: Results of statistical analysis presented in the previous table and the errors bar computed via Montecarlo simulations for each clusters.

Name HIP	V_{rot} sin i (km/s)	i (degree)	V_{rot} (km/s)	Stat V_{rot} (km/s)
20019	10.7 ± 2.7^a	85.71^e	10.7 ± 2.7	15 ± 2
20087	100.8 ± 5.0^b	125.08 ± 0.50^f	123.2 ± 6.2	129 ± 2
20661	16.3 ± 1.0^a	124.97 ± 0.92^g	19.9 ± 1.2	21 ± 2
20885	3^c	92.35 ± 0.24^h	3	3 ± 2
20894	80^d	46.2 ± 1.0^h	110.8	104 ± 2

(a) From Mermilliod et al. (2009)

(b) From Reiners (2003)

(c) From Gray (1982)

(d) From Abt & Morrell (1995)

(e) From Schiller & Milone (1987)

(f) From Torres et al. (1997a)

(g) From Torres et al. (1997b)

(h) From Torres et al. (1997c)

(b) (c) (d) are in WEBDA database

(c) (d) (e) don't give error bars

Table 7.3: Well known binary systems belonging to the Hyades cluster. Column 1 gives the Hipparcos ID of the primary stars with their projected rotational velocity in column 2. Column 3 gives the value of the inclination i used to get their V_{rot} done in column 4. Column 5 presents our estimated V_{rot} from the statistical inversion.

component. If we assume that in these system the rotational axes is perpendicular to the orbital plane, then the rotational axes inclination i can be derived from the orbital inclination. In this way we can estimate the true rotational velocity. In addition, for these stars we can compare the results of the statistical inversion of C-M formula on V_{rot} with the values derived using the orbital value of the inclination The two estimate of the true rotational velocity are summarized in Table 7.3. The two estimates are in good agreement.

7.3.2 Testing the procedure using stars of known rotational Period

The second test on the procedure is a comparison with the properties of stars of known rotation periods in the Hyades. We select stars for which we have the measurements of projected rotational velocity ($V_{rot}sini$) and the rotational period (P) at the same time. For this purpose we find the stars in common between the catalogue of (Röser et al., 2011), for the membership, the catalogue of (Mermilliod et al., 2009), to have the projected rotational velocity, and (Radick et al., 1987) and (Delorme et al., 2011) for the rotational period. The set we get count only of about 20 stars. For this stars we estimate the equatorial rotational velocity with statistical inversion and also from the period. Following the results of work (Kervella et al., 2004), we have a relation between the colour of the stars and the radius of the star. Remembering the relation between rotation period and equatorial velocity in the relation 7.3

$$V_{eq} = \frac{2\pi R}{P} \tag{7.3}$$

where V_{eq} is the equatorial velocity, R is the radius of the star and P is the period. Now we have two different estimate of the equatorial velocity, one from the statistical inversion and one from the period. They are compared in Fig. 7.11

As we see from the plot 7.11, there is a mild correlation between the two different estimates. Even if large differences are present, the presence of a correlation points in favour of a reasonable estimate of equatorial velocity.

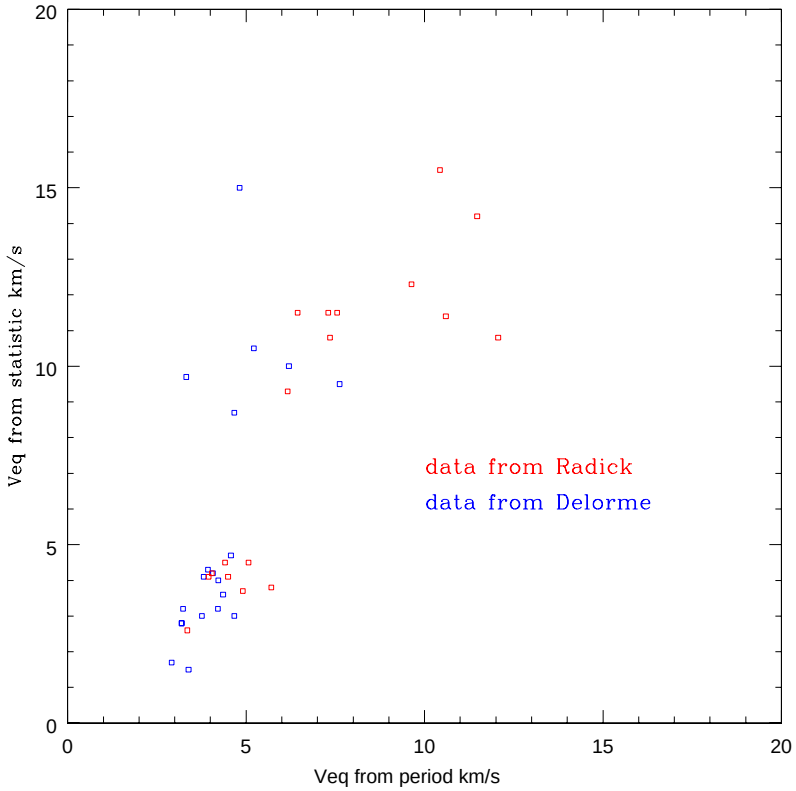

Figure 7.11: Equatorial rotational velocity estimate from the statistical inversion vs the estimate from the rotational period.

Chapter 8

Age estimate

In this chapter, first we will derive the age of our clusters using the stellar models including the rotation calculated in the previous chapters. Then we will discuss the age-rotational velocity relation of the cluster sample

8.1 Deriving the age of the clusters

In our clusters, stars in the evolved part of the main sequence have different rotational velocities. To derive the age of each star, we make use of set of stellar models calculated ad-hoc in the mass range of interest with the appropriate rotational velocity, and then we interpolate to derive the mass and the age.

8.1.1 The age of the Hyades

Fig 8.1 presents the turnoff region of the Hyades where stars of different rotational velocities are shown. The rotational velocities at the turnoff are ranging from V_{rot} higher than 200 km/s to 50 km/s.

In the 8.2 we plot the data of the Hyades in the turn off region with stellar models having rotational velocity of 50 and 150 km/s. We built different sets of models with rotational velocity from 0 km/s to 250 km/s and for different metallicities with the open cluster for which we want to have an age-mass determination.

Using the interpolation procedure on the new stellar models, we obtain a new age determination of 696 $\pm$ 100 Myr with a mass at the turn off of 2.7 $M_{\odot}$. The uncertainty on the age determination is obviously not related to a spread in age. This will be discuss this in the next section.

8.1.2 The age of the Hyades using Cesam with different physics

In the table 8.1 we compare our determination with the previous age determinations obtained using Cesam2k.

In (Perryman et al., 1998) Cesam isochrones with and without overshooting are used together with the first release of Hipparcos data to study the colour-magnitude diagram for Hyades open cluster (see 8.3)

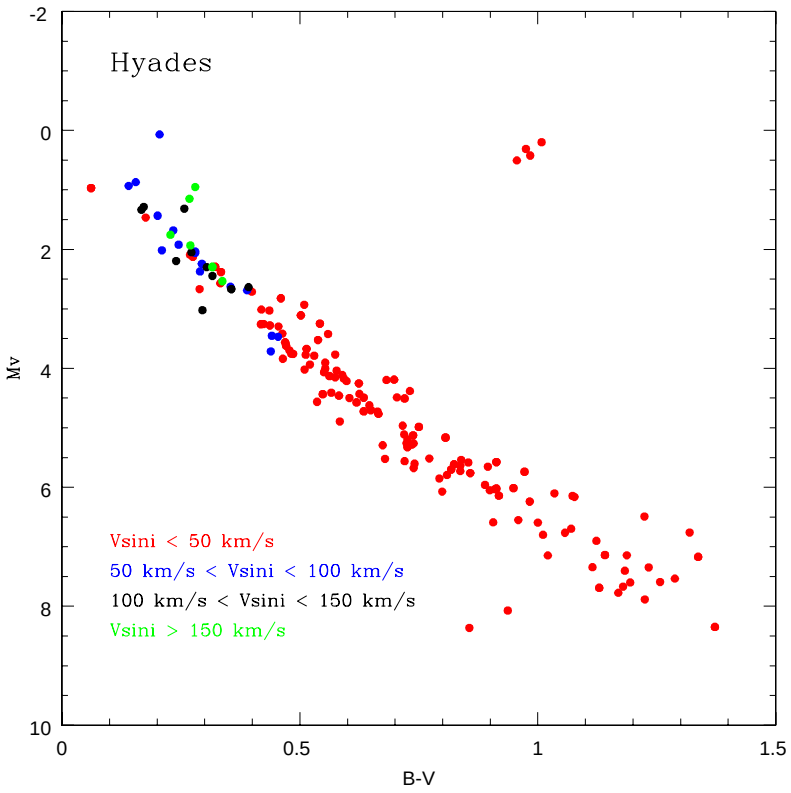

Figure 8.1: Colour diagram for Hyades cluster. The stars have different colour showing the rotational velocity: red for V_{rot} less than 50 km/s; blue for V_{rot} between 50 and 100 km/s; black for V_{rot} between 100 and 150 km/s; green for V_{rot} greater than 150 km/s.

The Helium abundance is estimated to be $Y = 0.26 \pm 0.02$ and an age of $625 \pm 50 Myr$ with overshooting. The authors adopted the calibration from (Alonso et al., 1996) which allows derivation of the $B-V$ colour as a function of T_{eff} and $[Fe/H]$ in order to have the transformation from the theoretical plane $(M_{bol}, logT_{eff})$ to the observational plane $(M_V, (B-V)$. In (Lebreton et al., 2001) Cesam stellar models are used for an analysis on 5 binary system in Hyades cluster in order to have constraints on cluster Helium content.

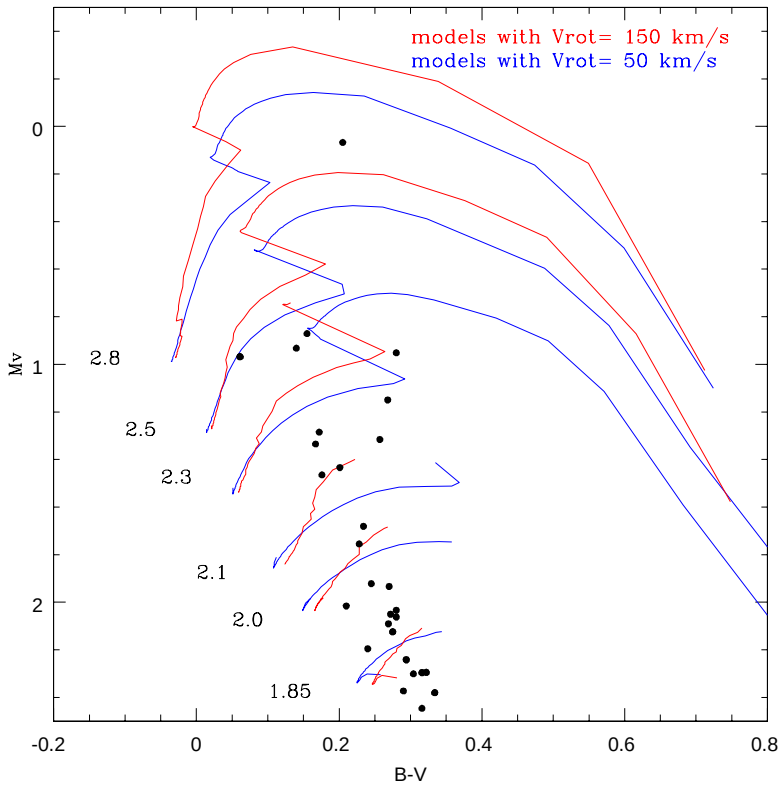

Figure 8.2: Data (black dots) for Hyades cluster in the turn off region with the models built with Cesam2k code. For clarity only a subset of the calculated models are plotted

The results of the work is an estimate of the Helium content, of about $Y = 0.255 \pm 0.009$ and of an age of 650 Myr with overshoot.

In the work of (Morel and Thévenin, 2002) the authors use Cesam models for another type of analysis. They focus on the role of the radiative diffusivity generated by the photon-ion collisions that is not presently taken into account in the microscopic diffusion coefficients. The photon-ion collisions are an efficient physical process that inhibits the large sedimentation of helium and heavy elements in outer layers of main sequence star

Cesam models	Reference	Age in Myr
Overshoot	Perryman et al.	625
overshoot	De Bruijne et al. 2001	625
No Overshoot, Y=0.26	Lebreton et al. 2001	650
Diffusion	Morel & Thévenin 2002	570
Rotation, no overshoot	This study	696

Table 8.1: Summary of the age determinations for the Hyades cluster done with Cesam2k code.

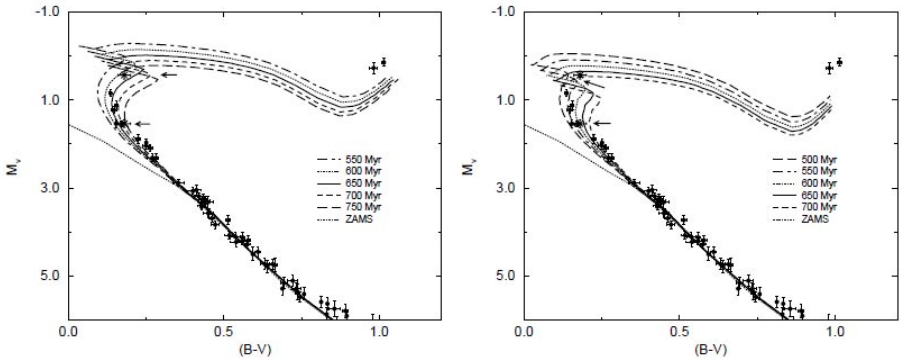

Figure 8.3: This plot is taken from Perryman et al. (1998). It shows the 69 single stars selected on the Hyades cluster. The isochrones are calculated with overshooting on left panel and without overshooting on right panel.

models. The ingredients for their model are taken from (Lebreton et al., 2001) and they don't use the overshooting. The cluster system that they use like a laboratory is Hyades cluster. The results for the colour-magnitude diagram is plotted in figure 8.5.

As we see in 8.4 the effect of the rotation on the age is of the order of 50 Myr. This estimate was made correcting the the colors and magnitudes of the isochrones calculated for Vsini=0 following the work of (Pérez Hernández et al., 1999) (see 8.4). These corrections are dependent on angular velocity and inclination angle.

(Lebreton et al., 2001) isochrones calculated without overshooting lead to an age estimated of 550 Myr, the inclusion of elemental diffusion in (Morel and Thévenin, 2002) leads to the age of 570 ± 15 Myr. This means the effect of elemental diffusion increase the age estimate.

We see clearly that the introduction of the rotation in the code give us an age determination about 15 % older than previous determinations.

8.1.3 Age determination of the Pleiades, Praesepe and Alpha Persei

Figs 8.6, 8.7, 8.8 presents the colour-magnitude diagrams of the studied clusters where the rotation velocity range is shown.

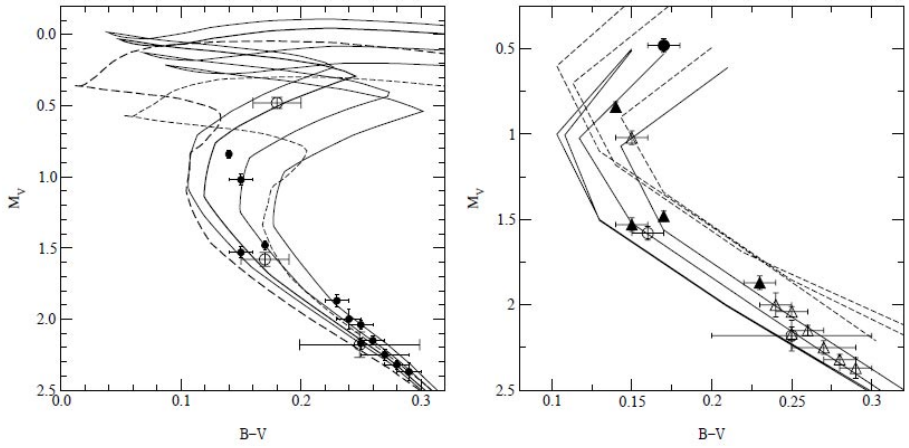

Figure 8.4: Turn off region for Hyades cluster (left panel). The data are from de Bruijne et al. (2001). The isochrones (with $[Fe/H] = 0.14$ and $Y = 0.26$) are with overshooting with ages (from left to right) of 600 Myr, 625 Myr, 700 Myr and 750 Myr for continuous line. The dashed lines are the isochrones with ages 550 Myr and 600 Myr and are without overshooting. The right panel shows the effect of rotation on the isochrones. From left to right $v_e sini = 0, 50, 100, 150 km/s$ and $i = 90°$ at $M_V = 0.5$.

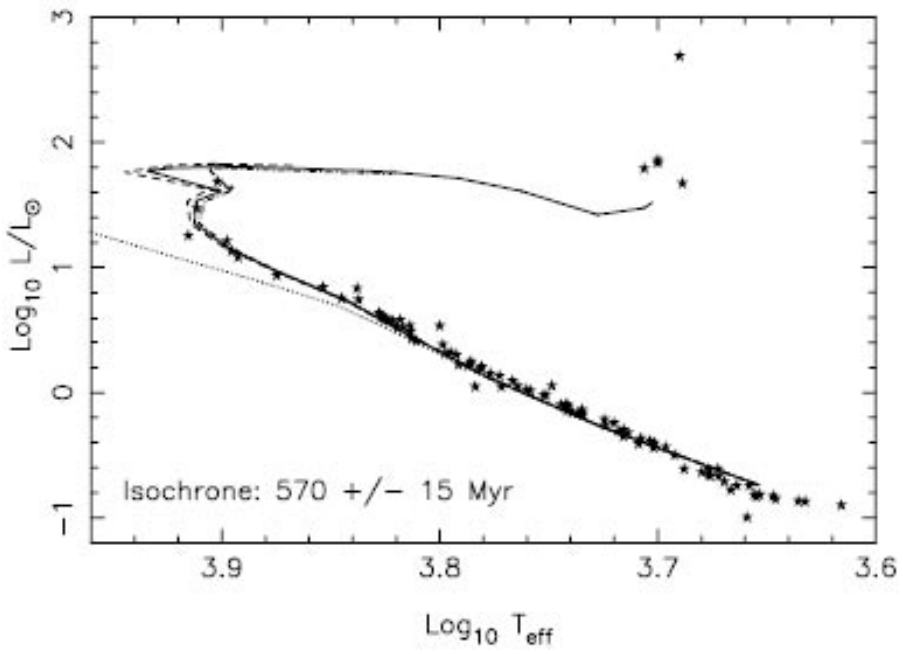

Figure 8.5: This plot is by Morel & Thévenin 2002. It shows the effect on Luminosity - effective Temperature diagram of elemental diffusion.

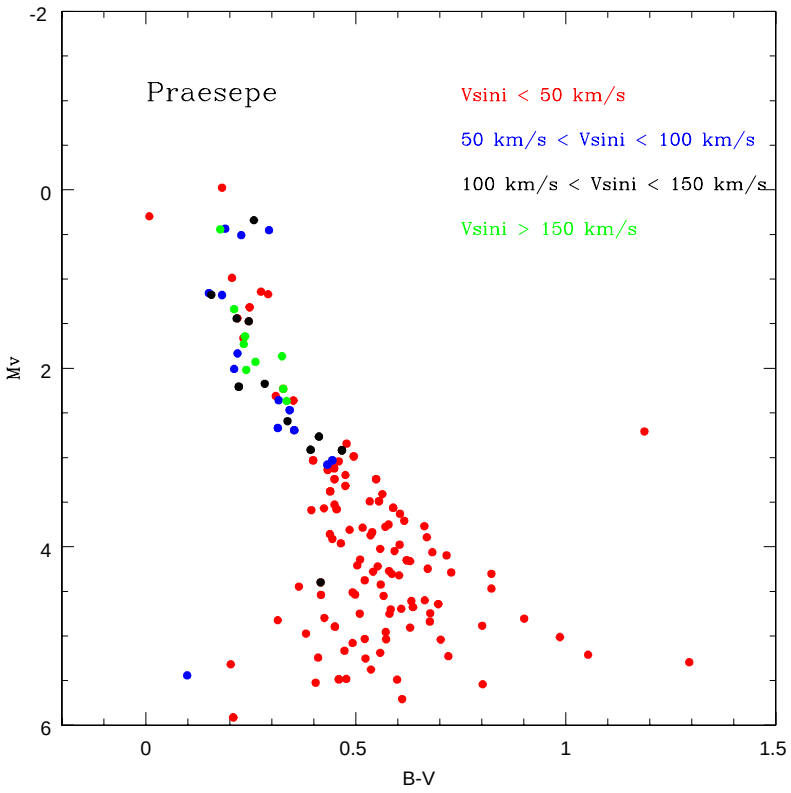

Figure 8.6: Colour diagram for Praesepe cluster. Red dots indicate stars V_{rot} less than 50 km/s; blue, stars V_{rot} between 50 and 100 km/s; black dots are stars with V_{rot} between 100 and 150 km/s; green dots are stars with V_{rot} greater than 150 km/s.

We make use of the evolved part of the main sequence to derive the age of the clusters, interpolating among the stellar masses with appropriate rotational velocities. The results are summarized in the table 8.2. For these clusters the previous age determinations are not done with Cesam2k code and are taken from van Leeuwen 2009 for Praesepe cluster and from (**?**).

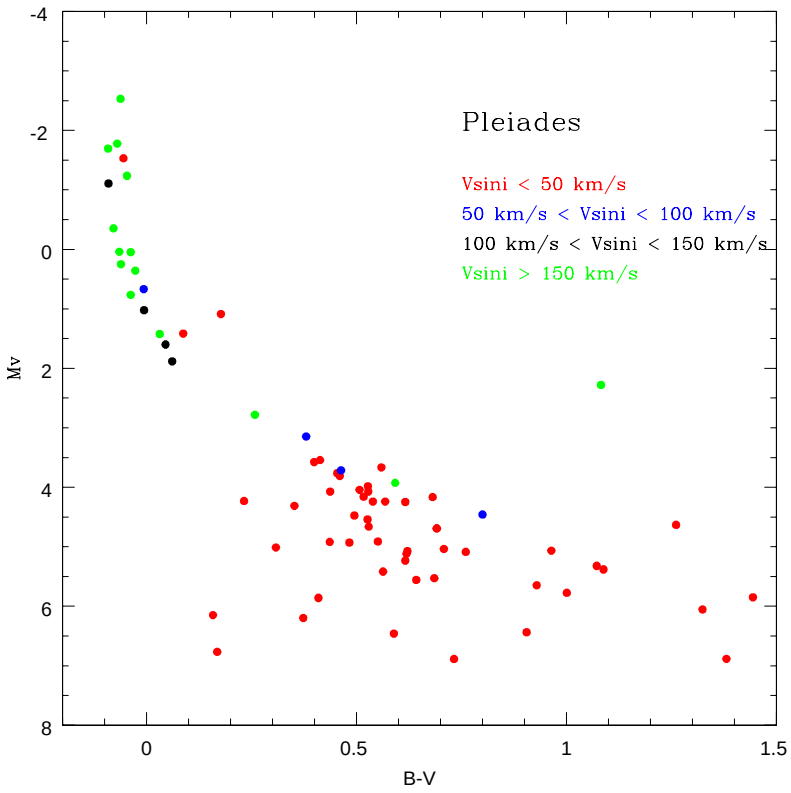

Figure 8.7: Colour diagram for Pleiades cluster. Different colours indicate the rotational velocity: red for V_{rot} less than 50 km/s; blue for V_{rot} between 50 and 100 km/s; black for V_{rot} between 100 and 150 km/s; green for V_{rot} greater than 150 km/s.

8.2 Discussion on the age determination

Our age estimates have large dispersion. This is possibly due to the fact that stars at the turnoff have similar masses, but rotational velocities ranging from 50 to 250 km/s as an effect of the inclination. We partially accounted for this using the Tsallis distribution.

Another effect that is not accounted for in Cesam2k models is the Von Zeipel effect. Slow rotators in the turn off region might not show the equatorial velocity, having low

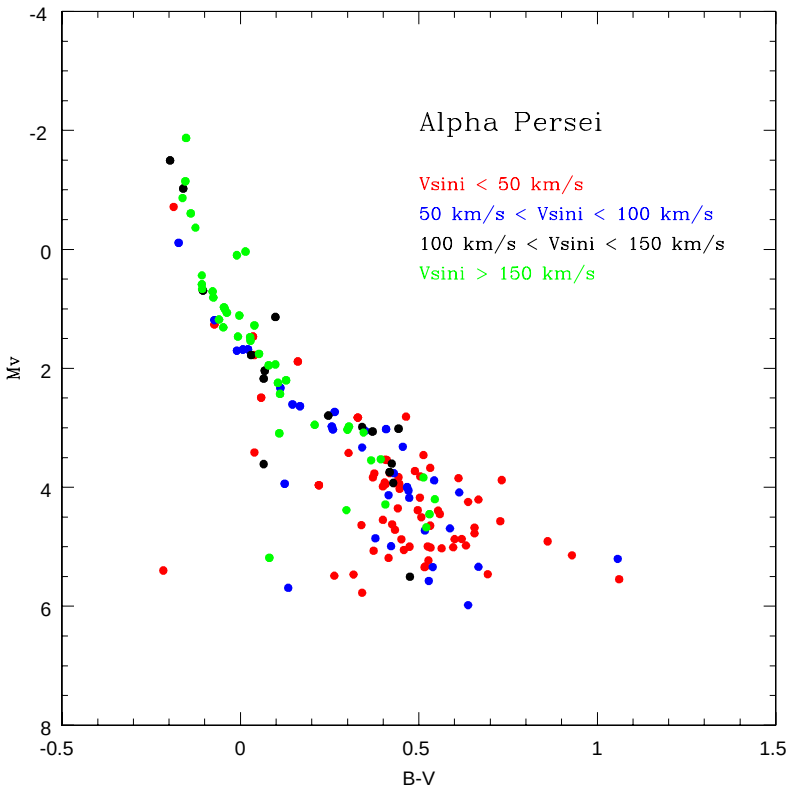

Figure 8.8: Colour diagram for Alpha Persei cluster. Different colours indicate the rotational velocity: red for V_{rot} less than 50 km/s; blue for V_{rot} between 50 and 100 km/s; black for V_{rot} between 100 and 150 km/s; green for V_{rot} greater than 150 km/s.

values of the inclination of spin axis.

If the star rotate rapidly, we know from the Von Zeipel effect that the star flatten and the pole region rotates at a velocity lower than the equatorial zone, but the temperature is hotter on the pole zone in comparison to the equatorial zone. This introduces a spread in color at the top of the main sequence, with slow rotators often hotter that faster rotators. The spread would be reduced applying a correction for the Von Zeipel effect. But the

Cluster	Previous age in Myr	this study age in Myr
Alpha Persei	75	120 ± 50
Pleiades	115	229± 80
Praesepe	794	812± 100

Table 8.2: Resume of the age determination for the Alpha Persei, Pleiades and Praesepe cluster done with Cesam2k code.

code Cesam2k is one dimensional evolutionary code and the effect is 2D. We calculate a correction for the one dimensional code temperature to account for this effect. The code provide us many parameter and the most important is the Luminosity of the star. When the star rotate we know from the Von Zeipel effect that the spherical symmetry is broken: the star flattens at the poles. We assume that the shape of the star becomes ellipsoidal. For the luminosity we have:

$$L = \sigma T^4 S$$

where S is the surface of the ellipsoid which is given by:

$$S = 4\pi R_{eq}^2 - 2\pi R_{eq}^2 F(e)$$

where the F(e) is a function of the eccentricity and it is

$$F(e) = 1 - (1 - e^2)\frac{arcSinh(e)}{e}$$

The eccentricity e is:

$$e = \sqrt{\frac{R_{eq}^2 - R_p^2}{R_{eq}^2}}$$

We know that the rotational velocity and angular velocity are related by:

$$\Omega = \frac{V_{eq}}{R_{eq}}$$

The equation for the energy equilibrium between pole zone, where is only the gravitational potential, and the equatorial zone, where we have also the rotational potential:

$$\frac{GM}{R_p^2} = \frac{V_{GM}}{R_{eq}^2} + \frac{1}{2}\Omega^2 R_{eq}^2$$

These equations can give us the polar and equatorial radius. We can use these quantities in the equation 2.3 and 2.4 of the effect Von Zeipel in order to have the polar and equatorial termperature for a given star that rotate at V_{eq}.

8.3 Age-rotational velocity relation

In this section, we discuss the relation age-rotational velocity for the cluster sample, using the statistical analysis of the the projected rotational velocity and the age estimates from the previous section.

In previous chapters, we derive the velocity distribution of the stars in the clusters using the Tsallis distribution. The peak of the distribution give the characteristic velocity of the system.

Using our age estimates for the clusters and literature values for Blanco 1, we fit a relation:

$$Log(V_{rot}) = aLog(t) + b$$

Where V_{rot} is the peak position of the rotational velocity distribution, t is the age of open cluster and a and b are the fit parameters. We found $a = -0.54$ that is very near to the power of the Skumanich law (see Fig 8.9 where the data and the results of the fit are shown).

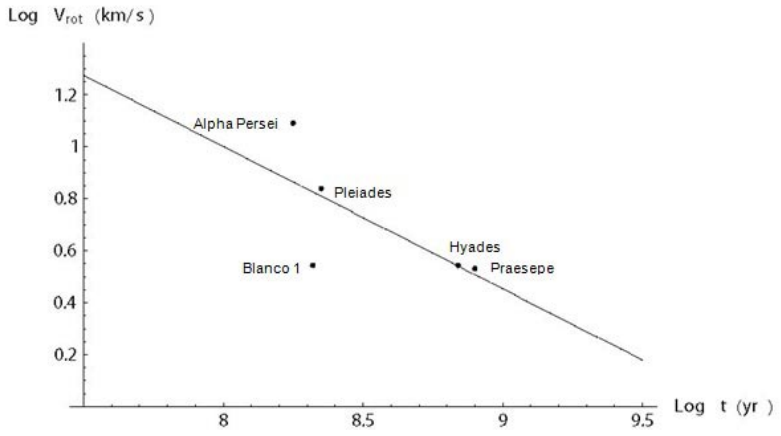

Figure 8.9: Peak rotational velocity of each cluster distribution vs the age.

Conclusions

In this PhD thesis we the study of rotation and it's influence on the interpretation of the characteristic of the open clusters, in particular for 5 clusters: Hyades, Praesepe, Pleiades, Blanco 1 and Alpha Persei. In particular, we will test the implementation of the rotational velocity in the stellar evolutionary code Cesam2K, calibrating the diffusion coefficients; we will calculate suitable sets of stellar models with ad-hoc rotational velocity to reproduce the data of the selected open clusters. Finally we will apply these models to the determination of the age of these clusters. In Chapter 1 we describe the general design of the Gaia mission, how it is organized and what kind of scientific problems it handles: the study of the Milky Way formation and evolution. We focus on the importance of the accurate stellar models for the mission. In Chapter 2 we discuss the rotation in stars: the status of the research in this field and in particular why the rotation is important in the study of relatively young low mass stars. We present the effect of rotation on the HR diagram, on the surface chemical abundances. Finally we discuss the von Zeipel effect. In Chapter 3 we present the observational framework, presenting the methods to measure the stellar rotation velocity. In the same chapter we discuss the Chandrasekhar-Munch method to statistically invert the projected rotational velocity distribution. In Chapter 4 we select from existing Catalogs, suitable data for 5 open clusters, having accurate memberships, magnitudes, colours, distances, and projected rotational velocities. We focus on Hyades, Praesepe, Pleiades, Blanco 1, Alpha Persei. In Chapter 5 we present the evolutionary code Cesam2k where the rotation was implemented and tested. In Chapter 6 we present the grids of stellar models at changing rotational velocities to be compared with the observations of our sample of open clusters. These models will be compared with existing grids of stellar models with rotation. In Chapter 7 we discuss how we obtain the true rotational velocity from the projected rotational velocity, the statistical inversion, its test with wide binary systems in Hyades cluster and using low mass stars having both $V sini$ determinations and rotational periods. In Chapter 8 we make use of the Cesa2k stellar models to derive the age of the open clusters. Finally we will verify whether the usual age-velocity relation (the Skumanich law) is verified.

We obtained an new age determinations for the open clusters we studied. We discuss on thi new determination, the source of possible errors and the trand of the new models with rootations. With this new age determinations we apply a simple linear fit to the relation between age and the peak position of the projected rotational velocity distributions that we discuss in the Chapter 7. We obtained a power law very near to the Skumanich law, but the diffence consist in the low statistical points. But this PhD work is essentially exploratory work on the effect of the rotation and so we discuss many aspect of this influence that remain very important in the study of open clusters.

Bibliography

Abney, W. D. W.: 1877, *MNRAS* **37**, 278

Adelberger, E. G., Austin, S. M., Bahcall, J. N., Balantekin, A. B., Bogaert, G., Brown, L. S., Buchmann, L., Cecil, F. E., Champagne, A. E., de Braeckeleer, L., Duba, C. A., Elliott, S. R., Freedman, S. J., Gai, M., Goldring, G., Gould, C. R., Gruzinov, A., Haxton, W. C., Heeger, K. M., Henley, E., Johnson, C. W., Kamionkowski, M., Kavanagh, R. W., Koonin, S. E., Kubodera, K., Langanke, K., Motobayashi, T., Pandharipande, V., Parker, P., Robertson, R. G., Rolfs, C., Sawyer, R. F., Shaviv, N., Shoppa, T. D., Snover, K. A., Swanson, E., Tribble, R. E., Turck-Chièze, S., and Wilkerson, J. F.: 1998, *Reviews of Modern Physics* **70**, 1265

Alecian, G. and Michaud, G.: 2005, *A&A* **431**, 1

Alecian, G., Michaud, G., and Tully, J.: 1993, *ApJ* **411**, 882

Alexander, D. R. and Ferguson, J. W.: 1994, *ApJ* **437**, 879

Allen, L. E. and Strom, K. M.: 1995, *AJ* **109**, 1379

Alonso, A., Arribas, S., and Martinez-Roger, C.: 1996, *A&A* **313**, 873

An, D., Terndrup, D. M., Pinsonneault, M. H., Paulson, D. B., Hanson, R. B., and Stauffer, J. R.: 2007, *ApJ* **655**, 233

Angulo, C., Arnould, M., Rayet, M., Descouvemont, P., Baye, D., Leclercq-Willain, C., Coc, A., Barhoumi, S., Aguer, P., Rolfs, C., Kunz, R., Hammer, J. W., Mayer, A., Paradellis, T., Kossionides, S., Chronidou, C., Spyrou, K., degl'Innocenti, S., Fiorentini, G., Ricci, B., Zavatarelli, S., Providencia, C., Wolters, H., Soares, J., Grama, C., Rahighi, J., Shotter, A., and Lamehi Rachti, M.: 1999, *Nuclear Physics A* **656**, 3

Artyukhina, N. M.: 1972, *Soviet Ast.* **16**, 317

Asplund, M., Carlsson, M., Garcia Perez, A. E., and Kiselman, D.: 2000, in *IAU Joint Discussion*, Vol. 8 of *IAU Joint Discussion*

Attridge, J. M. and Herbst, W.: 1992, *ApJ* **398**, L61

Aufdenberg, J. P., Mérand, A., Coudé du Foresto, V., Absil, O., Di Folco, E., Kervella, P., Ridgway, S. T., Berger, D. H., ten Brummelaar, T. A., McAlister, H. A., Sturmann, J., Sturmann, L., and Turner, N. H.: 2006, *ApJ* **645**, 664

Bailer-Jones, C. A. L., Smith, K. W., Tiede, C., Sordo, R., and Vallenari, A.: 2008, *MNRAS* **391**, 1838

Balachandran, S.: 1995, *ApJ* **446**, 203

Balachandran, S. C., Mallik, S. V., and Lambert, D. L.: 2011, *MNRAS* **410**, 2526

Barnes, S. A.: 2003, *ApJ* **586**, 464

Bastian, N. and de Mink, S. E.: 2009, *MNRAS* **398**, L11

Baumgardt, H., Dettbarn, C., and Wielen, R.: 2000, *A&AS* **146**, 251
Baxter, E. J., Covey, K. R., Muench, A. A., Fűrész, G., Rebull, L., and Szentgyorgyi, A. H.: 2009, *AJ* **138**, 963
Beck, P.: 2008, *Journal of Physics Conference Series* **118(1)**, 012046
Benz, W. and Mayor, M.: 1984, *A&A* **138**, 183
Bertelli, G., Nasi, E., Girardi, L., and Marigo, P.: 2009, *A&A* **508**, 355
Bertelli, G., Nasi, E., Girardi, L., and Marigo, P.: 2010, *VizieR Online Data Catalog* **350**, 80355
Böhm-Vitense, E.: 1958, *ZAp* **46**, 108
Bragaglia, A. and Tosi, M.: 2006, *AJ* **131**, 1544
Burgers, J. M.: 1969, *Flow Equations for Composite Gases*
Busse, F. H.: 1982, *ApJ* **259**, 759
Cameron, L. M.: 1985, *A&A* **147**, 39
Campa, A., Giansanti, A., Moroni, D., and Tsallis, C.: 2001, *Physics Letters A* **286**, 251
Canuto, V. M. and Mazzitelli, I.: 1991, *ApJ* **370**, 295
Cargile, P. A., James, D. J., and Jeffries, R. D.: 2010, *ApJ* **725**, L111
Carollo, D., Beers, T. C., Lee, Y. S., Chiba, M., Norris, J. E., Wilhelm, R., Sivarani, T., Marsteller, B., Munn, J. A., Bailer-Jones, C. A. L., Fiorentin, P. R., and York, D. G.: 2007, *Nature* **450**, 1020
Carrera, R. and Pancino, E.: 2011, *ArXiv e-prints*
Caughlan, G. R. and Fowler, W. A.: 1988, *Atomic Data and Nuclear Data Tables* **40**, 283
Cayrel de Strobel, G., Crifo, F., and Lebreton, Y.: 1997, in R. M. Bonnet, E. Høg, P. L. Bernacca, L. Emiliani, A. Blaauw, C. Turon, J. Kovalevsky, L. Lindegren, H. Hassan, M. Bouffard, B. Strim, D. Heger, M. A. C. Perryman, & L. Woltjer (ed.), *Hipparcos - Venice '97*, Vol. 402 of *ESA Special Publication*, pp 687–688
Chaboyer, B., Demarque, P., and Guenther, D. B.: 1999, *ApJ* **525**, L41
Chaboyer, B., Demarque, P., Guenther, D. B., and Pinsonneault, M. H.: 1995, *ApJ* **446**, 435
Chandrasekhar, S. and Münch, G.: 1950, *ApJ* **111**, 142
Charbonnel, C. and Talon, S.: 2008, in L. Deng and K. L. Chan (eds.), *IAU Symposium*, Vol. 252 of *IAU Symposium*, pp 163–174
Chiappini, C., Matteucci, F., and Gratton, R.: 1997, *ApJ* **477**, 765
Chiappini, C., Matteucci, F., and Romano, D.: 2001, *ApJ* **554**, 1044
Chiosi, C.: 2009, *Communications in Asteroseismology* **158**, 79
Choi, P. I. and Herbst, W.: 1996, *AJ* **111**, 283
Christensen-Dalsgaard, J. and Daeppen, W.: 1992, *A&A Rev.* **4**, 267
Collier Cameron, A., Campbell, C. G., and Quaintrell, H.: 1995, *A&A* **298**, 133
Converse, J. M. and Stahler, S. W.: 2008, *ApJ* **678**, 431
de Bruijne, J. H. J., Hoogerwerf, R., and de Zeeuw, P. T.: 2001, *A&A* **367**, 111
de Epstein, A. E. A. and Epstein, I.: 1985, *AJ* **90**, 1211
de Grijs, R.: 2010, *Royal Society of London Philosophical Transactions Series A* **368**, 693
Delorme, P., Collier Cameron, A., Hebb, L., Rostron, J., Lister, T. A., Norton, A. J., Pollacco, D., and West, R. G.: 2011, *MNRAS* **413**, 2218
Deutsch, A. J.: 1970, in A. Slettebak (ed.), *IAU Colloq. 4: Stellar Rotation*, pp 207–+

Dravins, D., Lindegren, L., Madsen, S., and Holmberg, J.: 1997, in R. M. Bonnet, E. Høg, P. L. Bernacca, L. Emiliani, A. Blaauw, C. Turon, J. Kovalevsky, L. Lindegren, H. Hassan, M. Bouffard, B. Strim, D. Heger, M. A. C. Perryman, & L. Woltjer (ed.), *Hipparcos - Venice '97*, Vol. 402 of *ESA Special Publication*, pp 733–738

Dufton, P. L., Smartt, S. J., Lee, J. K., Ryans, R. S. I., Hunter, I., Evans, C. J., Herrero, A., Trundle, C., Lennon, D. J., Irwin, M. J., and Kaufer, A.: 2006, *A&A* **457**, 265

Eddington, A. S.: 1926, *The Internal Constitution of the Stars*

Edwards, S., Strom, S. E., Hartigan, P., Strom, K. M., Hillenbrand, L. A., Herbst, W., Attridge, J., Merrill, K. M., Probst, R., and Gatley, I.: 1993, *AJ* **106**, 372

Eggen, O. J., Lynden-Bell, D., and Sandage, A. R.: 1962, *ApJ* **136**, 748

Eggleton, P. P., Faulkner, J., and Flannery, B. P.: 1973, *A&A* **23**, 325

Ekström, S., Georgy, C., Eggenberger, P., Meynet, G., Mowlavi, N., Wyttenbach, A., Granada, A., Decressin, T., Hirschi, R., Frischknecht, U., Charbonnel, C., and Maeder, A.: 2012, *A&A* **537**, A146

Endal, A. S. and Sofia, S.: 1978, *ApJ* **220**, 279

Ford, A., Jeffries, R. D., and Smalley, B.: 2005, *MNRAS* **364**, 272

Fossati, L., Bagnulo, S., Landstreet, J., Wade, G., Kochukhov, O., Monier, R., Weiss, W., and Gebran, M.: 2008, *A&A* **483**, 891

Freeman, K. and Bland-Hawthorn, J.: 2002, *ARA&A* **40**, 487

Gaige, Y.: 1993, *A&A* **269**, 267

Gatewood, G. and de Jonge, J. K.: 1994, *ApJ* **428**, 166

Gilmore, G.: 2002, in T. Lejeune & J. Fernandes (ed.), *Observed HR Diagrams and Stellar Evolution*, Vol. 274 of *Astronomical Society of the Pacific Conference Series*, pp 581–+

Gilmore, G. and Wyse, R. F. G.: 2001, in S. Deiters, B. Fuchs, A. Just, R. Spurzem, & R. Wielen (ed.), *Dynamics of Star Clusters and the Milky Way*, Vol. 228 of *Astronomical Society of the Pacific Conference Series*, pp 225–+

Gilmore, G., Wyse, R. F. G., and Kuijken, K.: 1989, *ARA&A* **27**, 555

Gratton, R. G., Sneden, C., Carretta, E., and Bragaglia, A.: 2000, *A&A* **354**, 169

Gray, R. O.: 1985, *JRASC* **79**, 237

Gray, R. O.: 1988, *JRASC* **82**, 336

Grevesse, N. and Noels, A.: 1993, in N. Prantzos, E. Vangioni-Flam, & M. Casse (ed.), *Origin and Evolution of the Elements*, pp 15–25

Gustafsson, B., Edvardsson, B., Eriksson, K., Jørgensen, U. G., Nordlund, Å., and Plez, B.: 2008, *A&A* **486**, 951

Hambly, N. C., Steele, I. A., Hawkins, M. R. S., and Jameson, R. F.: 1995, *A&AS* **109**, 29

Hamity, V. H. and Barraco, D. E.: 1996, *Physical Review Letters* **76**, 4664

Hartman, J. D., Bakos, G. Á., Kovács, G., and Noyes, R. W.: 2010, *MNRAS* **408**, 475

Helmi, A.: 2008, *A&A Rev.* **15**, 145

Hendry, M. A., O'dell, M. A., and Collier-Cameron, A.: 1993, *MNRAS* **265**, 983

Herbst, W., Bailer-Jones, C. A. L., and Mundt, R.: 2001, *ApJ* **554**, L197

Holland, K., Jameson, R. F., Hodgkin, S., Davies, M. B., and Pinfield, D.: 2000, *MNRAS* **319**, 956

Hou, J. L., Prantzos, N., and Boissier, S.: 2000, *A&A* **362**, 921

Iglesias, C. A. and Rogers, F. J.: 1996, *ApJ* **464**, 943
Irwin, J. and Bouvier, J.: 2009, in E. E. Mamajek, D. R. Soderblom, and R. F. G. Wyse (eds.), *IAU Symposium*, Vol. 258 of *IAU Symposium*, pp 363–374
Irwin, J., Hodgkin, S., Aigrain, S., Bouvier, J., Hebb, L., and Moraux, E.: 2008, *MNRAS* **383**, 1588
Irwin, J., Hodgkin, S., Aigrain, S., Hebb, L., Bouvier, J., Clarke, C., Moraux, E., and Bramich, D. M.: 2007, *MNRAS* **377**, 741
Jackson, R. J. and Jeffries, R. D.: 2010, *MNRAS* **402**, 1380
Jackson, R. J., Jeffries, R. D., and Maxted, P. F. L.: 2009, *MNRAS* **399**, L89
Jeffries, R. D.: 2007a, *MNRAS* **376**, 1109
Jeffries, R. D.: 2007b, *MNRAS* **381**, 1169
Jones, B. F. and Cudworth, K.: 1983, *AJ* **88**, 215
Jones, B. F. and Stauffer, J. R.: 1991, *AJ* **102**, 1080
Kafka, S. and Honeycutt, R. K.: 2006, *AJ* **132**, 1517
Kawaler, S. D.: 1988, *ApJ* **333**, 236
Kervella, P., Thévenin, F., Di Folco, E., and Ségransan, D.: 2004, *A&A* **426**, 297
Kharchenko, N. V., Piskunov, A. E., Röser, S., Schilbach, E., and Scholz, R.-D.: 2004, *Astronomische Nachrichten* **325**, 740
Klypin, A., Kravtsov, A. V., Valenzuela, O., and Prada, F.: 1999, *ApJ* **522**, 82
Koenigl, A.: 1991, *ApJ* **370**, L39
Kraft, R. P.: 1965, *ApJ* **142**, 681
Kraus, A. L. and Hillenbrand, L. A.: 2007, *AJ* **134**, 2340
Krishnamurthi, A., Terndrup, D. M., Pinsonneault, M. H., Sellgren, K., Stauffer, J. R., Schild, R., Backman, D. E., Beisser, K. B., Dahari, D. B., Dasgupta, A., Hagelgans, J. T., Seeds, M. A., Anand, R., Laaksonen, B. D., Marschall, L. A., and Ramseyer, T.: 1998, *ApJ* **493**, 914
Kucinskas, A., Lindegren, L., and Vansevicius, V.: 2005, in C. Turon, K. S. O'Flaherty, & M. A. C. Perryman (ed.), *The Three-Dimensional Universe with Gaia*, Vol. 576 of *ESA Special Publication*, pp 695–+
Latora, V., Rapisarda, A., and Tsallis, C.: 2002, *Physica A Statistical Mechanics and its Applications* **305**, 129
Lavagno, A., Kaniadakis, G., Rego-Monteiro, M., Quarati, P., and Tsallis, C.: 1998, *Astrophysical Letters Communications* **35**, 449
Lebreton, Y., Fernandes, J., and Lejeune, T.: 2001, *A&A* **374**, 540
Lebreton, Y., Gomez, A. E., Mermilliod, J. C., and Perryman, M. A. C.: 1997, in R. M. Bonnet, E. Høg, P. L. Bernacca, L. Emiliani, A. Blaauw, C. Turon, J. Kovalevsky, L. Lindegren, H. Hassan, M. Bouffard, B. Strim, D. Heger, M. A. C. Perryman, & L. Woltjer (ed.), *Hipparcos - Venice '97*, Vol. 402 of *ESA Special Publication*, pp 231–236
Lejeune, T.: 2002, in T. Lejeune and J. Fernandes (eds.), *Observed HR Diagrams and Stellar Evolution*, Vol. 274 of *Astronomical Society of the Pacific Conference Series*, p. 159
Lima, J. A. S. and Plastino, A. R.: 2000, *Brazilian Journal of Physics* **30**, 176
Lydon, T. J. and Sofia, S.: 1995, *ApJS* **101**, 357

Maeder, A.: 1998, in I. Howarth (ed.), *Properties of Hot Luminous Stars*, Vol. 131 of *Astronomical Society of the Pacific Conference Series*, pp 85–+
Maeder, A.: 2009, *Physics, Formation and Evolution of Rotating Stars*
Maeder, A. and Meynet, G.: 2000, *ARA&A* **38**, 143
Maeder, A. and Zahn, J.-P.: 1998, *A&A* **334**, 1000
Makarov, V. V.: 2006, *AJ* **131**, 2967
Mathis, S., Palacios, A., and Zahn, J.-P.: 2004, *A&A* **425**, 243
Mathis, S. and Zahn, J.-P.: 2004, *A&A* **425**, 229
Matt, S. and Pudritz, R. E.: 2005, *ApJ* **632**, L135
Matt, S. P., Pinzón, G., de la Reza, R., and Greene, T. P.: 2010, *ApJ* **714**, 989
Meibom, S., Mathieu, R. D., and Stassun, K. G.: 2009, *ApJ* **695**, 679
Melia, F. and Falcke, H.: 2001, *ARA&A* **39**, 309
Ménard, F. and Duchêne, G.: 2004, *A&A* **425**, 973
Mermilliod, J.-C., Mayor, M., and Udry, S.: 2009, *VizieR Online Data Catalog* **3498**, 80949
Mermilliod, J.-C., Platais, I., James, D. J., Grenon, M., and Cargile, P. A.: 2008a, *A&A* **485**, 95
Mermilliod, J.-C., Queloz, D., and Mayor, M.: 2008b, *A&A* **488**, 409
Messina, S., Desidera, S., Turatto, M., Lanzafame, A. C., and Guinan, E. F.: 2010, *A&A* **520**, A15+
Messina, S., Rodonò, M., and Cutispoto, G.: 2004, *Astronomische Nachrichten* **325**, 660
Mestel, L.: 1953, *MNRAS* **113**, 716
Meynet, G. and Maeder, A.: 2000, *A&A* **361**, 101
Michaud, G. and Proffitt, C. R.: 1993, in W. W. Weiss & A. Baglin (ed.), *IAU Colloq. 137: Inside the Stars*, Vol. 40 of *Astronomical Society of the Pacific Conference Series*, pp 246–259
Mihalas, D., Dappen, W., and Hummer, D. G.: 1988, *ApJ* **331**, 815
Miller, A. A., Irwin, J., Aigrain, S., Hodgkin, S., and Hebb, L.: 2008, *MNRAS* **387**, 349
Molla, M., Ferrini, F., and Diaz, A. I.: 1997, *ApJ* **475**, 519
Moore, B., Ghigna, S., Governato, F., Lake, G., Quinn, T., Stadel, J., and Tozzi, P.: 1999, *ApJ* **524**, L19
Morel, P. and Lebreton, Y.: 2008, *Ap&SS* **316**, 61
Morel, P. and Thévenin, F.: 2002, *A&A* **390**, 611
Munari, U., Zwitter, T., and Milone, E. F.: 2004, in R. W. Hilditch, H. Hensberge, & K. Pavlovski (ed.), *Spectroscopically and Spatially Resolving the Components of the Close Binary Stars*, Vol. 318 of *Astronomical Society of the Pacific Conference Series*, pp 422–429
Nicolet, B.: 1981, *A&A* **104**, 185
Paczynski, B.: 1986, *ApJ* **304**, 1
Palacios, A., Talon, S., Charbonnel, C., and Forestini, M.: 2003, *A&A* **399**, 603
Percival, S. M., Salaris, M., and Kilkenny, D.: 2003, *A&A* **400**, 541
Pérez Hernández, F., Claret, A., Hernández, M. M., and Michel, E.: 1999, *A&A* **346**, 586
Perryman, M. A. C., Brown, A. G. A., Lebreton, Y., Gomez, A., Turon, C., Cayrel de Strobel, G., Mermilliod, J. C., Robichon, N., Kovalevsky, J., and Crifo, F.: 1998, *A&A*

331, 81
Pillitteri, I., Micela, G., Sciortino, S., and Favata, F.: 2003, *A&A* **399**, 919
Pinsonneault, M. H., Kawaler, S. D., Sofia, S., and Demarque, P.: 1989, *ApJ* **338**, 424
Portinari, L. and Chiosi, C.: 1999, *A&A* **350**, 827
Prosser, C. F.: 1992, *AJ* **103**, 488
Prosser, C. F., Shetrone, M. D., Dasgupta, A., Backman, D. E., Laaksonen, B. D., Baker, S. W., Marschall, L. A., Whitney, B. A., Kuijken, K., and Stauffer, J. R.: 1995, *PASP* **107**, 211
Radick, R. R., Thompson, D. T., Lockwood, G. W., Duncan, D. K., and Baggett, W. E.: 1987, *ApJ* **321**, 459
Rajagopal, A. K.: 1996, *Physical Review Letters* **76**, 3469
Rambaux, N., Couedtic, J., Laskar, J., and Sozzetti, A.: 2009, in M. Heydari-Malayeri, C. Reyl'E, & R. Samadi (ed.), *SF2A-2009: Proceedings of the Annual meeting of the French Society of Astronomy and Astrophysics*, pp 73–+
Rebull, L. M., Stauffer, J. R., Megeath, S. T., Hora, J. L., and Hartmann, L.: 2006, *ApJ* **646**, 297
Reid, I. N. and Mahoney, S.: 2000, *MNRAS* **316**, 827
Rogers, F. J., Swenson, F. J., and Iglesias, C. A.: 1996, *ApJ* **456**, 902
Rosales-Ortega, F. F., Kennicutt, R. C., Sánchez, S. F., Díaz, A. I., Pasquali, A., Johnson, B. D., and Hao, C. N.: 2010, *MNRAS* **405**, 735
Röser, S., Schilbach, E., Piskunov, A. E., Kharchenko, N. V., and Scholz, R.-D.: 2011, *A&A* **531**, A92
Royer, F., Zorec, J., and Gómez, A. E.: 2007, *A&A* **463**, 671
Salpeter, E. E.: 1959, *ApJ* **129**, 608
Schatzman, E.: 1962, *Annales d'Astrophysique* **25**, 18
Schatzman, E.: 1969, *A&A* **3**, 331
Searle, L. and Zinn, R.: 1978, *ApJ* **225**, 357
Shatsova, R. B.: 1981, *Soviet Astronomy Letters* **7**, 398
Shu, F., Najita, J., Ostriker, E., Wilkin, F., Ruden, S., and Lizano, S.: 1994, *ApJ* **429**, 781
Shu, F. H., Adams, F. C., and Lizano, S.: 1987, *ARA&A* **25**, 23
Sills, A. and Deliyannis, C. P.: 2000, *ApJ* **544**, 944
Silva, Jr., R., Plastino, A. R., and Lima, J. A. S.: 1998, *Physics Letters A* **249**, 401
Smiljanic, R., Gauderon, R., North, P., Barbuy, B., Charbonnel, C., and Mowlavi, N.: 2009, *A&A* **502**, 267
Smith, K. W., Bailer-Jones, C. A. L., Elting, C., and Tiede, C.: 2008, in C. A. L. Bailer-Jones (ed.), *American Institute of Physics Conference Series*, Vol. 1082 of *American Institute of Physics Conference Series*, pp 29–36
Soares, B. B., Carvalho, J. C., Do Nascimento, Jr., J. D., and de Medeiros, J. R.: 2006, *Physica A Statistical Mechanics and its Applications* **364**, 413
Soderblom, D. R., King, J. R., Hanson, R. B., Jones, B. F., Fischer, D., Stauffer, J. R., and Pinsonneault, M. H.: 1998, *ApJ* **504**, 192
Soderblom, D. R., Laskar, T., Valenti, J. A., Stauffer, J. R., and Rebull, L. M.: 2009, *AJ* **138**, 1292

Sofue, Y., Honma, M., and Omodaka, T.: 2009, *PASJ* **61**, 227
Spiegel, E. A. and Zahn, J.-P.: 1970, *Comments on Astrophysics and Space Physics* **2**, 178
Springel, V., Frenk, C. S., and White, S. D. M.: 2006, *Nature* **440**, 1137
Stahler, S. W.: 1988, *ApJ* **332**, 804
Stauffer, J., Hamilton, D., Probst, R., Rieke, G., and Mateo, M.: 1989, *ApJ* **344**, L21
Stauffer, J. R., Schultz, G., and Kirkpatrick, J. D.: 1998, *ApJ* **499**, L199+
Stello, D. and Nissen, P. E.: 2001, *A&A* **374**, 105
Struve, O.: 1945, *Popular Astronomy* **53**, 201
Sweet, P. A.: 1950, *MNRAS* **110**, 548
Talon, S., Zahn, J.-P., Maeder, A., and Meynet, G.: 1997, *A&A* **322**, 209
Taruya, A. and Sakagami, M.-a.: 2002, *Physica A Statistical Mechanics and its Applications* **307**, 185
Tassoul, J.-L.: 1978, *Theory of rotating stars*
Thompson, M. J., Christensen-Dalsgaard, J., Miesch, M. S., and Toomre, J.: 2003, *ARA&A* **41**, 599
Tisserand, P., Le Guillou, L., Afonso, C., Albert, J. N., Andersen, J., Ansari, R., Aubourg, É., Bareyre, P., Beaulieu, J. P., Charlot, X., Coutures, C., Ferlet, R., Fouqué, P., Glicenstein, J. F., Goldman, B., Gould, A., Graff, D., Gros, M., Haissinski, J., Hamadache, C., de Kat, J., Lasserre, T., Lesquoy, É., Loup, C., Magneville, C., Marquette, J. B., Maurice, É., Maury, A., Milsztajn, A., Moniez, M., Palanque-Delabrouille, N., Perdereau, O., Rahal, Y. R., Rich, J., Spiro, M., Vidal-Madjar, A., Vigroux, L., Zylberajch, S., and The EROS-2 Collaboration: 2007, *A&A* **469**, 387
Torres, G., Stefanik, R. P., and Latham, D. W.: 1997a, *ApJ* **485**, 167
Torres, G., Stefanik, R. P., and Latham, D. W.: 1997b, *ApJ* **474**, 256
Torres, G., Stefanik, R. P., and Latham, D. W.: 1997c, *ApJ* **479**, 268
Tsallis, C.: 1988, *Journal of Statistical Physics* **52**, 479
van der Kruit, P. C. and Freeman, K. C.: 2011, *ArXiv e-prints*
van Leeuwen, F.: 1980, in J. E. Hesser (ed.), *Star Clusters*, Vol. 85 of *IAU Symposium*, pp 157–162
van Leeuwen, F.: 1999, in D. Egret & A. Heck (ed.), *Harmonizing Cosmic Distance Scales in a Post-HIPPARCOS Era*, Vol. 167 of *Astronomical Society of the Pacific Conference Series*, pp 52–71
van Leeuwen, F.: 2009, *A&A* **497**, 209
Vink, J. S., Drew, J. E., Harries, T. J., Oudmaijer, R. D., and Unruh, Y.: 2005, *MNRAS* **359**, 1049
von Zeipel, H.: 1924, *MNRAS* **84**, 665
Weber, E. J. and Davis, Jr., L.: 1967, *ApJ* **148**, 217
Westerlund, B. E., Lundgren, K., Pettersson, B., Garnier, R., and Breysacher, J.: 1988, *A&AS* **76**, 101
Xue, X. X., Rix, H. W., Zhao, G., Re Fiorentin, P., Naab, T., Steinmetz, M., van den Bosch, F. C., Beers, T. C., Lee, Y. S., Bell, E. F., Rockosi, C., Yanny, B., Newberg, H., Wilhelm, R., Kang, X., Smith, M. C., and Schneider, D. P.: 2008, *ApJ* **684**, 1143
Zahn, J.-P.: 1974, in P. Ledoux, A. Noels, & A. W. Rodgers (ed.), *Stellar Instability and*

Evolution, Vol. 59 of *IAU Symposium*, pp 185–194
Zahn, J. P.: 1975, *Memoires of the Societe Royale des Sciences de Liege* **8**, 31
Zahn, J.-P.: 1992, *A&A* **265**, 115
Zahn, J.-P., Ranc, C., and Morel, P.: 2010, *A&A* **517**, A7+
Zorec, J. and Royer, F.: 2012, *A&A* **537**, A120